

Seventh Framework Programme

Theme 6

Environment



Project: 603864 – HELIX

Full project title:

High-End cLimate Impacts and eXtremes

D9.3 Technical report detailing the results from the uncertainty and sensitivity analysis

Part A: Climate Change impact assessment of the Ganga River Basin using hydrological modelling.

Part B: Chapter One: Assessment on the uncertainty of the high flows (floods) and low flows (hydrological droughts) of the Brahmaputra River

Part B: Chapter Two: Assessment of the uncertrainty and sensitivity of climate change on the production of Boro rice in Bangladesh using DSSAT crop model

Original Due date of deliverable: 31/10/16

Actual date of submission: 31/10/16

Contributors to the Report

IIT Delhi

BUET Bangladesh

PART A: Climate Change Impact Assessment of the Ganga River Basin using Hydrological Modelling

Technical Report No D9.3

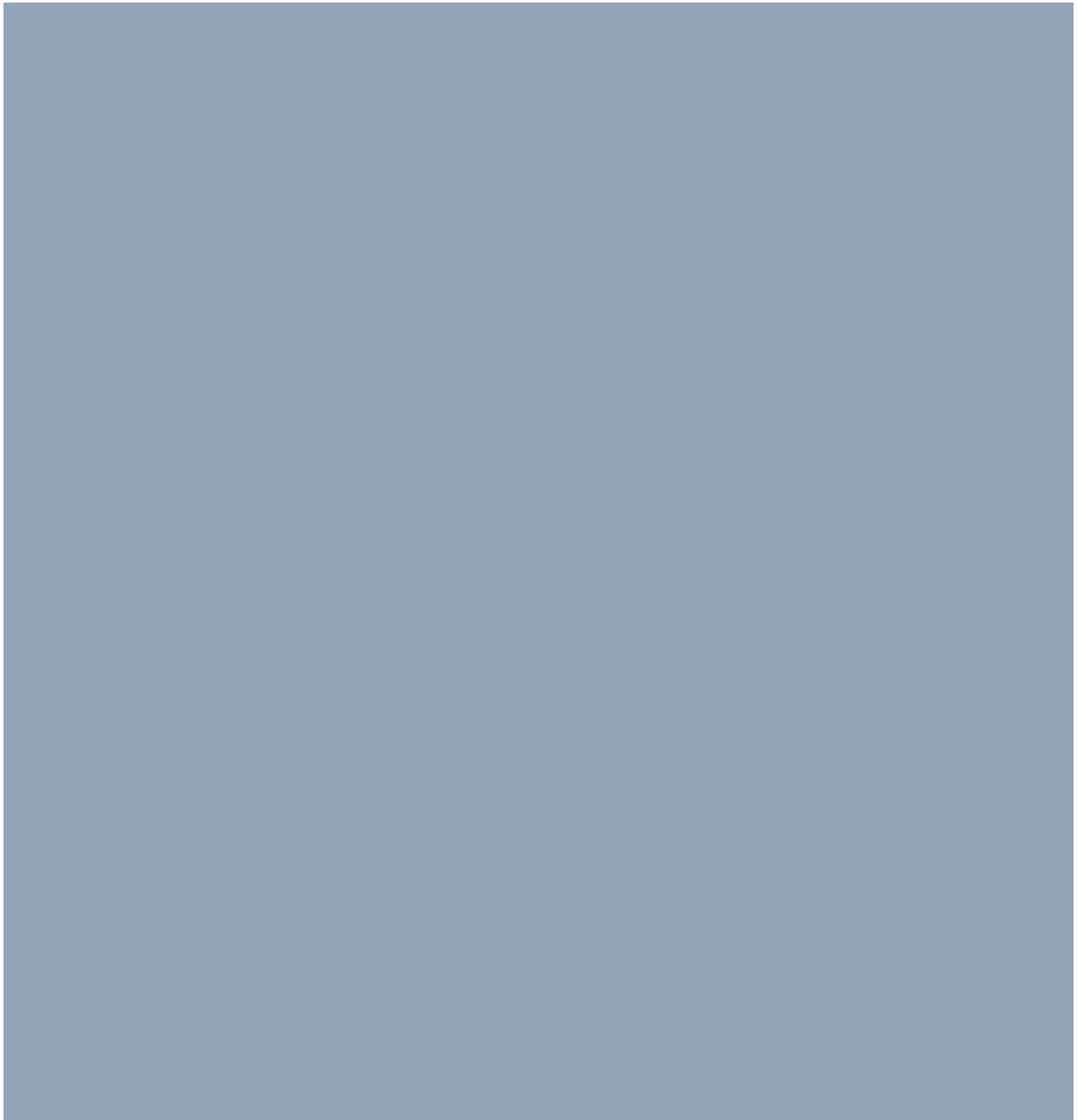


Table of Contents

TABLE OF CONTENTS	4
LIST OF FIGURES	5
LIST OF TABLES	6
<u>CLIMATE CHANGE IMPACTS USING HIGH RESOLUTION RCMS FOR IPCC AR5 RCP 8.5 SCENARIO: DETAILING THE RESULTS FROM THE UNCERTAINTY AND SENSITIVITY ANALYSIS FOR SPECIFIC WARMING LEVEL</u>	<u>7</u>
THE HYDROLOGIC SIMULATION WITH CLIMATE CHANGE SCENARIO	7
SPECIFIC WARMING LEVEL	8
UNCERTAINTY IN CLIMATE CHANGE PROJECTIONS ON HYDROLOGY OF THE GANGA RIVER BASIN	9
CHANGE IN CLIMATE	9
CHANGE IN WATER BALANCE COMPONENTS	19
CHANGE IN EXTREMES	25
Drought Analysis	25
Peak Discharge Analysis	28
CHANGE IN CROP GROWTH	29
SENSITIVITY ANALYSIS	31
CO ₂ FERILIZATION	31

List of Figures

FIGURE 1 PROJECTED CHANGE IN ANNUAL MAXIMUM, MINIMUM TEMPERATURE AND ANNUAL PRECIPITATION FOR THE GANGA BASIN FOR RCP8.5 SCENARIO AT SPECIFIC GLOBAL WARMING LEVELS OF SWL1.5, SWL2 AND SWL4	10
FIGURE 2 PROJECTED LONG TERM MONTHLY MAXIMUM TEMPERATURE WITH UNCERTAINTY BANDS (RANGES) FOR THE GANGA BASIN - BASELINE, RCP8.5 SCENARIO AT SPECIFIC GLOBAL WARMING LEVELS OF SWL1.5, SWL2 AND SWL4	12
FIGURE 3 PROJECTED LONG TERM MONTHLY MINIMUM TEMPERATURE WITH UNCERTAINTY BANDS (RANGES) FOR THE GANGA BASIN - BASELINE, RCP8.5 SCENARIO FOR SWL1.5, SWL2 AND SWL4	14
FIGURE 4 MULTI MODEL RANGE RELATIVE TO MULTI MODEL MEAN FOR LONG TERM MONTHLY TEMPERATURE FOR THE GANGA BASIN - BASELINE, RCP8.5 SCENARIO FOR SWL1.5, SWL2 AND SWL4....	16
FIGURE 5 PROJECTED LONG TERM MONTHLY PRECIPITATION WITH UNCERTAINTY BANDS (RANGES) FOR THE GANGA BASIN - BASELINE, RCP8.5 SCENARIO FOR SWL1.5, SWL2 AND SWL4	17
FIGURE 6 MULTI MODEL RANGE RELATIVE TO MULTI MODEL MEAN FOR LONG TERM MONTHLY PRECIPITATION FOR THE GANGA BASIN - BASELINE, RCP8.5 SCENARIO FOR SWL1.5, SWL2 AND SWL4 ...	19
FIGURE 7 PROJECTED CHANGE IN ANNUAL STREAM FLOW AND EVAPOTRANSPIRATION FOR THE GANGA BASIN	20
FIGURE 8 PROJECTED LONG TERM ANNUAL PRECIPITATION, STREAM FLOW AND EVAPOTRANSPIRATION FOR MULTI MODELS FOR THE GANGA BASIN - BASELINE, RCP8.5 SCENARIO FOR SWL1.5, SWL2 AND SWL4... 21	21
FIGURE 9 PROJECTED CHANGE IN LONG TERM ANNUAL PRECIPITATION, STREAM FLOW AND EVAPOTRANSPIRATION RELATIVE TO BASELINE FOR MULTI MODELS FOR THE GANGA BASIN - BASELINE, RCP8.5 SCENARIO FOR SWL1.5, SWL2 AND SWL4	23
FIGURE 10 ANNUAL WATER BALANCE COMPONENTS SIMULATED USING MULTIPLE CORDEX RCM MODELS FOR THE GANGA BASIN.....	24
FIGURE 11 PROJECTED CHANGE IN EXTREME WEATHER EVENT - DROUGHT FOR THE GANGA BASIN	26
FIGURE 12 BOXPLOT OF PROJECTED CHANGE IN EXTREME WEATHER EVENT - DROUGHT FOR THE GANGA BASIN	27
FIGURE 13 PROJECTED CHANGE IN EXTREME WEATHER EVENT - PEAK DISCHARGE AT FARAKKA FOR THE GANGA BASIN	28
FIGURE 14 BOXPLOT OF PROJECTED CHANGE IN EXTREME WEATHER EVENT - PEAK DISCHARGE FOR THE GANGA BASIN	29
FIGURE 15 PROJECTED CHANGE IN CROP WATER PRODUCTIVITY AND ADDITIONAL IRRIGATION REQUIREMENT - GANGA BASIN	30
FIGURE 16 SENSITIVITY OF ELEVATED CO ₂ ON CROP GROWTH	32

List of Tables

TABLE 1 AVAILABLE BIAS CORRECTED DATA AT RCP85.....	7
TABLE 2 CMIP5 MODELS AND TIME OF PASSING OF A GIVEN SWL WITH THE RCP85 FORCING.....	8

Climate Change Impacts using High Resolution RCMs for IPCC AR5 RCP 8.5 Scenario: Detailing the Results from the Uncertainty and Sensitivity Analysis for Specific Warming Level

The Hydrologic Simulation with Climate Change Scenario- Previous work

In the previous work, the hydrological model has been run using climate scenarios for near (MC) and long term (EC) periods (2021 – 2050, 2071-2100, respectively) with the assumption that the land use is not changing over time. The hydrological simulations are run with 11 high resolution RCM models (Table 1), and for 3 time periods (Baseline, mid century and end Century) for RCP scenarios 8.5 (bias corrected). Thus the number of hydrological model simulations carried out was 33 simulations for the Ganga basin.

Table 1 Available Bias Corrected data at RCP85

Sl	Model	Remark
CSIRO-CCAM-1391M		
1	WAS-44i_ACCESS1-0_r1_CSIRO-CCAM-1391M_day	
2	WAS-44i_CCSM4_r1_CSIRO-CCAM-1391M_day	
3	WAS-44i_CNRM-CM5_r1_CSIRO-CCAM-1391M_day	
4	WAS-44i_GFDL-CM3_r1_CSIRO-CCAM-1391M_day	Not Used (no precipitation data available)
5	WAS-44i_MPI-ESM-LR_r1_CSIRO-CCAM-1391M_day	
MPI-CSC-REMO2009		
1	WAS-44_MPI-M-MPI-ESM-LR_r1i1p1_MPI-CSC-REMO2009_v1_day	
SMHI-RCA4		
1	WAS-44_CNRM-CERFACS-CNRM-CM5_r1i1p1_SMHI-RCA4_v2_day	
2	WAS-44_ICHEC-EC-EARTH_r12i1p1_SMHI-RCA4_v2_day	
3	WAS-44_IPSL-IPSL-CM5A-MR_r1i1p1_SMHI-RCA4_v2_day	
4	WAS-44_MIROC-MIROC5_r1i1p1_SMHI-RCA4_v2_day	
5	WAS-44_MPI-M-MPI-ESM-LR_r1i1p1_SMHI-RCA4_v2_day	
6	WAS-44_NOAA-GFDL-GFDL-ESM2M_r1i1p1_SMHI-RCA4_v2_day	
Data Source: Technical University of Crete		

The present segment of the study is aimed at quantifying uncertainties from multiple climate model data derived impacts on the water resources of the Ganga Basin using Specific Warming Levels (SWL) under Helix objectives. SWAT hydrological model has been re-run for SWL1.5, SWL2, SWL4 scenarios. Due to non availability of extended time series climate data beyond 2100, SWL6 could not be run.

Model uncertainty arising from different SWLs relative to baseline has been discussed in the following paragraphs. Baseline period has been considered from 1981-2010.

The well known distributed hydrological model SWAT has been deployed for the purpose. Scenarios have been generated for assessing implications on quantity of water on account of multiple regional climate model climate data.

The outputs of these scenarios have been analyzed to evaluate the possible impacts on some of the important hydrological entities such as the runoff, baseflow, soil moisture, ground water recharge and actual evapotranspiration. The impacts have been expressed as change in the future periods with respect to the baseline.

Specific Warming Level

HELIX assesses potential climate change impacts and adaptation for global warming above 2°C. Development of coherent, internally-consistent global scenarios of the combined natural and human world at 1.5, 2, 4 and 6°C global warming, including reaching this level early (2060s) or later (after 2100) has been carried out under WP3. Based on a set of selected CMIP5 forcing data and associated timing of passing a specific SWL has been arrived at. These CMIP5 models span a good range of fast/slow warming rates and wet/dry conditions in the HELIX target regions. Table 2 gives the details of the models and their respective time of passing of selected SWLs.

Table 2 CMIP5 models and time of passing of a given SWL with the RCP85 forcing

Member	Model	Ensemble	RCP85			
			SWL1.5	SWL2	SWL4	SWL6
r0	ERA interim					
r1	IPSL-CM5A-LR	r1i1p1	2015	2030	2068	2102
r2	GFDL-ESM2M	r1i1p1	2040	2055	2113	2186
r3	HadGEM2-ES	r1i1p1	2027	2039	2074	2110
r4	EC-EARTH	r12i1p1	2019	2035	2083	
r5	GISS-E2-H	r1i1p1	2022	2038	2102	2244
r6	IPSL-CM5A-MR	r1i1p1	2020	2034	2069	

Uncertainty in Climate Change Projections on Hydrology of the Ganga River Basin

Uncertainty is associated with each stage of climate change hydrological impact assessments (Nawaz and Adeloje, 2006¹; Gosling et al., 2011²). Uncertainty can arise from (a) definition of greenhouse gas emissions scenarios with which GCMs are forced; (b) climate model structural uncertainty (c) downscaling of GCM projections to finer spatial resolution. However, in the present case it has been decided to deal with the uncertainty in the climate change key parameters of precipitation and temperature (both minimum and maximum).

Change in Climate

The key parameters of precipitation and temperature have been taken up to explore their variation across the models at the temporal and spatial scale. Figure 1, depicts the spatial variation in the projected future change in annual minimum and maximum temperature and precipitation under specific warming levels of SWL1.5, SWL2 and SWL4 with respect to the baseline scenario for all the eleven models.

It may be observed from the figure that there is appreciable variation across the models for all the three entities of minimum temperature, maximum temperature and precipitation. The change in the minimum annual temperature itself is ranging between 0.8 to 2.1°C under SWL1.5, 1.3 to 2.8°C under SWL2, and between 3.3 to 5°C under SWL4 scenario. It may also be seen that the variation in the change in the annual minimum temperature for SWL1.5 and SWL2 is relatively lower across the models in comparison to the variation observed across the models for SWL4 scenario.

Similarly, the change in the maximum annual temperature is ranging between ranging between 0.7 to 1.8°C under SWL1.5, 1.1 to 2.5°C under SWL2, and between 2.5 to 5°C under SWL4 scenario. It may also be seen again that the variation in the change in the annual maximum temperature for for SWL1.5 and SWL2 is relatively lower across the models in comparison to the variation observed across the models for SWL4 scenario.

Higher warming is projected for some parts of Ganga basin than average temperature global warming for SWL1.5, SWL2 and SWL4 levels both in minimum and maximum temperatures.

In case of precipitation, most of the models show marginal increase/decrease in annual precipitation from -7% to 11% under SWL1.5, to 9%-15% under SWL2 and -18% to 24% under SWL4 specific warming levels. SMHI-RCA4 RCM with MIROC5 and GFDL-ESM2M forcing do not achieve specific global warming level of 4°C till end of century. RCM cordex models namely REMO2009 (MPI GCM forcing)and SMHI-RCA4 (MPI and GFDL-ESM2M GCM forcing) show projected marginal decrease in precipitation whereas rest of the 8 models show projected increase in precipitation.

These uncertainties in the key weather inputs are bound to reflect in all the impacts being computed using these parameters in hydrological models.

¹ Nawaz, N.R., Adeloje, A.J., 2006. Monte Carlo assessment of sampling uncertainty of climate change impacts on water resources yield in Yorkshire, England. *Clim. Change* 78, 257–292.

² Gosling, S.N., Taylor, R.G., Arnell, N.W., Todd, M.C., 2011a. A comparative analysis of projected impacts of climate change on river runoff from global and catchment scale hydrological models. *Hydrol. Earth Syst. Sci.* 15, 279–294.

Figure 1 Projected change in annual maximum, minimum temperature and annual precipitation for the Ganga basin for RCP8.5 Scenario at specific global warming levels of SWL1.5, SWL2 and SWL4

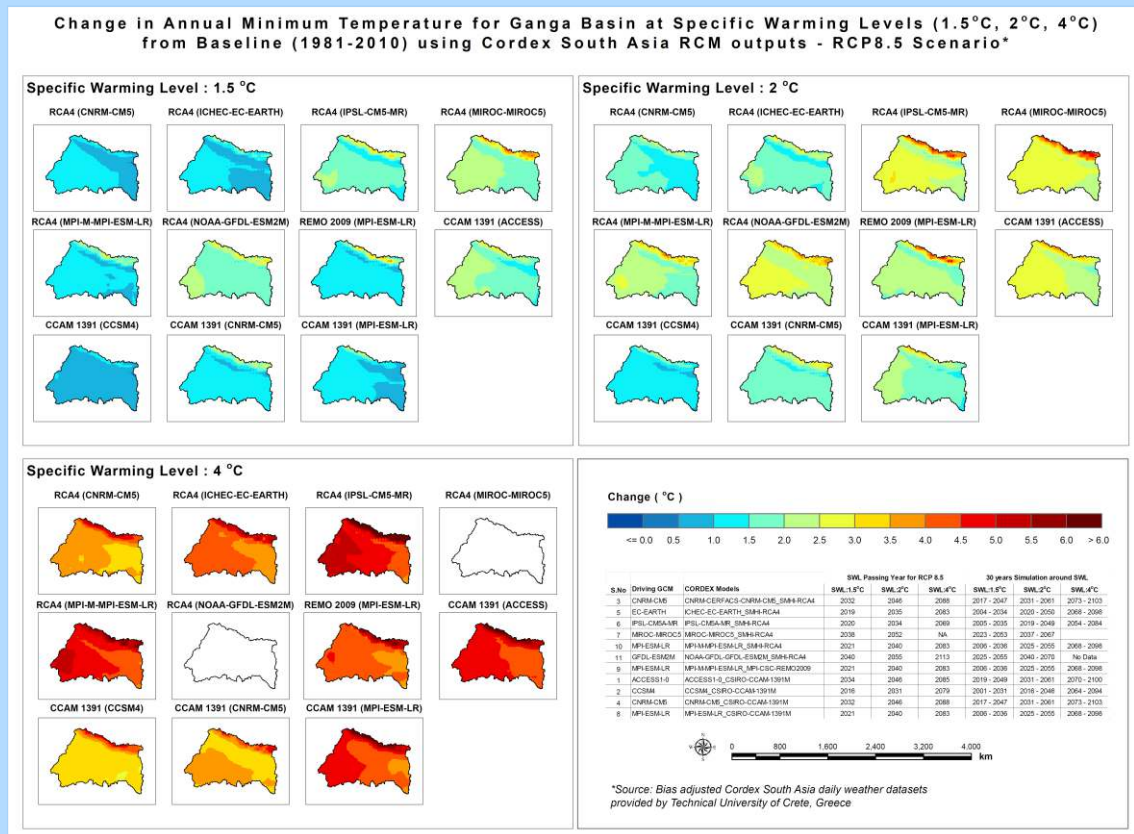
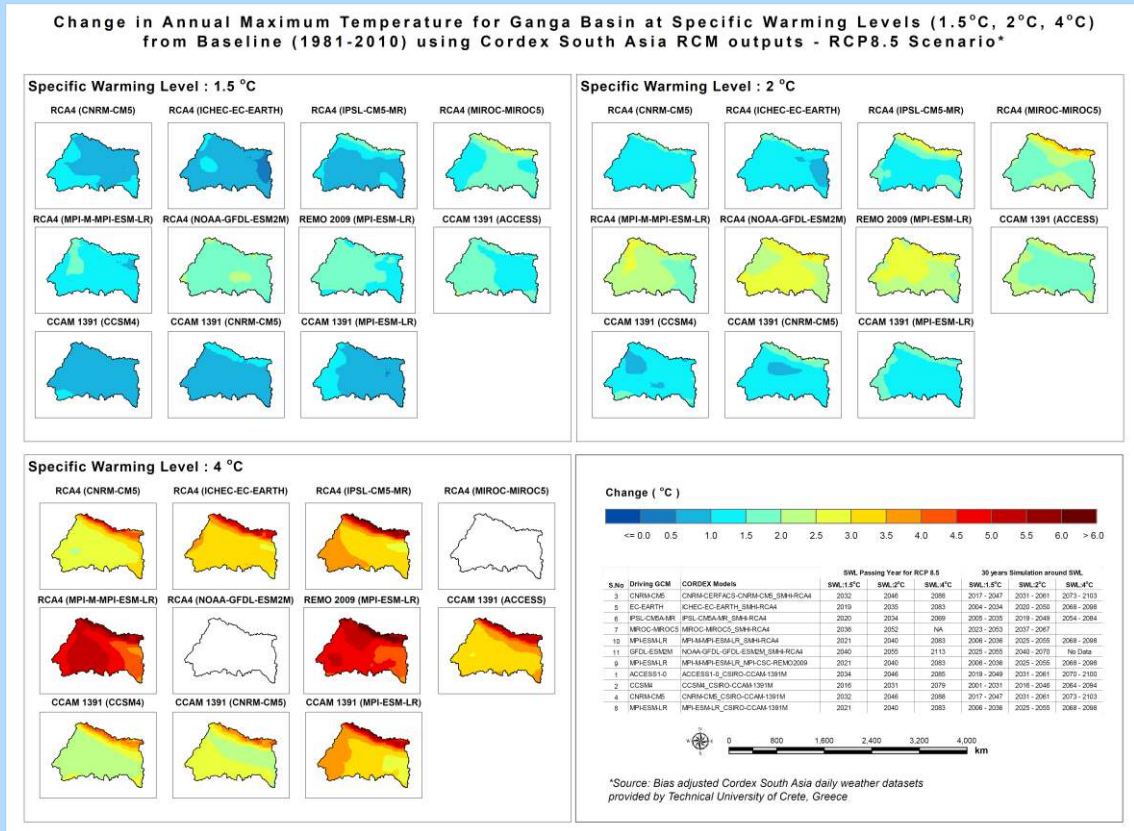
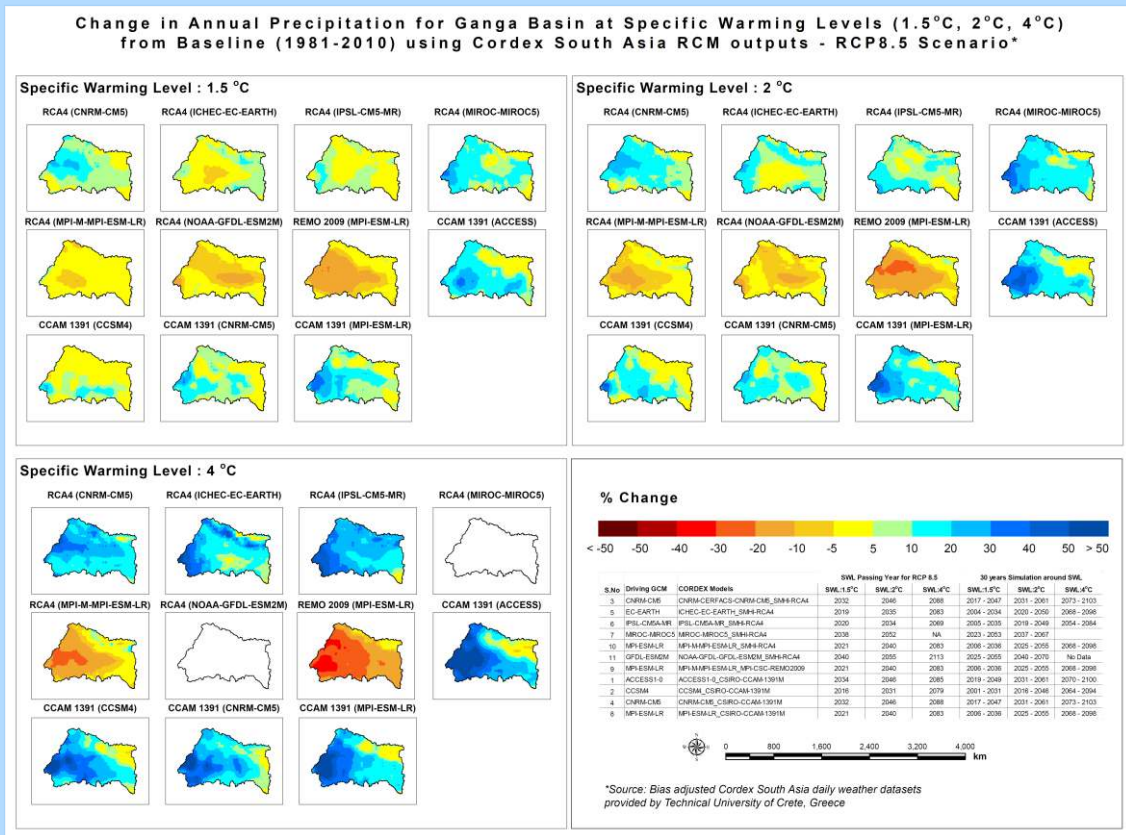


Figure 1 Projected change in annual maximum, minimum temperature and annual precipitation for the Ganga basin for RCP8.5 Scenario at specific global warming levels of SWL1.5, SWL2 and SWL4



The uncertainty amongst the climate models has also been depicted temporally using the monthly interval for all the three parameters of maximum temperature, minimum temperature and precipitation. Figure 2 presents the maximum monthly temperature for various models under baseline, SWL1.5, SWL2 and SWL4 for RCP8.5 scenarios. It may be noted that the maximum monthly temperature for all the models for Baseline scenario is the same for all the 11 models used.

There has been variation of up to 2.0°C to 2.4°C in maximum temperature under SWL1.5 and SWL4 respectively between the different models. The months from January to June show more variation in the maximum temperature. This spread has further increased for SWL4, where variation for the month of is as much as 2.4°C.

Figure 2 Projected long term monthly maximum temperature with uncertainty bands (ranges) for the Ganga basin - Baseline, RCP8.5 Scenario at specific global warming levels of SWL1.5, SWL2 and SWL4

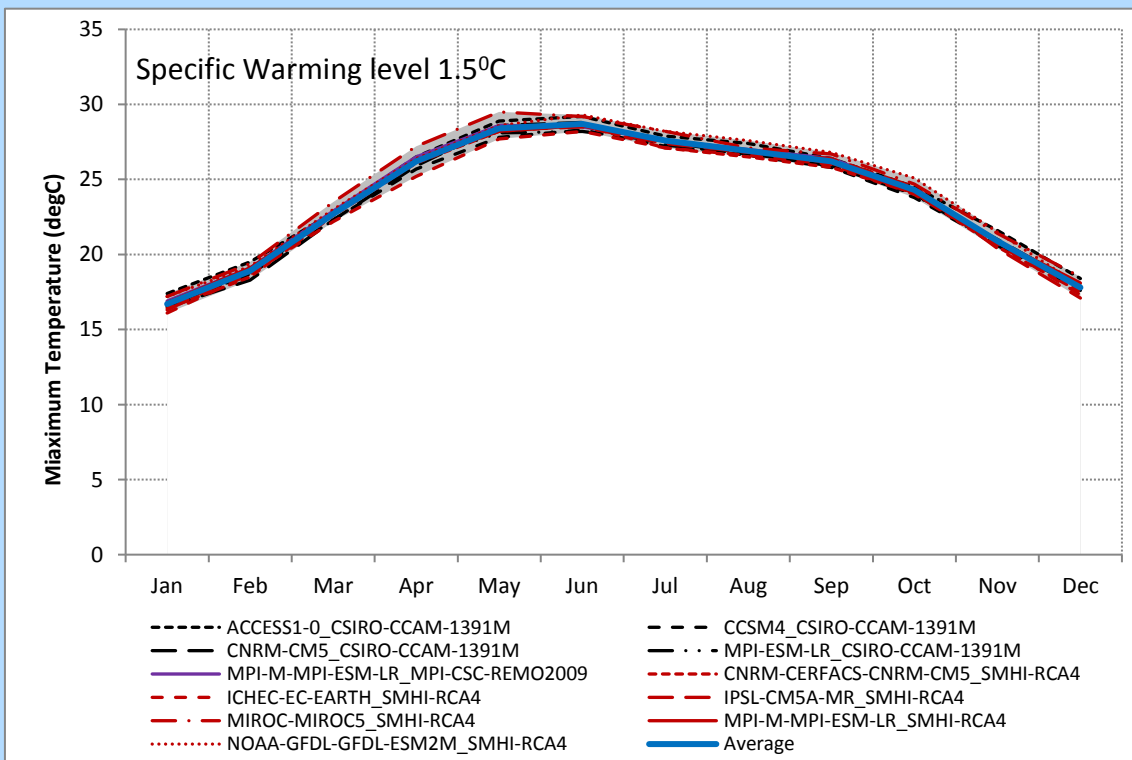
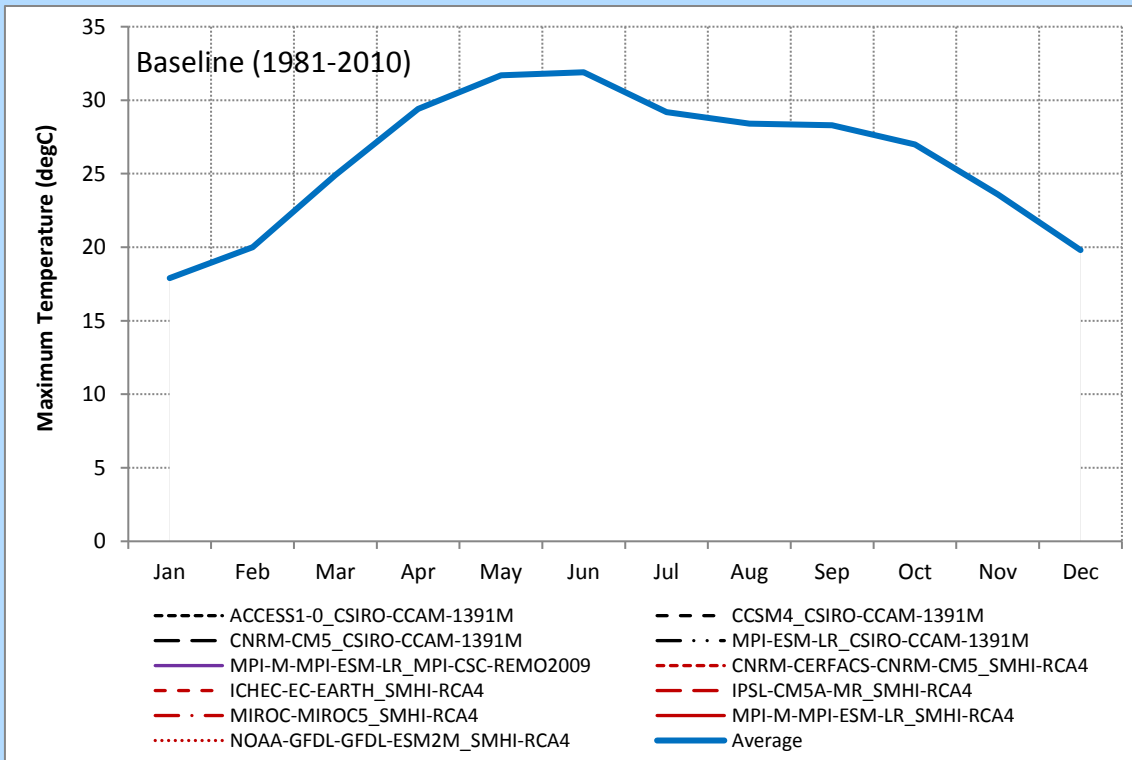
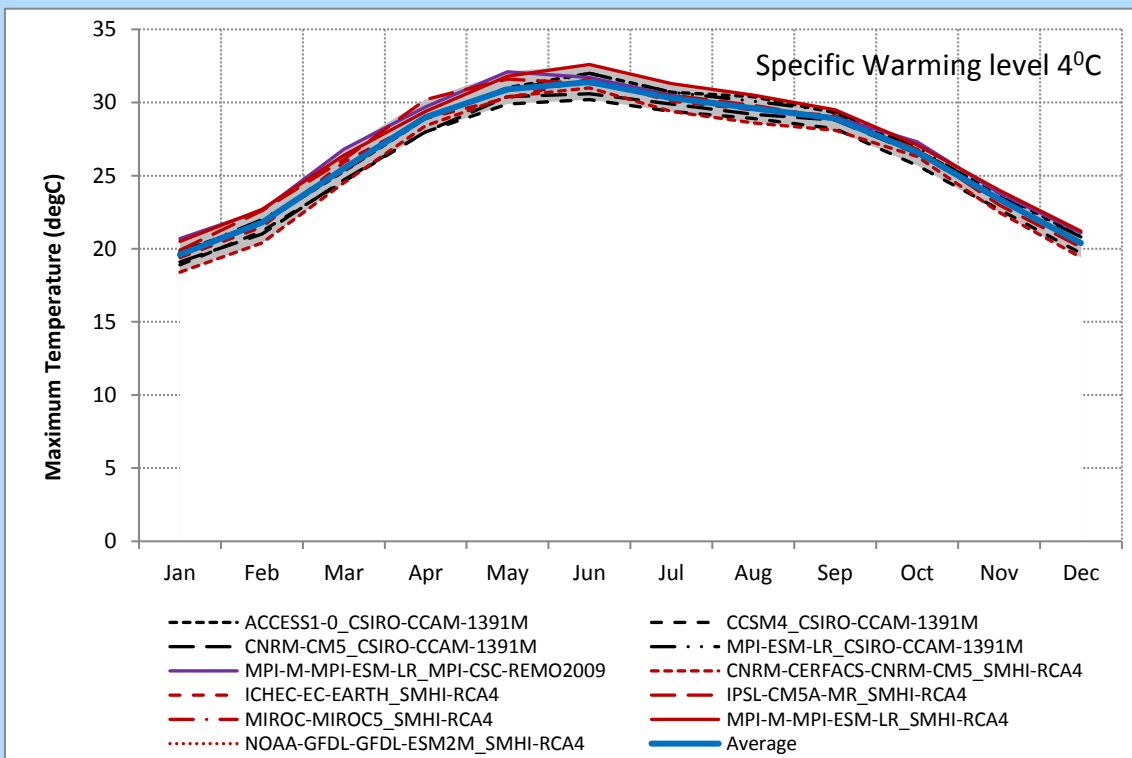
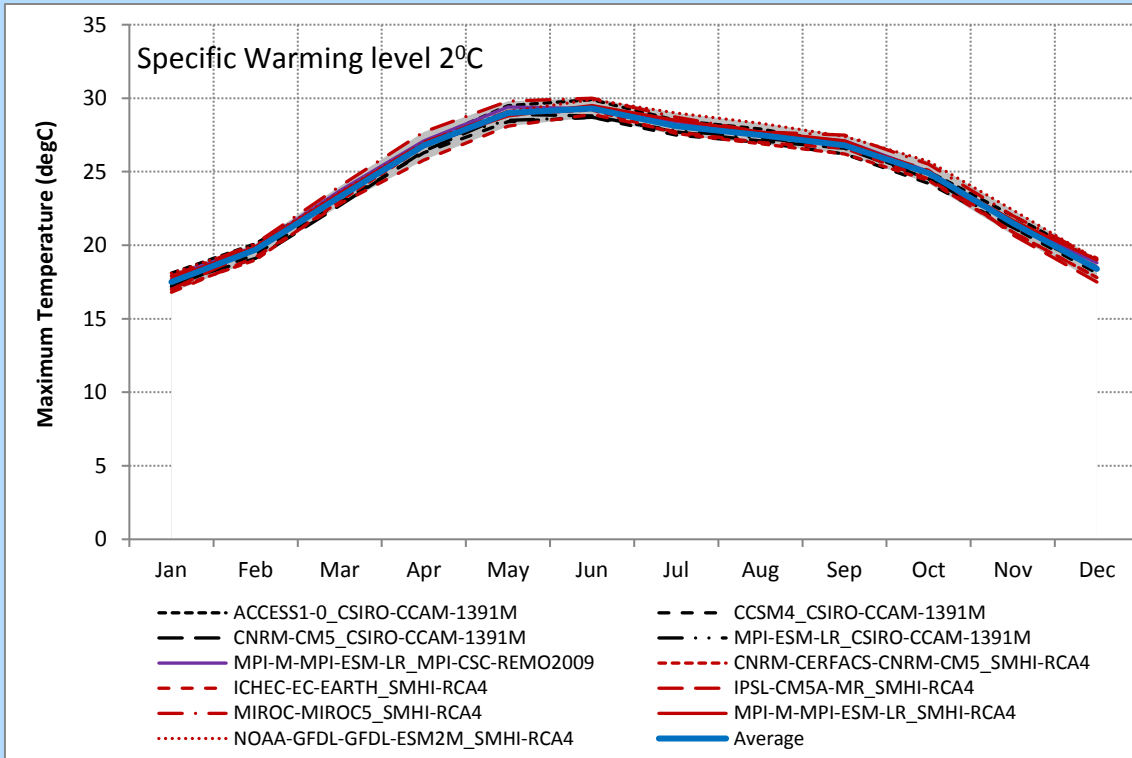


Figure 2 Projected long term monthly maximum temperature with uncertainty bands (ranges) for the Ganga basin - Baseline, RCP8.5 Scenario at specific global warming levels of SWL1.5, SWL2 and SWL4



Similarly, the Figure 3 presents the minimum monthly temperature for various models under baseline, Baseline, RCP8.5 Scenario for SWL1.5, SWL2 and SWL4. The minimum monthly temperature for all the

models for baseline scenario is the same for all the 11 models used which is expected because of the bias correction. There has been variation of up to 2.6°C in minimum temperature under SWL2 between the different models. The months of April, May, October and November show more variation in the minimum temperature than the other months. This spread appears to have further increased for SWL2.

Figure 3 Projected long term monthly minimum temperature with uncertainty bands (ranges) for the Ganga basin - Baseline, RCP8.5 Scenario for SWL1.5, SWL2 and SWL4

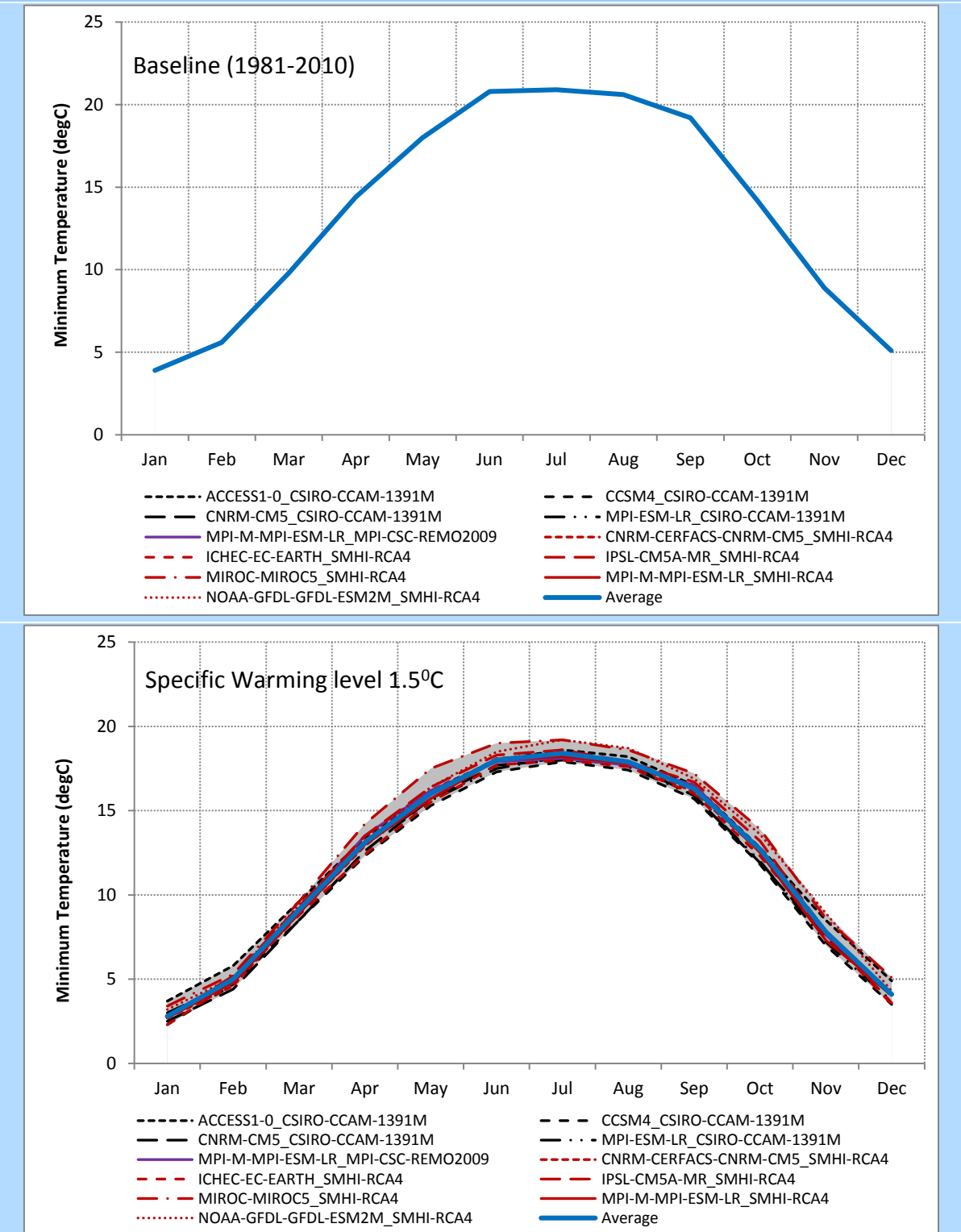
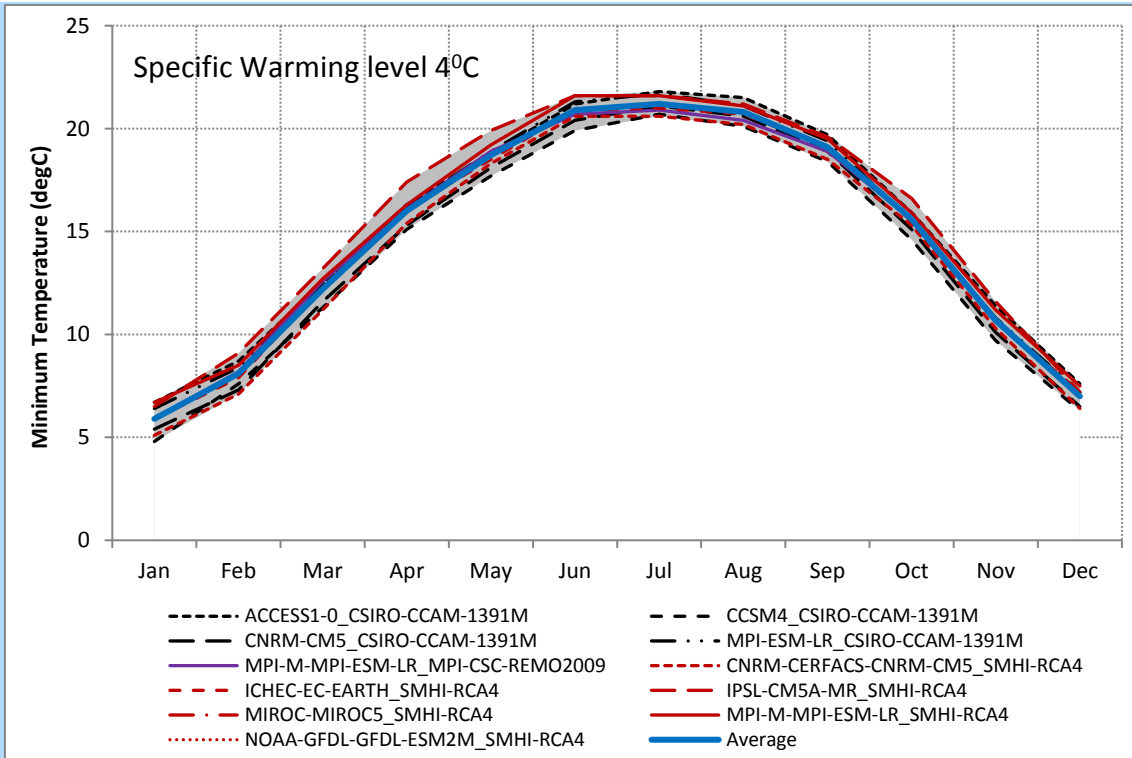
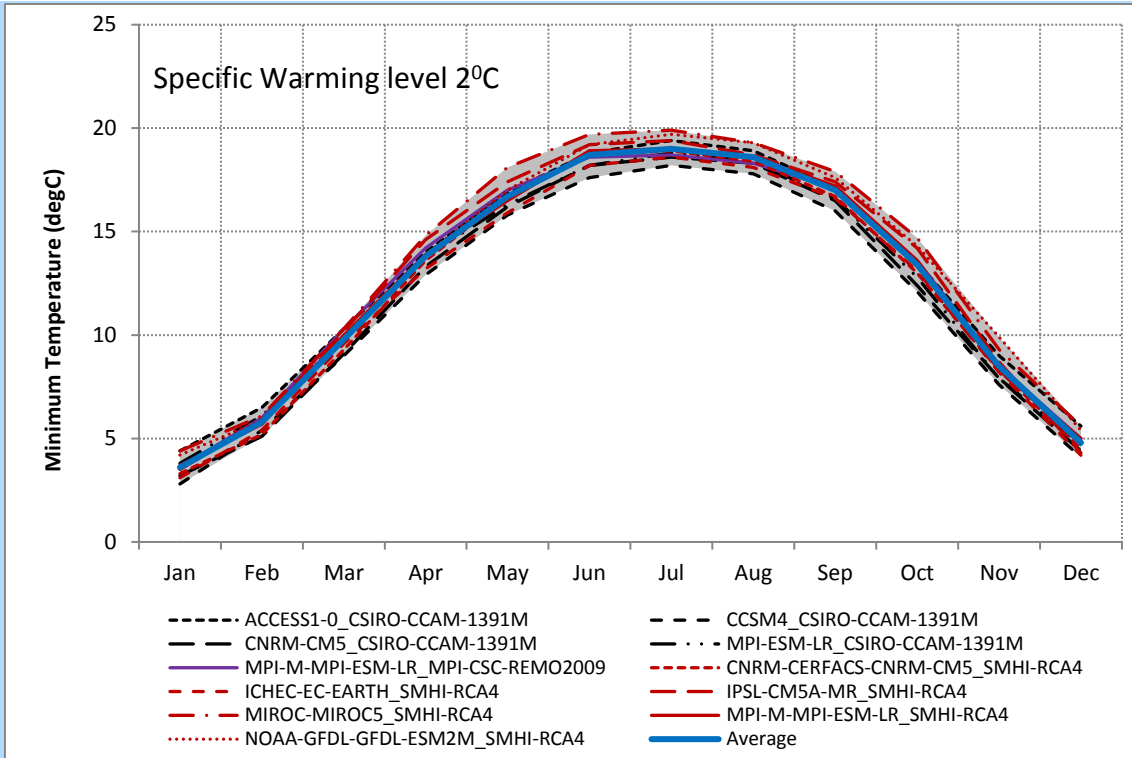
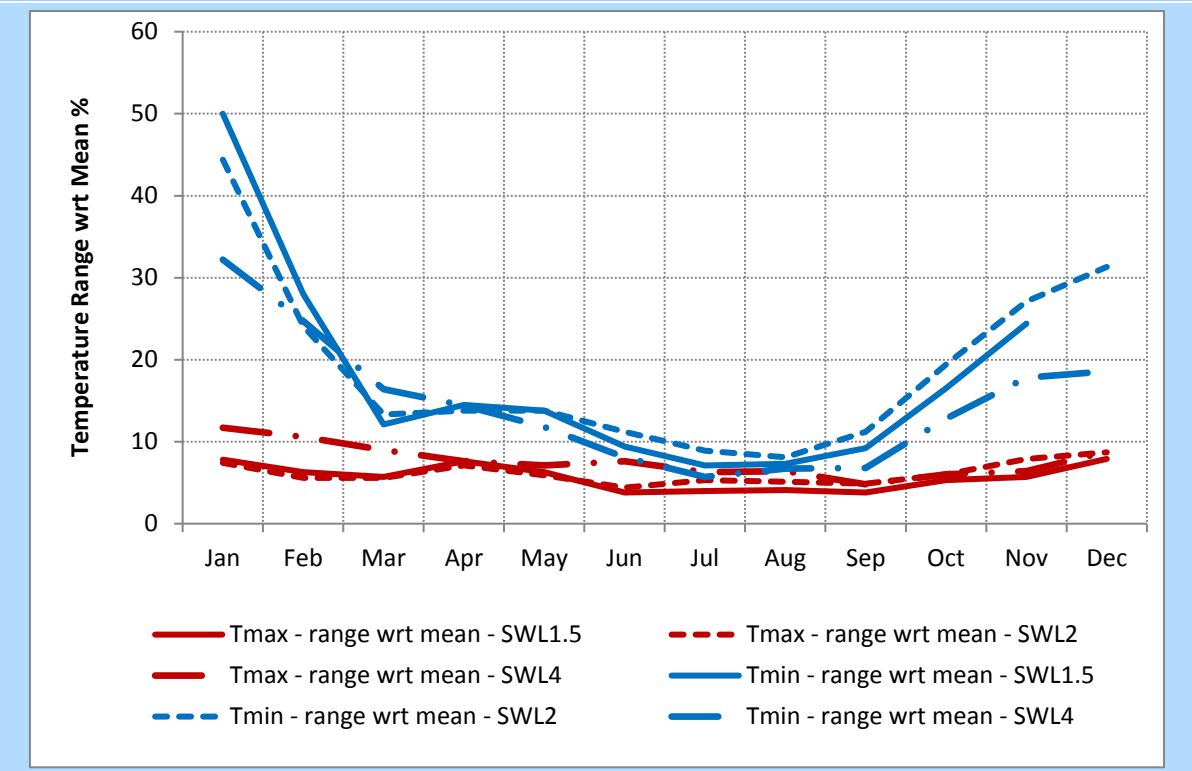


Figure 3 Projected long term monthly minimum temperature with uncertainty bands (ranges) for the Ganga basin - Baseline, RCP8.5 Scenario for SWL1.5, SWL2 and SWL4



The uncertainty between the models has also been depicted in Figure 4 by computing the multi model range relative to multi model mean for different months for maximum and minimum temperature under RCP8.5 scenario for SWL1.5, SWL2 and SWL4. It can be noted that the order of magnitude of variation between the minimum temperatures is much more in comparison to the maximum temperature. This trend is reversed only for the months of July and August under SWL4o. It may also be noticed that this range is highly pronounced during the months of January, February, October, November and December.

Figure 4 Multi model range relative to multi model mean for long term monthly temperature for the Ganga basin - Baseline, RCP8.5 Scenario for SWL1.5, SWL2 and SWL4



Similar analysis to depict the uncertainty in the precipitation has been performed and is depicted in Figure 5 for baseline, RCP8.5 Scenario at specific global warming levels of SWL1.5, SWL2 and SWL4 for different models. It may be noted that the long-term mean monthly precipitation for all the models for baseline scenario is the same but for the IPSL-CMSA-MR_SMHI-RCA4 model. There has been variation of close to 28 mm, 46 mm and 91 mm in monthly precipitation under SWL1.5, SWL2 and SWL4 respectively between the different models. The months of July and August show more variation in the monthly precipitation. This spread is further projected to increase under SWL4, where variation for the month of June has increased to about 43 mm. The maximum variation remains for the months of non monsoon months. Large variations in the model have been observed for SWL4 scenario.

Figure 5 Projected long term monthly precipitation with uncertainty bands (ranges) for the Ganga basin - Baseline, RCP8.5 Scenario for SWL1.5, SWL2 and SWL4

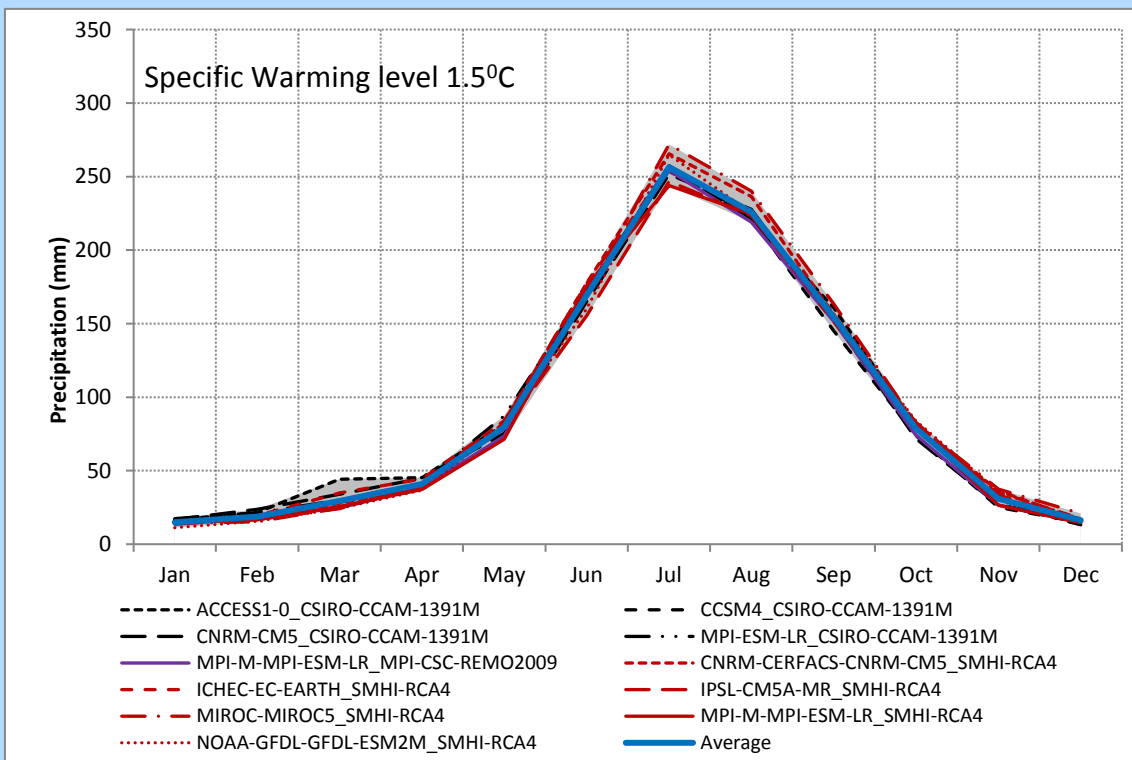
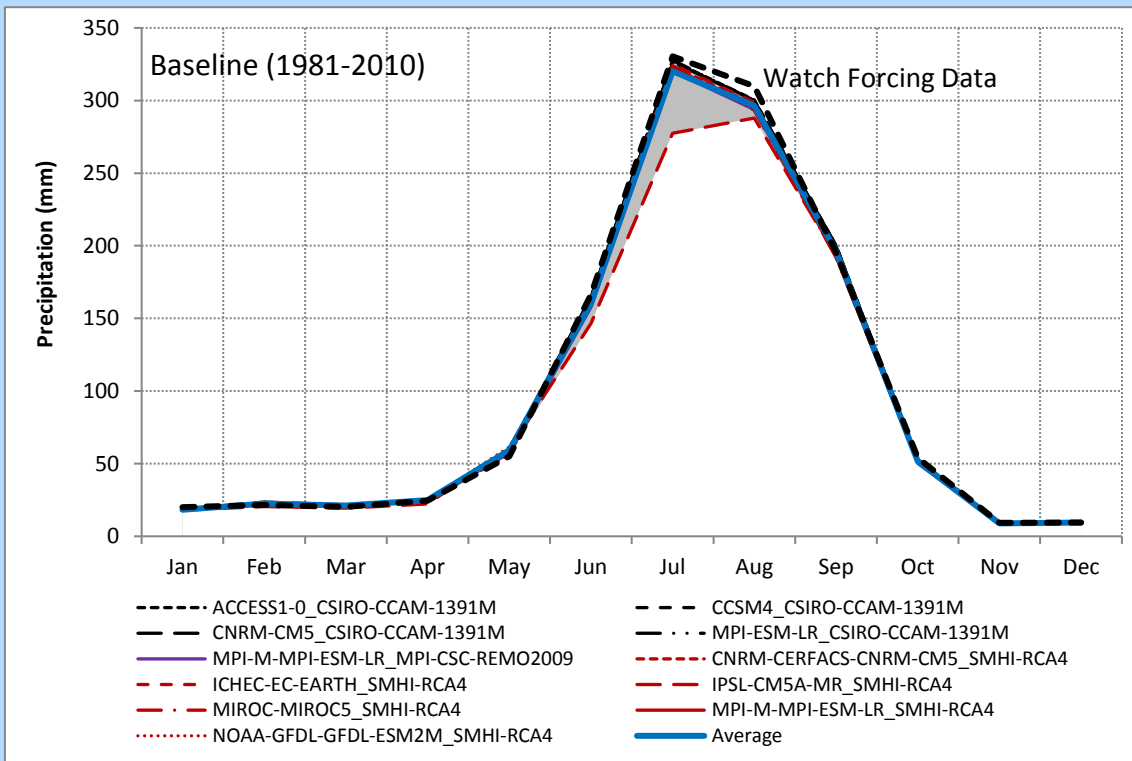
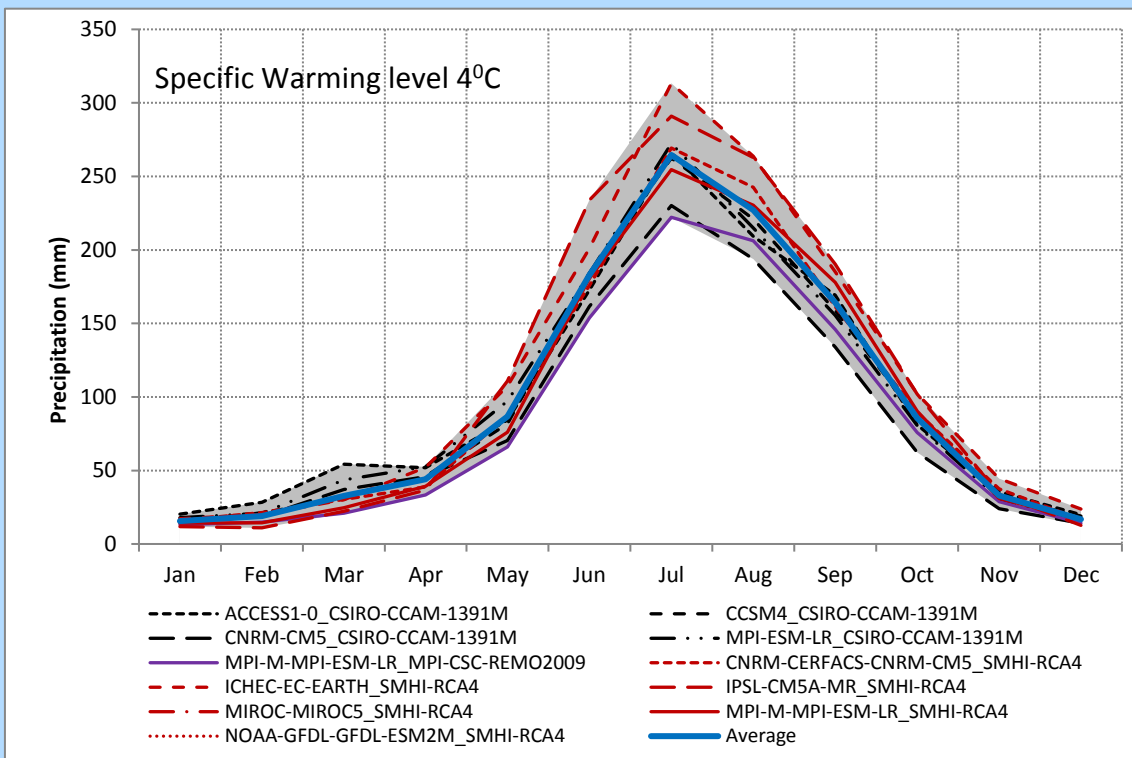
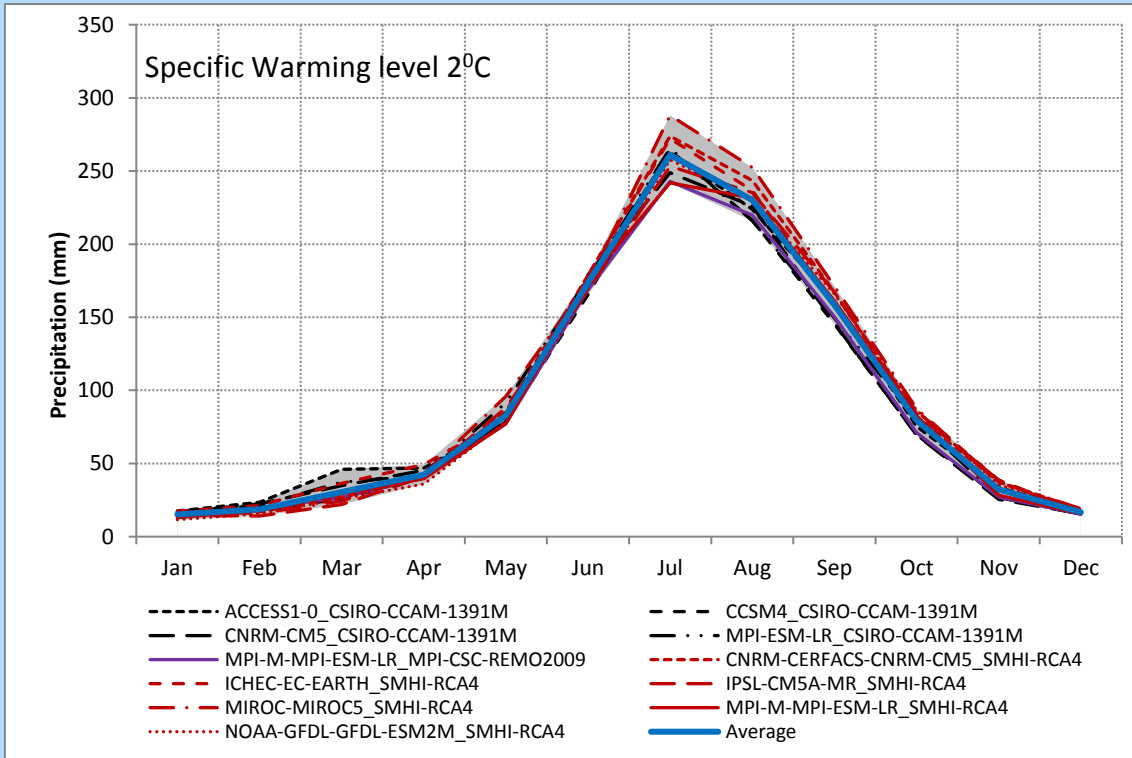
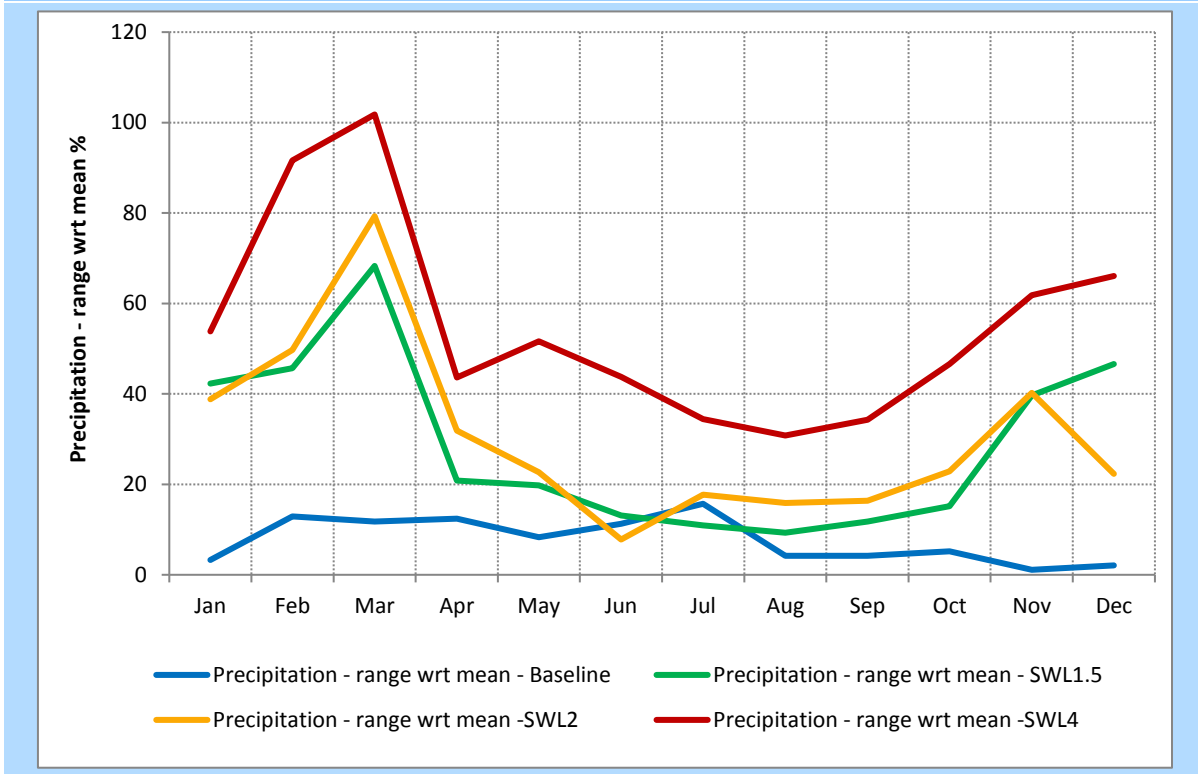


Figure 5 Projected long term monthly precipitation with uncertainty bands (ranges) for the Ganga basin - Baseline, RCP8.5 Scenario for SWL1.5, SWL2 and SWL4



The uncertainty across the models for precipitation has also been depicted in Figure 6 by computing the multi model range relative to multi model mean for different months for precipitation under baseline, RCP8.5 scenario for SWL1.5, SWL2 and SWL4. It can be noted that the order of magnitude of variation in the projected precipitation is the maximum for SWL4.

Figure 6 Multi model range relative to multi model mean for long term monthly precipitation for the Ganga basin - Baseline, RCP8.5 Scenario for SWL1.5, SWL2 and SWL4



It may also be noticed that the variation is maximum for the non-monsoon months when the magnitude of precipitation is very small. However, for the monsoon months also this variation ranges from 20% to 43% for SWL4 scenario and from 10% to 12% for SWL2 scenario. All these inputs are potential sources of uncertainties in the impact assessment.

Change in Water Balance Components

The present segment of the study is aimed at quantifying the impacts of climate change on the water resources of the Ganga Basin using the hydrological simulation methodology. The well known distributed hydrological model SWAT has been deployed for the purpose. Scenarios have been generated for assessing implications on quantity of water on account of various climate change scenarios.

The hydrological model has been run using climate scenarios for SWLs with the assumption that the land use is not changing over time. The hydrological simulations are run with 11 high resolution RCM models (Table 1), and for 3 SWLs (1.5°C, 2°C and 4°C) for RCP scenarios 8.5 (bias corrected). Thus the number of hydrological model simulations carried out was 44 simulations, including baseline for the Ganga basin.

Two important water balance components i.e., water yield and evapotranspiration have been taken to quantify the change in these components under RCP8.5 scenario for SWL1.5, SWL2 and SWL4 scenarios with respect to the baseline scenario for each of the 11 identified models of RCP8.5 and have been presented in Figure 7. It may be observed that there is a considerable variation in the water yield and evapotranspiration between the models. There are models that are showing general increase in the water yield under SWL1.5 scenario whereas there are models that are showing considerable decrease in under the same scenario. Large spatial variation in water yield can be seen is several models. REMO2009 and SMHI-RCA4 RCM models with MPI GCM forcing show dry bias and CCAM 1391 shows wet bias under Access and CCSM4 GCM forcing. However, under SWL4 scenario most of the models are showing significant increase in water yield except for REMO2009 and SMHI-RCA4 RCM models with MPI GCM forcing.

With respect to the evapotranspiration most of the models depict marginal to no change in the evapotranspiration under SWL1.5 and SWL2, however under SWL4 reduction in evapotranspiration is projected. The outcome on the evapotranspiration is quite complex since there are so many factors such as temporal distribution of precipitation, CO₂ level, temperature, wind velocity, landuse etc., that affect the evapotranspiration.

Figure 7 Projected change in annual stream flow and evapotranspiration for the Ganga basin

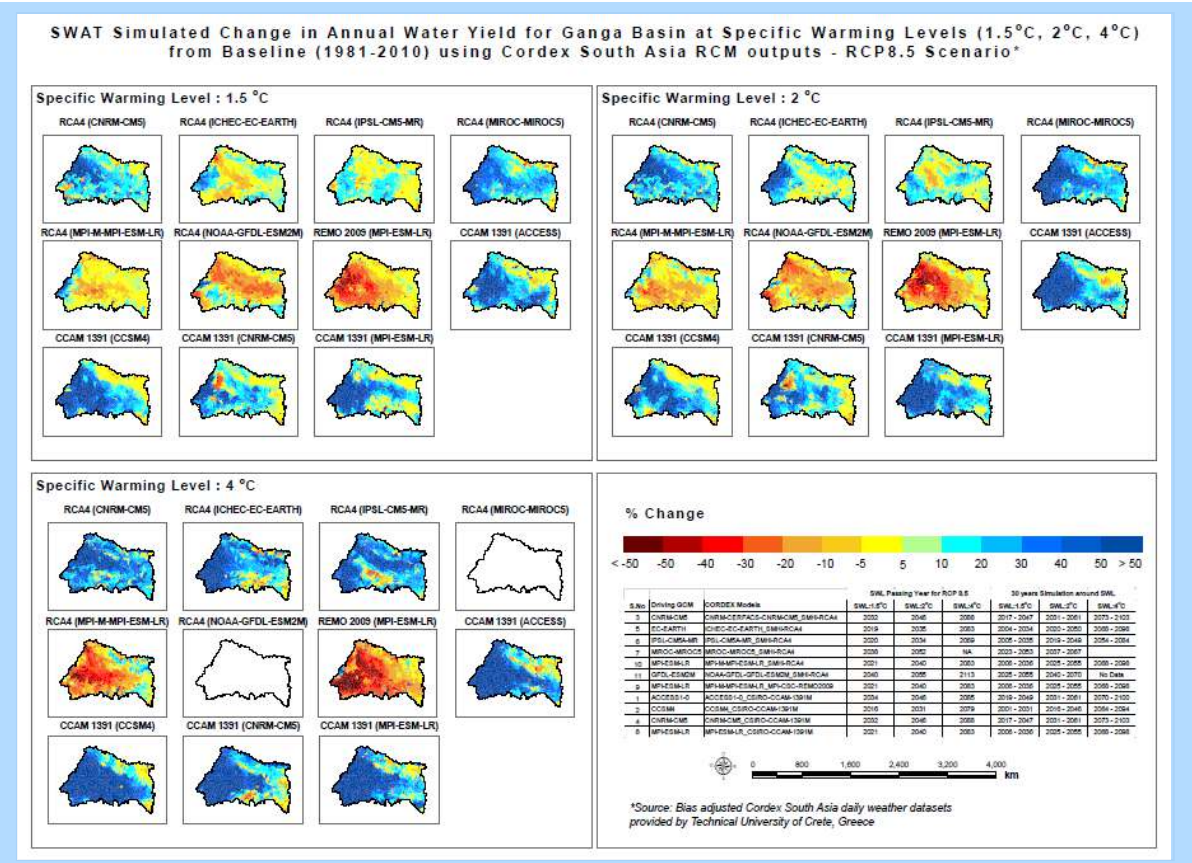


Figure 7 Projected change in annual stream flow and evapotranspiration for the Ganga basin

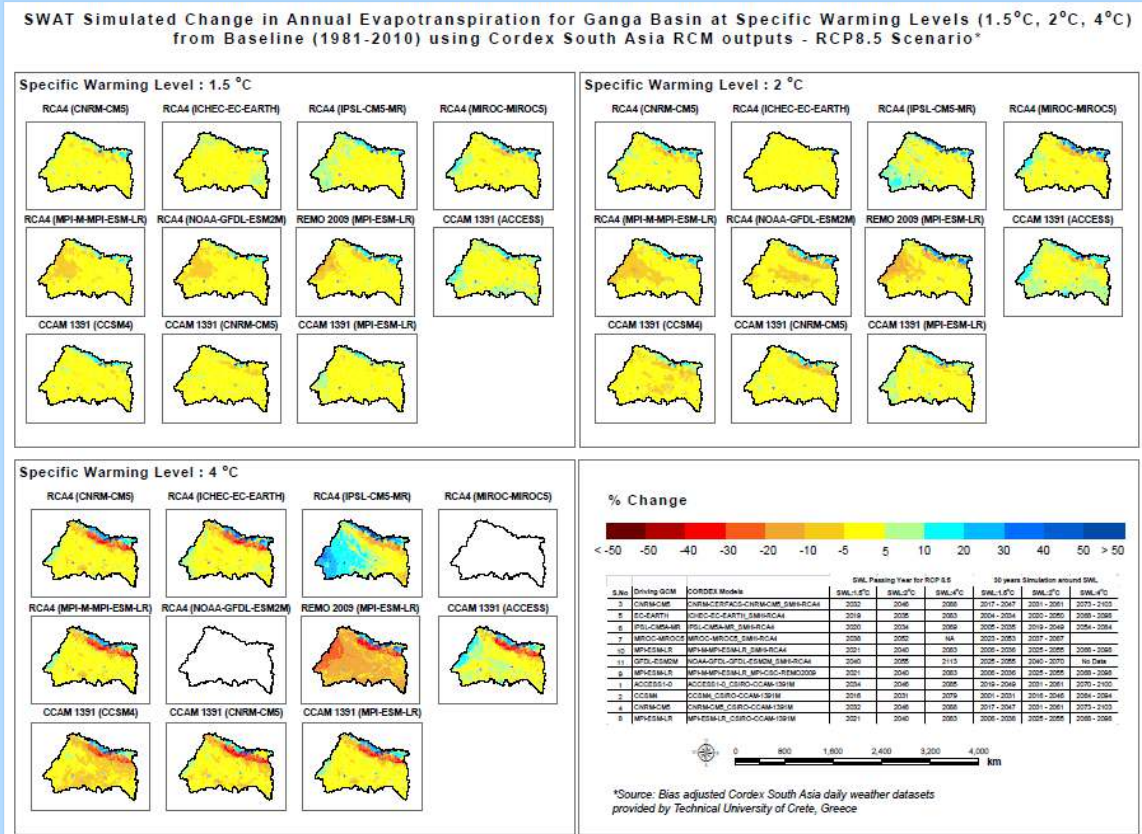


Figure 8 shows long term precipitation, stream flow and evapotranspiration for the entire Ganga basin for 11 Cordex models.

Figure 8 Projected long term annual precipitation, stream flow and evapotranspiration for multi models for the Ganga basin - Baseline, RCP8.5 Scenario for SWL1.5, SWL2 and SWL4

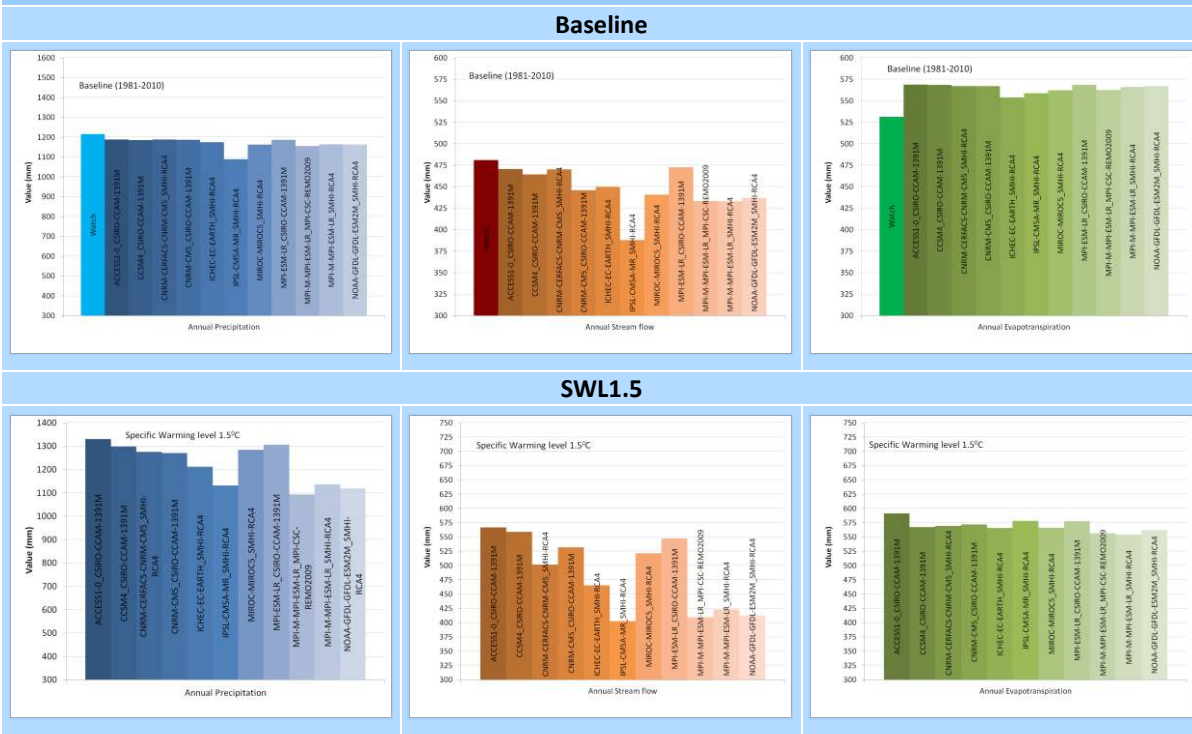
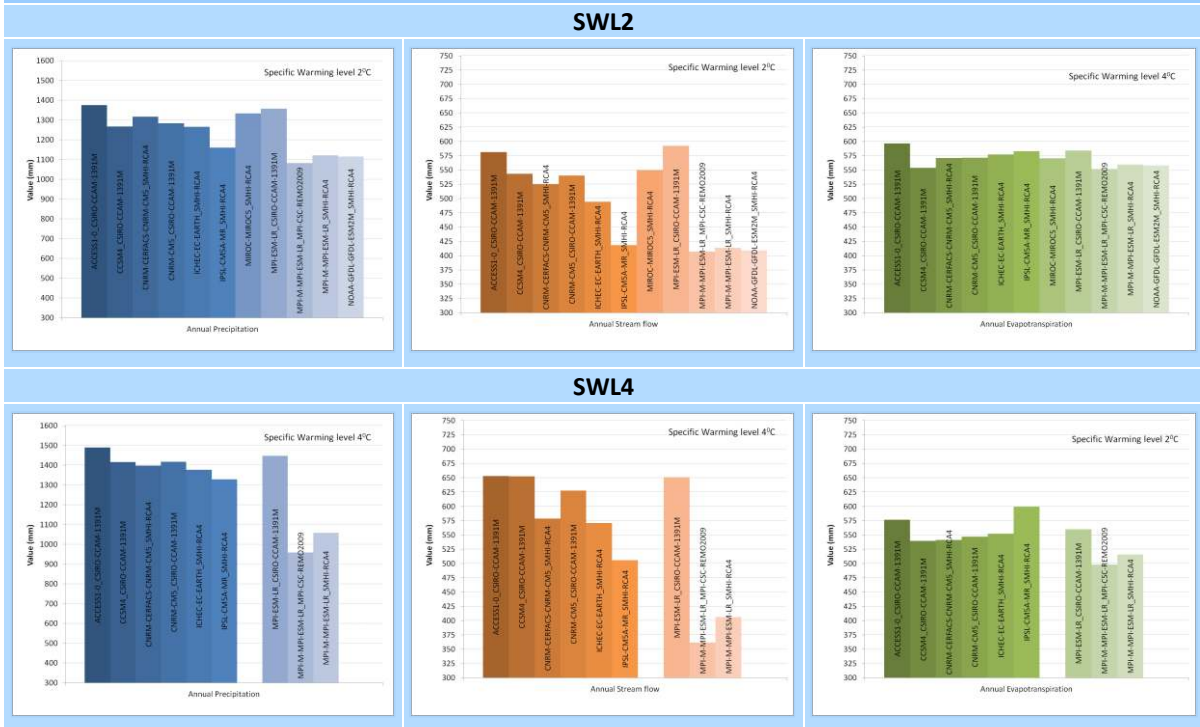


Figure 8 Projected long term annual precipitation, stream flow and evapotranspiration for multi models for the Ganga basin - Baseline, RCP8.5 Scenario for SWL1.5, SWL2 and SWL4



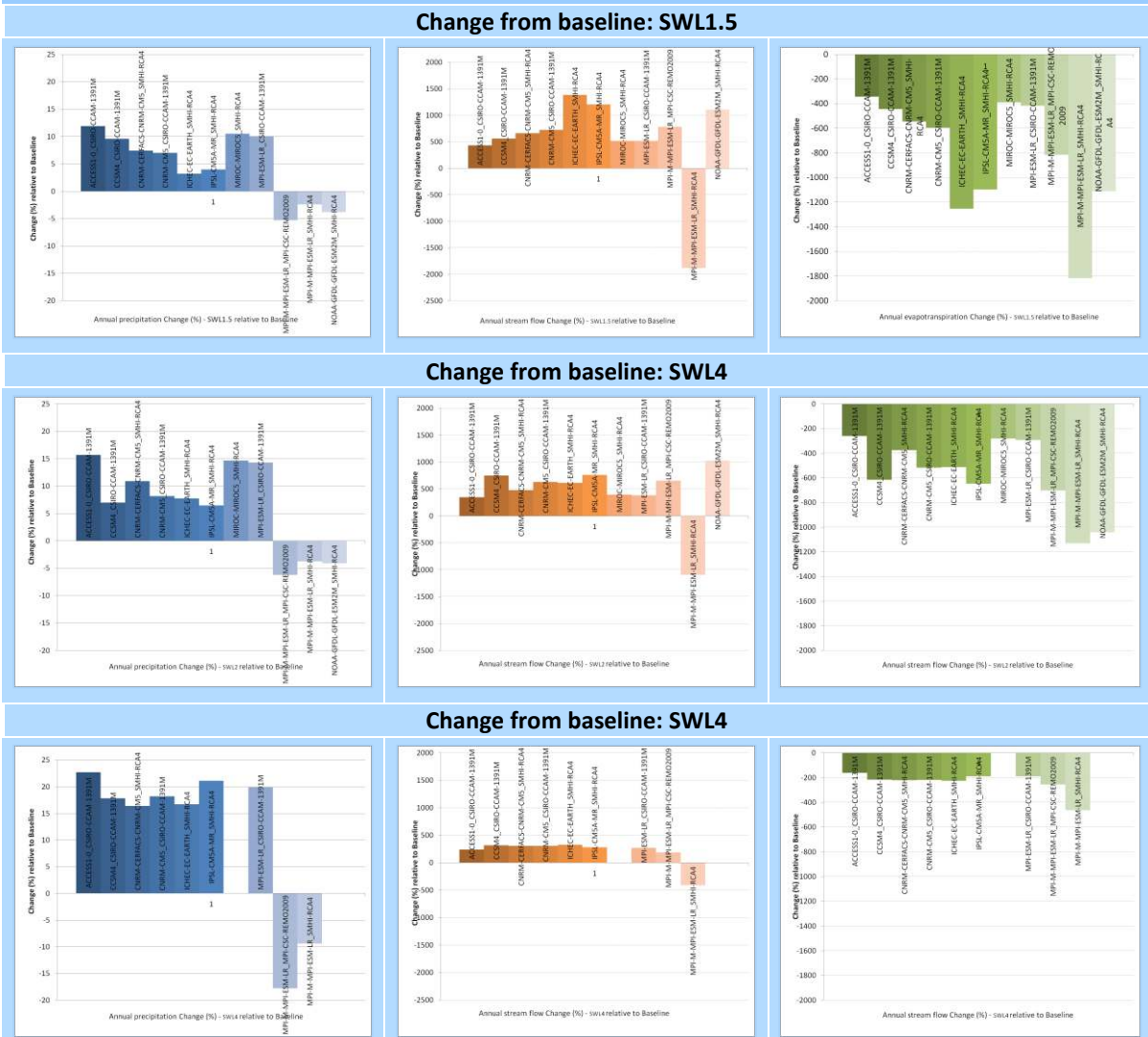
Model sequence

1. ACCESS1-0_CSIRO-CCAM-1391M,
2. CCSM4_CSIRO-CCAM-1391M,
3. CNRM-CERFACS-CNRM-CM5_SMHI-RCA4,
4. CNRM-CM5_CSIRO-CCAM-1391M,
5. ICHEC-EC-EARTH_SMHI-RCA4,
6. IPSL-CM5A-MR_SMHI-RCA4,
7. MIROC-MIROC5_SMHI-RCA4,
8. MPI-ESM-LR_CSIRO-CCAM-1391M,
9. MPI-M-MPI-ESM-LR_MPI-CSC-REMO2009,
10. MPI-M-MPI-ESM-LR_SMHI-RCA4,
11. NOAA-GFDL-GFDL-ESM2M_SMHI-RCA4

Baseline results are depicted with model run using WATCH reanalysis data to compare the inter model difference in reproducing the current conditions. It can be seen from the figure that simulated evapotranspiration is higher by 30 to 40 mm in all 11 models. All models except IPSL-CM5A-MR_SMHI-RCA4 replicate the current precipitation amount well. Uncertainty increases towards SWL2 and SWL4, especially in MPI-M-MPI-ESM-LR_MPI-CSC-REMO2009, MPI-M-MPI-ESM-LR_SMHI-RCA4 and NOAA-GFDL-GFDL-ESM2M_SMHI-RCA4 models.

Figure 9 shows change in stream flow and evapotranspiration as percentage of the change in precipitation. As it can be seen that increase (or decrease) in water balance components is not directly proportional to increase (or decrease) in precipitation.

Figure 9 Projected change in long term annual precipitation, stream flow and evapotranspiration relative to baseline for multi models for the Ganga basin - Baseline, RCP8.5 Scenario for SWL1.5, SWL2 and SWL4

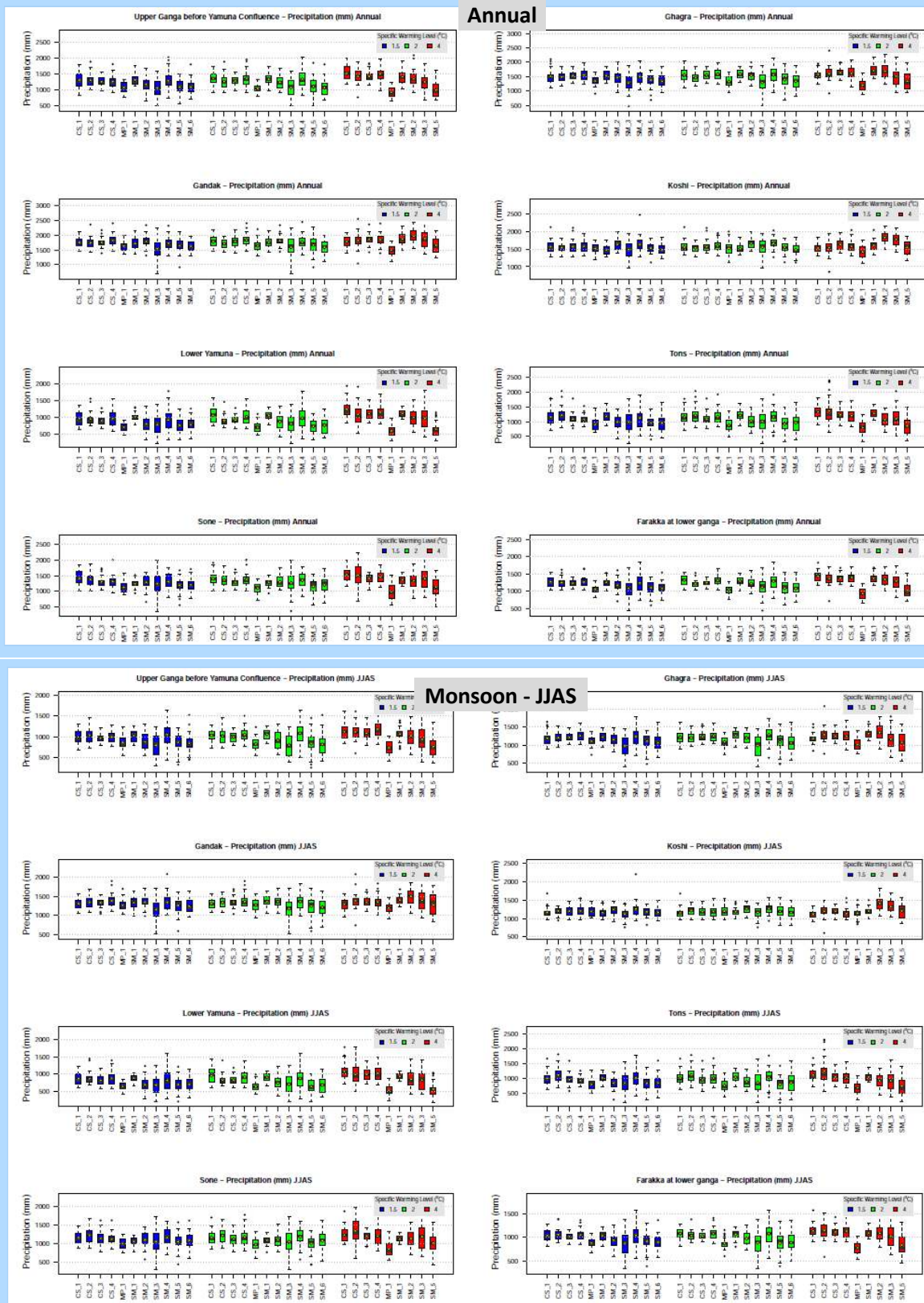


Model sequence

1. ACCESS1_0_CSIRO-CCAM-1391M, 2. CCSM4_CSIRO-CCAM-1391M, 3. CNRM-CERFACS-CNRM-CM5_SMHI-RCA4,
4. CNRM-CM5_CSIRO-CCAM-1391M, 5. ICHEC-EC-EARTH_SMHI-RCA4, 6. IPSL-CM5A-MR_SMHI-RCA4,
7. MIROC-MIROC5_SMHI-RCA4, 8. MPI-ESM-LR_CSIRO-CCAM-1391M, 9. MPI-M-MPI-ESM-LR_MPI-CSC-REMO2009,
10. MPI-M-MPI-ESM-LR_SMHI-RCA4, 11. NOAA-GFDL-GFDL-ESM2M_SMHI-RCA4

Figure 10 shows comparison of model response to precipitation on water balance components for entire Ganga basin as box plots.

Figure 10 Annual water balance components simulated using multiple CORDEX RCM models for the Ganga basin



It can be seen that the uncertainties between models increase towards SWL2 and SWL4 scenarios. MPI-M-MPI-ESM-LR_MPI-CSC-REMO2009 shows different distribution as compared to other models.

Change in Extremes

The outputs from the hydrological model have been used to assess the impact of the climate change on the river basins in terms of occurrence of droughts and floods. The rainfall, runoff and actual evapotranspiration have been selected from the available model output since they mainly govern the two extreme impacts due to climate change, namely droughts and floods.

Drought Analysis

Drought indices are widely used for the assessment of drought severity by indicating relative dryness or wetness effecting water sensitive economies.

Soil moisture index developed (Narasimhan and Srinivasan, 2005³) to monitor drought severity using SWAT output to incorporate the spatial variability has been used in the present study to focus on the agricultural drought where severity implies cumulative water deficiency. Weekly information has been derived using daily SWAT outputs which in turn have been used for subsequent analysis of drought severity.

The severity of droughts effects is proportional to the relative change in climate. For example, if a climate that usually has very slight deviations from the normal experiences a moderate dry period, the effects would be quite dramatic. On the other hand, a very dry period would be needed in a climate that is used to large variations to produce equally dramatic effects. In the current context scale 1 (Index between 0 to -1) represent the drought developing stage and scales 2 (Index between -1 to -4) represent mild to moderate and extreme drought condition. Higher water stress conditions may call for additional irrigation supplies for agriculture.

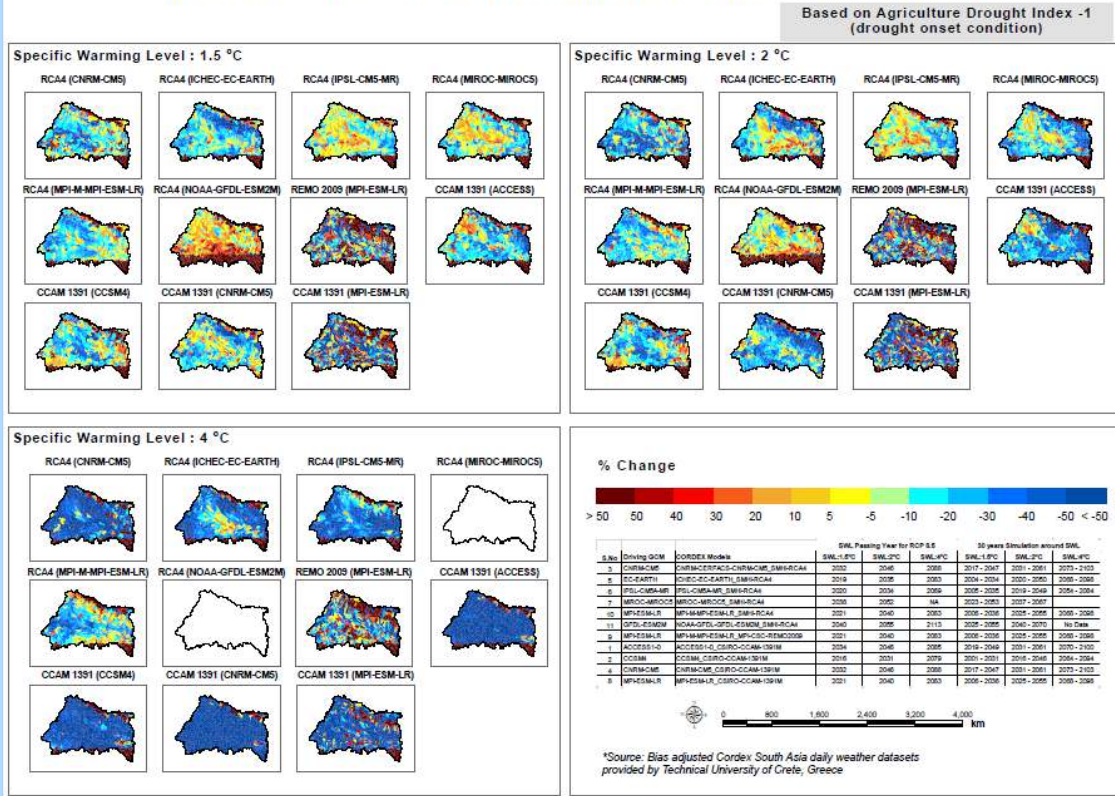
Figure 11 depicts the change in drought conditions under two scales as discussed above. There is a large spatial variation between models under scale 1 for RCP8.5 Scenario at specific global warming levels of SWL1.5, SWL2 and SWL4. Most of the models show decrease in drought onset conditions under SWL4 except for MPI-M-MPI-ESM-LR_MPI-CSC-REMO2009 and MPI-M-MPI-ESM-LR_SMHI-RCA4 models. Similar variations are seen under moderate to sever drought conditions in these two models (increase) while rest of the models show decrease in drought events. However, situation is likely to become better for SWL4 scenario for most of the models.

Figure 12 shows comparison of model response to drought conditions for entire Ganga basin as box plots. Uncertainty in models is higher under SWL4 scenario.

³ Narasimhan, B. and Srinivasan, R., 2005. Development and evaluation of Soil Moisture Deficit Index (SMDI) and Evapotranspiration Deficit Index (ETDI) for agricultural drought monitoring, Agricultural and Forest Meteorology 133 (2005) 69–88

Figure 11 Projected change in extreme weather event - Drought for the Ganga basin

Percentage Change in Monsoon Drought Weeks for Ganga Basin at Specific Warming Levels (1.5°C, 2°C, 4°C) from Baseline (1981-2010) using Cordex South Asia RCM outputs - RCP8.5 Scenario*



Percentage Change in Monsoon Drought Weeks for Ganga Basin at Specific Warming Levels (1.5°C, 2°C, 4°C) from Baseline (1981-2010) using Cordex South Asia RCM outputs - RCP8.5 Scenario*

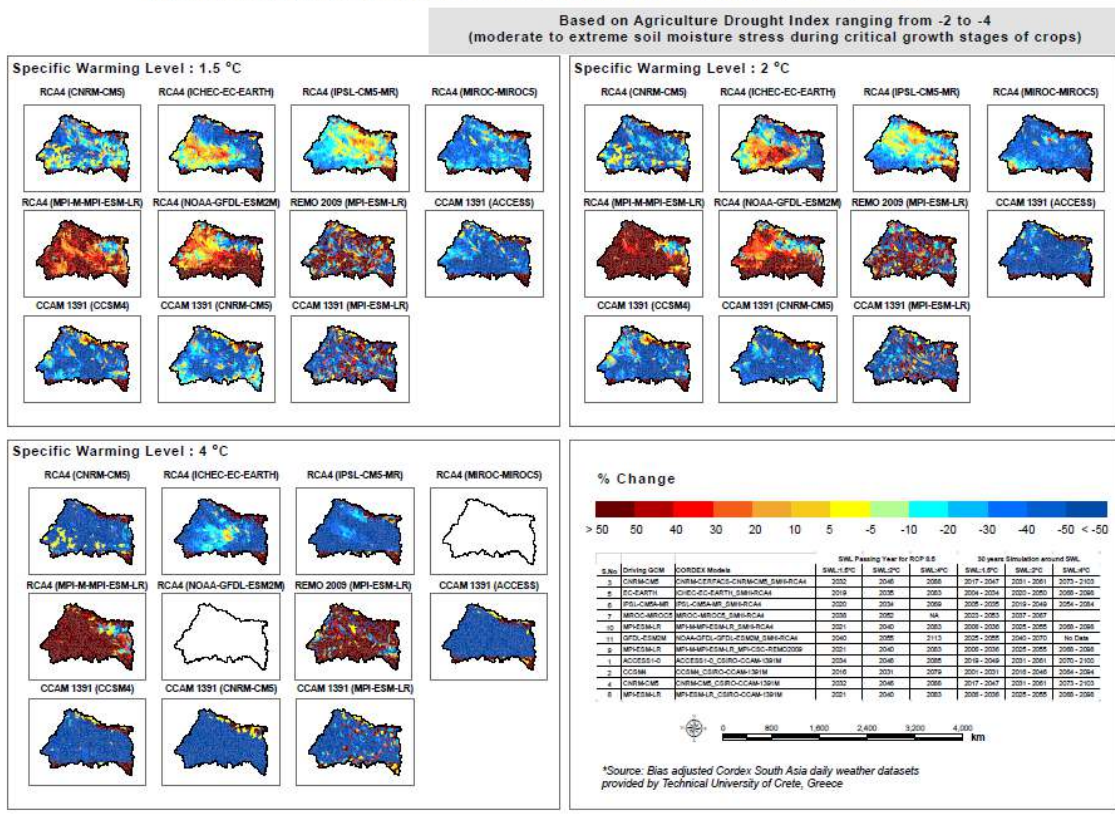
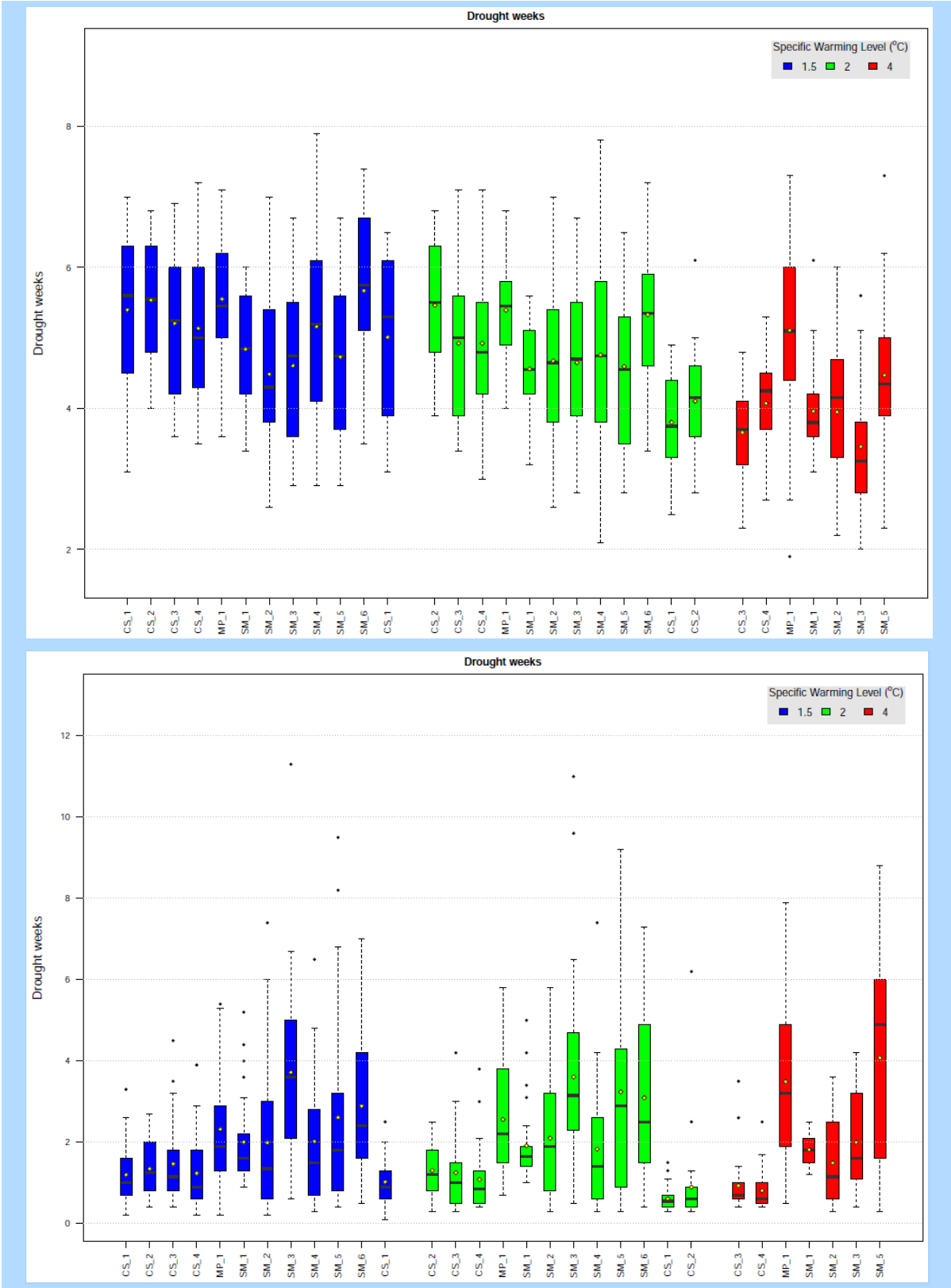


Figure 12 Boxplot of Projected change in extreme weather event - Drought for the Ganga basin

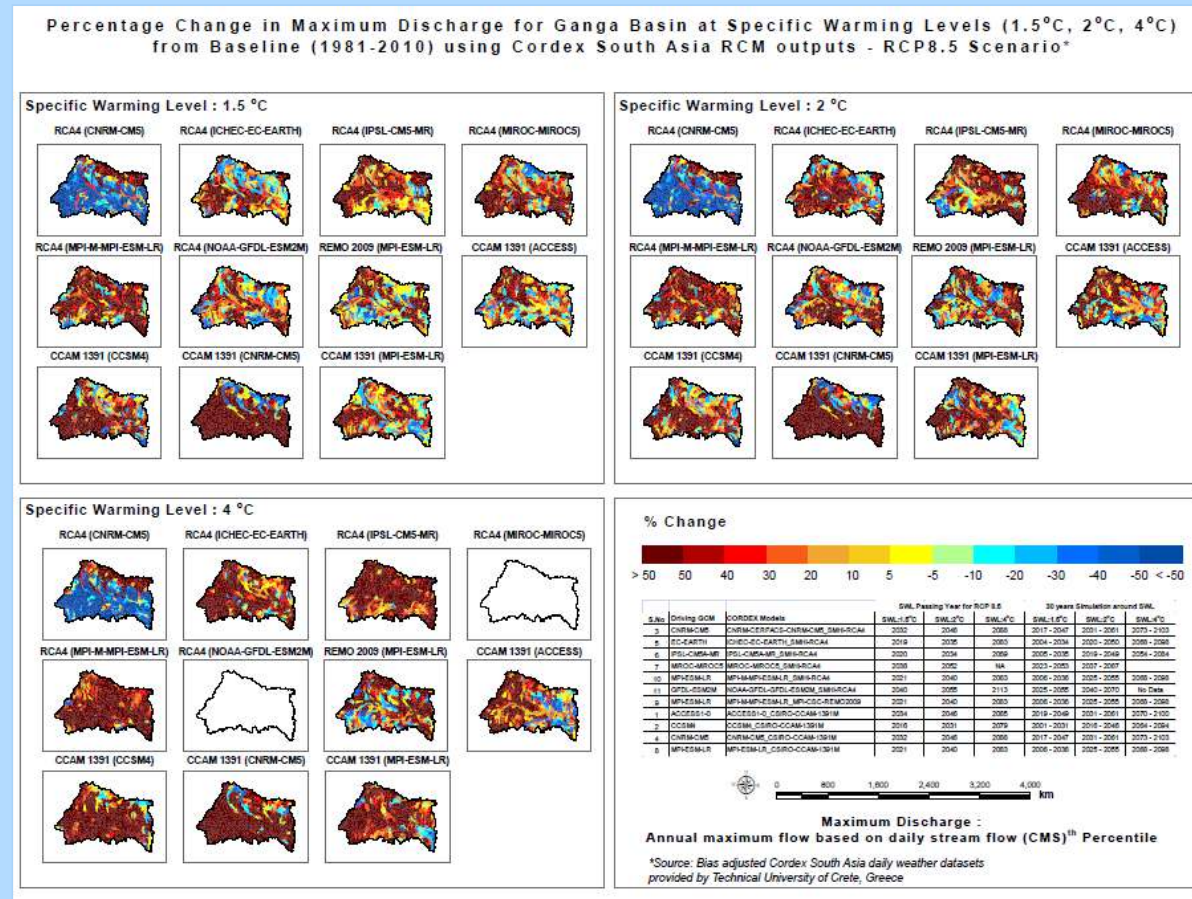


Model Code: ACCESS1-0_CSIRO-CCAM-1391M:CS_1, CCSM4_CSIRO-CCAM-1391M:CS_2, CNRM-CERFACS-CNRM-CM5_SMHI-RCA4:SM_1, CNRM-CM5_CSIRO-CCAM-1391M:CS_3, ICHEC-EC-EARTH_SMHI-RCA4:SM_2, IPSL-CM5A-MR_SMHI-RCA4:SM_3, MIROC-MIROC5_SMHI-RCA4:SM_4, MPI-ESM-LR_CSIRO-CCAM-1391M:CS_4, MPI-M-MPI-ESM-LR_MPI-CSC-REMO2009:MP_1, MPI-M-MPI-ESM-LR_SMHI-RCA4:SM_5, NOAA-GFDL-GFDL-ESM2M_SMHI-RCA4:SM_6

Peak Discharge Analysis

Projected change in peak stream flow floods has been carried out using the daily outflow discharge taken for each sub-basin from the SWAT output. These discharges have been analysed with respect to the maximum annual peaks. Figure 13 depicts peak discharge.

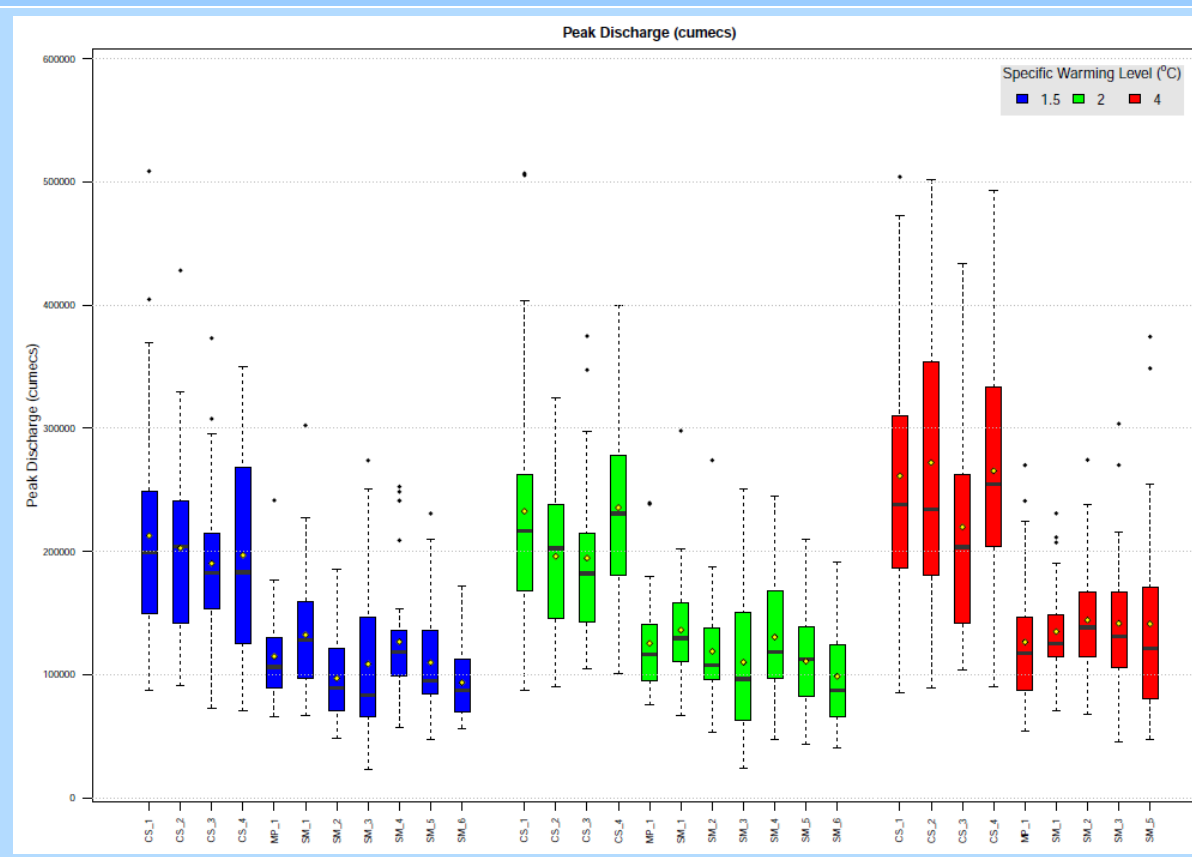
Figure 13 Projected change in extreme weather event - Peak discharge at Farakka for the Ganga basin



There is a good agreement between the models on the magnitude of peak discharge for all specific warming levels.

Figure 14 shows comparison of model response to flood conditions for entire Ganga basin as box plots. Uncertainty in models is higher under SWL4 scenario.

Figure 14 Boxplot of Projected change in extreme weather event - Peak discharge for the Ganga basin



Change in Crop Growth

Change in crop growth has been analysed based on average crop yield, evapotranspiration and amount of irrigation applied. Change in water productivity (crop yield per cubic metre of water consumption from rainfed and irrigated agriculture) has been calculated using average crop yield (rice and wheat) and evapotranspiration. Figure 15 shows the change in water productivity and additional irrigation water requirement for SWL1.5, SWL2 and SWL4 respectively relative to baseline condition. MPI-M-MPI-ESM-LR_MPI-CSC-REMO2009 and NOAA-GFDL-GFDL-ESM2M_SMHI-RCA4 show marginal decrease in productivity and decrease in additional irrigation requirement. This may be attributed to early maturity of crops due to higher temperature.

Figure 15 Projected change in crop water productivity and additional irrigation requirement - Ganga basin

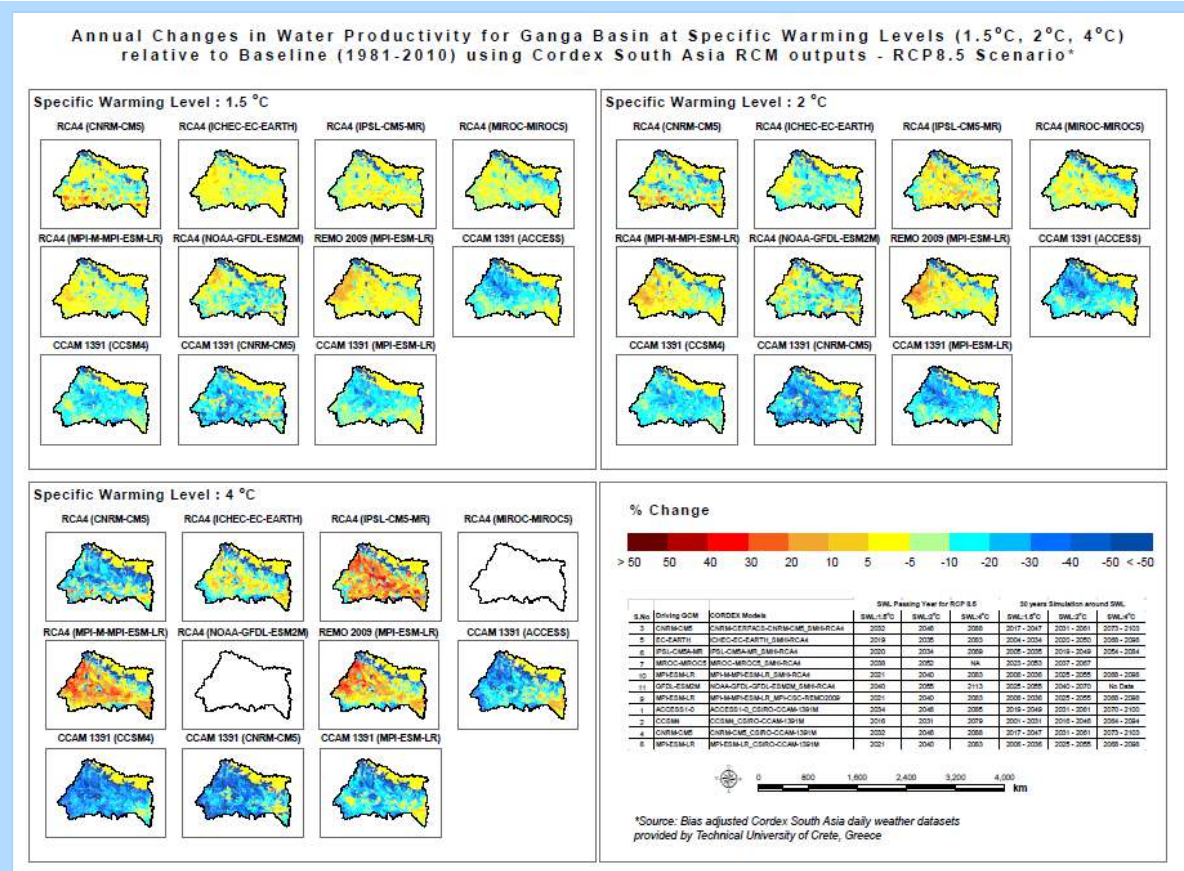
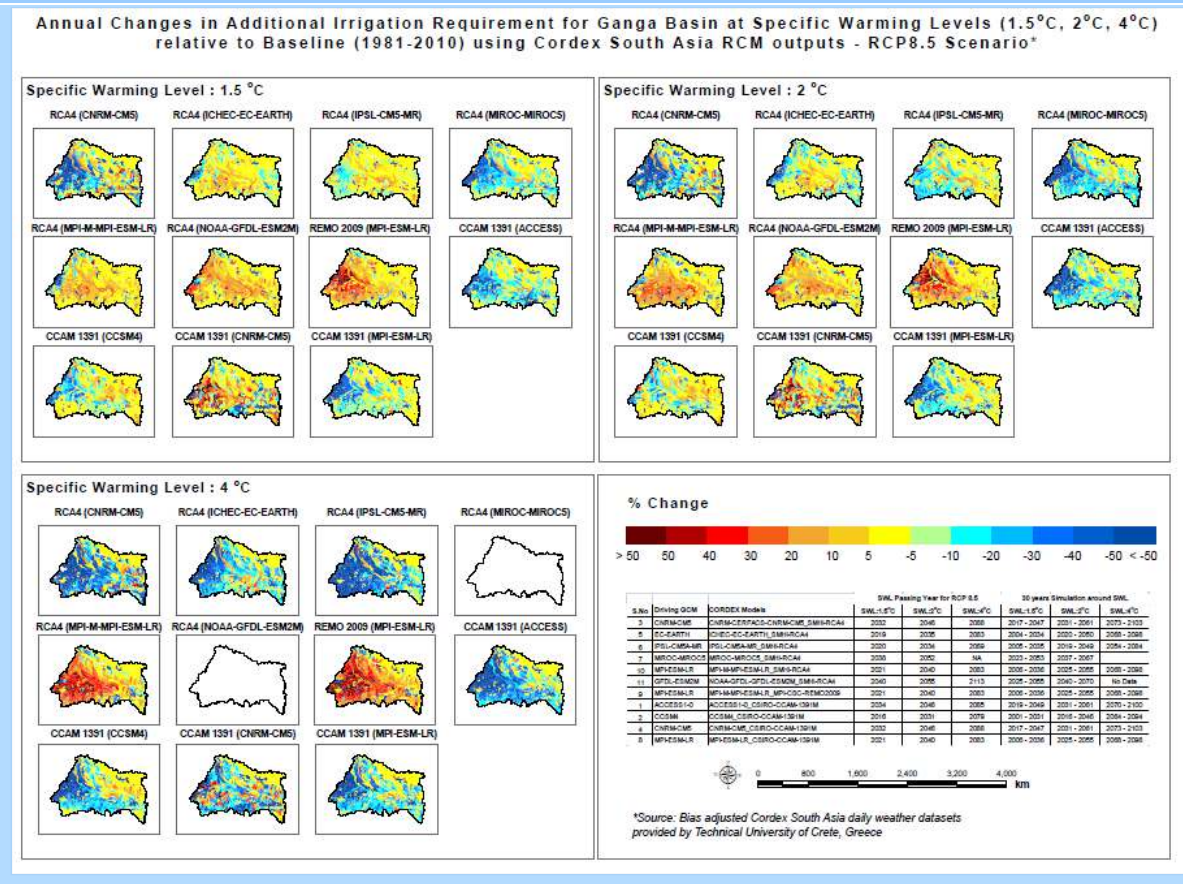


Figure 15 Projected change in crop water productivity and additional irrigation requirement - Ganga basin

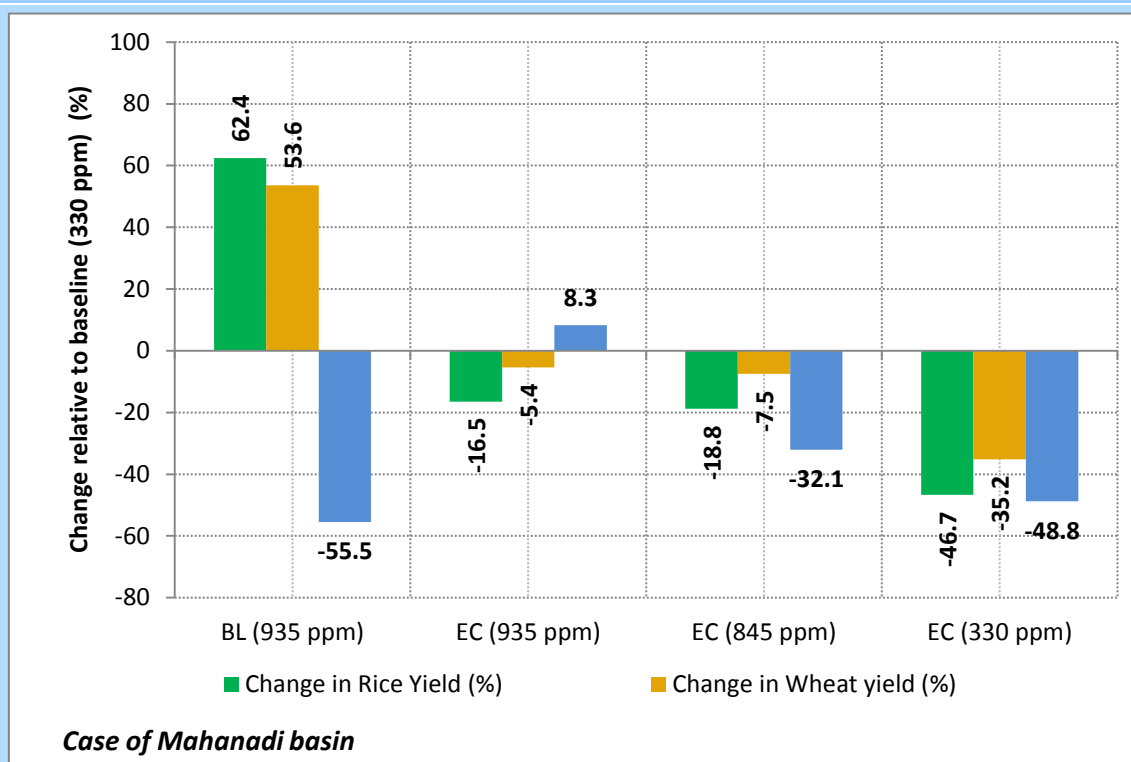


Sensitivity Analysis

CO₂ Fertilization

Sensitivity analysis has been carried out for a pilot basin to assess the impact of CO₂ concentration on crop yield and water requirement. It can be seen from Figure 16 that with higher temperature higher CO₂ is not always beneficial. A combination of 845 ppm CO₂ and temperature towards end-century impacts in decrease in yield and at the same time irrigation water requirement also reduces. This combination of temperature and CO₂ increase the water use efficiency in plants.

Figure 16 Sensitivity of elevated CO₂ on crop growth



BL_935	Yield is high, Low Irrigation	Advantage CO ₂ Fertilization
EC_935	Yield is marginally low, Irrigation is marginally high	Disadvantage High Temperature + High CO ₂
EC_845	Yield is low, Irrigation is Low	Advantage CO ₂ Fertilization in terms of Water saving
EC_330	Lowest Yield, low irrigation	Disadvantage Low CO ₂ +High Temperature

Seventh Framework Programme

Theme 6

Environment



Project: 603864 – HELIX

Full project title:

High-End cLimate Impacts and eXtremes

D9.3 Technical report detailing the results from the uncertainty and sensitivity analysis

Part B: Chapter one. Assessment on the uncertainty of the high flows (floods) and low flows (hydrological droughts) of the Brahmaputra River

Chapter two. Assessment of the uncertrainty and sensitivity of climate change on the production of Boro rice in Bangladesh using DSSAT crop model

TABLE OF CONTENTS

	<u>Page No.</u>
TABLE OF CONTENTS	ii
LIST OF TABLES	iv
LIST OF FIGURES	v
EXECUTIVE SUMMARY	vi
CHAPTER ONE ASSESSMENT ON THE UNCERTAINTY OF THE HIGH FLOWS (FLOODS) AND LOW FLOWS (HYDROLOGICAL DROUGHTS) OF THE BRAHMAPUTRA RIVER.....	1
1.1 Introduction.....	1
1.2 Study area.....	3
1.3 Materials and methods	5
1.3.1 Description of SWAT model	5
1.3.2 Input data and model setup	6
1.3.2.1 Topography, land use/land cover, soil data.....	6
1.3.2.2 Weather data	7
1.3.2.3 Model setup.....	7
1.3.3 Calibration and validation of SWAT model	7
1.3.3.1 Observed discharge data	7
1.3.3.2 Calibration and validation	8
1.3.4 Climate change impact analysis	10
1.3.4.1 Future climate projections.....	10
1.3.4.2 Analysis of extreme discharges.....	13
1.4 Results.....	14
1.4.1 Calibration and validation of SWAT model	14
1.4.2 Climate change impact analysis	16
1.4.2.1 Changes in frequency of annual maximum discharge	18
1.4.2.2 Changes in magnitude of annual maximum discharge.....	20
1.4.2.3 Changes in timing of annual maximum discharge	21
1.4.2.4 Changes in frequency of annual minimum discharge	22
1.4.2.5 Changes in magnitude of annual minimum discharge	24
1.4.2.6 Changes in timing of annual minimum discharge.....	25
1.4.2.7 Changes in median of mean monthly discharge.....	26
1.5 Summary	29
CHAPTER TWO ASSESSMENT OF THE UNCERTAINTY AND SENSITIVITY OF CLIMATE CHANGE ON THE PRODUCTION OF BORO RICE IN BANGLADESH USING DSSAT CROP MODEL .	31
2.1 Introduction.....	31

2.2 Materials and methods	32
2.2.1 Study area.....	33
2.2.2 Selection of crop simulation model.....	34
2.2.3 Integrating field data in DSSAT	35
2.2.4 Selection of rice variety	35
2.2.5 Weather data	36
2.2.6 Climatic data	37
2.2.7 Crop management	38
2.2.8 Calibration and validation	40
2.3 Results and discussion	42
2.3.1 Climatic scenarios	42
2.3.2 Change of the yield	44
2.3.3 Sensitivity of the increasing CO ₂ on yield	46
2.4 Summary	49
REFERENCES	50

LIST OF TABLES

Table 1.1 Parameters used for calibration of SWAT model, ranked by sensitivity.....	8
Table 1.2 CORDEX-South Asia climate projections used in the study.....	11
Table 1.3 Performance of SWAT model during the calibration and validation periods.....	16
Table 1.4 Percentage change in annual maximum discharge for different return periods.....	20
Table 1.5 Percentage change in properties of probability density function of annual maximum discharge.....	21
Table 1.6 Percentage change in annual minimum discharge for different return periods.....	23
Table 1.7 Percentage change in properties of probability density function of annual minimum discharge.	25
Table 1.8 Median of percentage changes of mean monthly discharge.	29
Table 2.1 Key information of the BR29 variety of Boro rice.	35
Table 2.2 Details of the bias corrected ensembles of regional climate models.....	38
Table 2.3 Crop management data for simulations of BR29 in DSSAT.	40
Table 2.4 Default values of the genetic coefficients of Boro rice.....	41
Table 2.5 Values of the genetic coefficients in some important locations (divisions).....	42

LIST OF FIGURES

Fig. 1.1 Location and details of the Brahmaputra River basin.....	5
Fig. 1.2 Changes in ensemble range of basin averaged temperature compared to pre-industrial period.....	12
Fig. 1.3 Changes in ensemble range of basin averaged precipitation.....	12
Fig. 1.4 Comparison of observed and simulated hydrographs.....	15
Fig. 1.5 Changes in ensemble range of annual mean discharge.....	17
Fig. 1.6 Changes in ensemble range of annual maximum discharge.....	17
Fig. 1.7 Changes in ensemble range of annual minimum discharge.....	18
Fig. 1.8 Return period curves of annual maximum discharge for different time periods.....	19
Fig. 1.9 Probability density functions of annual maximum discharge for different time periods.....	21
Fig. 1.10 Timing of annual maximum discharge for different time periods.....	22
Fig. 1.11 Return period curves of annual minimum discharge for different time periods.....	23
Fig. 1.12 Probability density functions of annual minimum discharge for different time periods.....	25
Fig. 1.13 Timing of annual minimum discharge for different time periods.....	26
Fig. 1.14 Boxplot of mean monthly discharge for different time periods.....	27
Fig. 1.15 Boxplot of percentage change in mean monthly discharge.....	28
Fig. 2.1 District maps of Bangladesh.....	34
Fig. 2.2 Thirty four ground base measuring stations of Bangladesh Meteorological Department.....	37
Fig. 2.3 BR29 variety of Boro rice in Bangladesh.....	39
Fig. 2.4 Changes of the maximum temperature (top) and minimum temperature (bottom) in 2021-2050 (left) and 2070-2099 (right).....	43
Fig. 2.5 Change of rainfall in 2021-2050 (left) and 2070-2099 (right).....	44
Fig. 2.6 (a) Change of Boro yield in 2021-2050 and (b) Change of Boro yield in 2070-2099.....	45
Fig. 2.7 Change of yield of Boro rice in 2021-2050.....	46
Fig. 2.8 Change of yield of Boro rice in 2070-2099.....	46
Fig. 2.9 Comparison of the yield change in fixed (380 ppm) and elevated (500 ppm) CO ₂ in 2021-2050.....	48
Fig. 2.10 Comparison of the yield change in fixed (380 ppm) and elevated (950ppm) CO ₂ in 2070-2099.....	48

EXECUTIVE SUMMARY

The release of the new generation high resolution downscaled projections of the fifth phase of the Coupled Model Inter-comparison Project (CMIP5) over the CORDEX-SA (Coordinated Downscaling Experiment) domain provides an opportunity to assess the risks from the hydrological extremes. The Brahmaputra carries the highest annual flow (about 67%) to Bangladesh from China, India and Bhutan which is likely to experience changes of high flows (floods) and low flows (hydrological drought) due to climate change. This study assessed the impact of climate change on the frequency, magnitude and timing of extreme discharges and the mean monthly discharges of Brahmaputra River at Bahadurabad gaging station inside Bangladesh. The hydrological model SWAT was calibrated and validated for the Brahmaputra River basin using weather data from TRMM and ERA-Interim and observed discharge data at Bahadurabad gaging station of BWDB from 2000 to 2013. It was found to have very good NSE and R2 values (>0.8) during both calibration and validation periods. The calibrated model was then used with bias corrected weather data from an ensemble of 11 climate projections with the emission scenario of RCP8.5 collected from the CORDEX-South Asia domain database. The results of the analysis of simulated discharges show that the floods will become more frequent in the future and their magnitudes will become greater, i.e. they will become more severe, but the mean timing of flood events will not change while the low flow extremes will become less frequent in the future and their magnitudes will become greater, i.e. they will become less severe, but the mean timing of the low flow extremes will not change. The mean monthly discharges will increase for most of the months in the future and a few months will see a slight decrease. But for all time periods the month of May will see the highest increase in discharge compared to the other months.

Rice is the staple food for about 156 million people of the country. With the present population growth rate of 2 million per year, the total population would be 238 million by 2050. Bangladesh will require more than 55.0 million tons of rice to feed its people by the year 2050. Impact of extreme climate change on the production of Boro rice in Bangladesh has been evaluated using the DSSAT 4.6 crop modeling software. The model was calibrated using BR29 variety of Boro rice for the years 2007-2010 and validated for 2011-2014 incorporating BBS data with statistical parameters RMSE and NSE. There are 8 genetic coefficients for BR29 variety of Boro rice which are the calibration parameters of Boro rice in DSSAT 4.6. Impact of future climate is analysed considering baseline period of 30 years from 1991-2010. The future yield was analysed for the near future during 2030's (2021-2050) and the far future during 2080's (2070-2099) using 7 bias corrected ensembles of regional climate models (RCMs) for whole Bangladesh divided in 64 districts. The soil profile data was integrated in DSSAT by extracting the available 14 soil databases of Bangladesh in WISE 1.1 soil database. The results show that, for most

of the districts, the yield is negative, reaching over 20% decrease in some regions. The maximum temperature rise exceeds 1.5°C in 2030's and 4°C in 2080's whereas the minimum temperature rises up to 5°C in 2090's. This rise in daily temperature over the growing period of Boro rice indicates the adverse impact of temperature on crops. However, the increase in the amount of Carbon dioxide increases the yield up to a certain limit, but this increase is not significant compared to the negative impacts of the rise of temperature. Almost all the regions has increased in the elevated CO₂ level than the fixed CO₂ emission in 2030's and 2080's based on the sensitivity analysis. However, the range of unpredictability in rice yield has increased with the elevated CO₂ emissions. This might indicate the complex correlation between temperature and elevated CO₂ emission in the yield of crop. The model also shows a significant change in the yield or rice with the change of transplantation date. This shifting of transplantation date helps to predict the optimum transplantation date that would result in harvesting the maximum yield of rice.

CHAPTER ONE

ASSESSMENT ON THE UNCERTAINTY OF THE HIGH FLOWS (FLOODS) AND LOW FLOWS (HYDROLOGICAL DROUGHTS) OF THE BRAHMAPUTRA RIVER

1.1 Introduction

An increase in global average temperature due to climate change is likely to intensify the global hydrological cycle, which in turn will impact regional water resources (Oki and Kanae 2006; Arnell 1999). For instance, any change either in the frequency or total amount of precipitation over a river basin can cause change in the magnitude and timing of the river's discharge, thereby changing the mean discharges along with the intensity of floods and droughts (Immerzeel 2008). The impacts on regional water resources due to climate change are still uncertain and under investigation, especially the impacts on extreme events such as floods and droughts (Andersen and Shepherd 2013). Although estimating the changes in future mean discharges is necessary for overall water resources management, quantifying the future extreme discharges is of greater urgency because future changes in hydrological extremes are thought to be greater than hydrological mean conditions (Huang et al 2015). Increased floods and droughts have the obvious potential to cause massive damage to society and environment in many ways, including the decline of crop yields, thus increasing the risk of poverty and hunger (Abbaspour et al 2009). Therefore, it has become imperative that the impacts of climate change on regional water resources are quantified with meaningful spatial and temporal resolutions for long term strategic planning of any country (Uniyal et al 2015).

The Brahmaputra is a transboundary river originating in China and ending in Bangladesh and it is the fourth largest river of the world in terms of average discharge of approximately 20,000 m³/s (Jian et al 2009). It drains water from approximately 520,000 km² area of China, India, Bhutan and Bangladesh (Immerzeel 2008). An estimated 66 million people depend on water from this river for their livelihood

through subsistence agriculture and thus any change in the river's discharge due to climate change may have a negative impact on this large population (Hasson et al 2013; Immerzeel et al 2010). A decrease in discharge during dry season when the basin requires water for irrigation systems translates into a threat to food security (Gain 2011). On the other hand, an increase in discharge during monsoon season translates into increase of major flooding events particularly in the lowermost riparian country, Bangladesh. About 67% of the total annual discharge of Bangladesh comes from the Brahmaputra River (Immerzeel 2008). A warming climate will impact the snow and glacier melt processes of the Brahmaputra River basin. In addition, the precipitation falling over the basin will also be affected. Precipitation in this region is connected to the Indian summer monsoon, which is projected to be impacted by climate change. Therefore, the likelihood increases that the discharges of the Brahmaputra River will change with a changing climate (Pervez and Henebry 2015; Nepal and Shrestha 2015). Given the importance of the Brahmaputra River to its riparian countries, this study made an attempt at estimating the changes in future extreme and mean discharges of the river due to climate change.

One of the key constraints in estimating the change in future river discharges with reasonable accuracy is the multiple levels of uncertainty associated with simulating the future discharges. Ouyang et al (2015) divided the uncertainties into: (1) uncertainty related to different global circulation models (GCMs), (2) uncertainty related to different emission scenarios/representative concentration pathways (RCPs), (3) uncertainty of downscaling methods/regional climate models (RCMs) and (4) uncertainty of hydrological models that simulate the river discharges. An additional uncertainty in simulating extreme discharges is the natural variability of such rare events. Of all these, the largest uncertainty is considered to arise from different GCM structures (Xu and Luo 2015). Given these limitations, if only a few future climate projections are used as forcing to run hydrological models, the simulated discharges will likely be biased. Hence it has been suggested to use an ensemble of climate projections to better account for the uncertainty (Huang et al 2015). This study therefore used an ensemble of 11 different climate projections made by different RCMs that are driven by multiple GCMs. In order to focus on the impacts of high-end climate change on the discharges of the Brahmaputra River, only the emission scenario of

RCP8.5 from the Fifth Assessment Report (AR5) of the Intergovernmental Panel on Climate Change (IPCC) was selected for all 11 climate projections. The pathway RCP8.5 assumes continued anthropogenic greenhouse gas emissions throughout the 21st century. Hence, this represents the highest CO₂ concentrations in the atmosphere and the highest rise in global temperatures, out of all the 4 emission scenarios (IPCC 2013).

Out of the many hydrological models presently available, this study selected the Soil and Water Analysis Tool (SWAT) (Arnold et al 1998) for simulating future discharges for the 11 different climate projections. SWAT has recently become one of the most commonly used hydrological models around the world for investigating climate change impacts on regional water resources because of its flexibility and robustness (Jha et al 2006). Earlier studies have shown that SWAT is suitable for modeling large basins such as the Brahmaputra and it has also been used to assess climate change impacts in the Indian subcontinent near the Brahmaputra (Gosain et al 2011; Narsimlu et al 2015, Bharati et al 2016). The broad goals of this study were to (1) calibrate and validate the SWAT model for the Brahmaputra River basin, (2) use the calibrated model to simulate future river discharges for the 11 selected climate projections, (3) analyze the simulated discharges to estimate the future change in frequency, magnitude and timing of both annual maximum and minimum discharges and (4) analyze the simulated discharges to estimate the future change in mean monthly discharges.

1.2 Study area

The Brahmaputra River originates in the glaciated Kailas range of southern Tibet, China at about 5300 m amsl (above mean sea level) and then travels approximately 2900 km through China, India and Bangladesh before meeting with the Ganges River which ultimately discharges in the Bay of Bengal (Gain et al 2011). Around 50.5% of the Brahmaputra River basin falls within China, 33.6% in India, 8.1% in Bangladesh and 7.8% in Bhutan (Immerzeel 2008). The physiography of the basin consists of: (1) the Tibetan plateau having elevations above 3500 m amsl and covering 44.4% of the basin, (2) the Himalayan belt having elevation from 100 to 3500 m amsl and covering 28.6% of the basin and (3) the

lowland floodplains having elevations below 100 m amsl and covering 27% of the basin (Gain et al 2011). The northern part of the basin over the Tibetan plateau has a cold and dry mountain climate while the southern lower elevation part of the basin has a warm and humid tropical monsoon climate. The southern part also receives high amounts of widespread precipitation because of the influence of the Indian summer monsoon. The different physiographic zones of the basin have different average temperature and precipitation. In the Tibetan plateau, the average minimum temperature is about -12 °C and the average maximum temperature is about 27 °C. In the Himalayan belt, a high variation in the temperature is observed because of the large elevation range. In the lowland floodplain, the average minimum temperature is about 9 °C and the average maximum temperature is about 35 °C. The coldest months in the basin are generally December and January while the warmest months are the period from May to August (Pervez and Henebry 2015). The upper reaches of the basin lies in the Himalayan rain-shadow area, but the remaining parts of the basin are heavily influenced by the summer monsoon. The mean annual rainfall in the basin is about 2300 mm while spatial variability ranges from 1200 mm to over 6000 mm. Of the total annual rainfall, about 60-70% falls in the monsoon season (June to September) and another 20-25% falls in the pre-monsoon season (March to May). Above the elevations of 1500 m amsl, some precipitation falls as snow. The lowermost reaches of the river are usually flooded during the monsoon and becomes a braided river in the dry season (Nepal and Shrestha 2015).

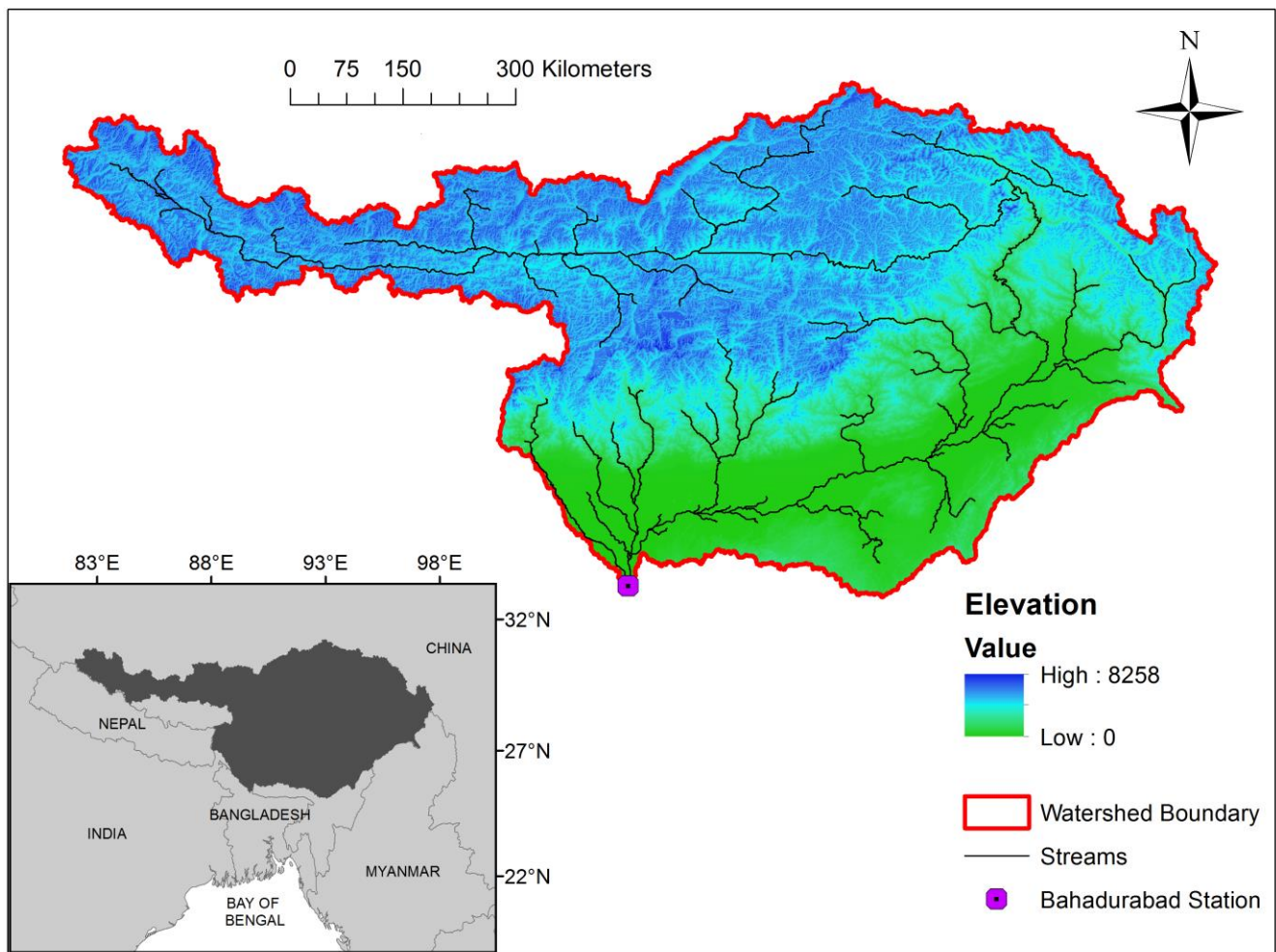


Fig. 1.1 Location and details of the Brahmaputra River basin.

1.3 Materials and methods

1.3.1 Description of SWAT model

SWAT is a physically based, semi-distributed, basin-scale, computationally efficient, continuous time hydrological model that operates on a daily/sub-daily time step. It divides a basin into sub-basins by overlaying land use/land cover map, soil map and digital elevation model (DEM). The sub-basins are further divided the sub-basins into lumped units called hydrologic response units (HRU) which are the percentage of a sub-basin area that has a unique combination of soil, land use/land cover and slope properties. Using moisture and energy inputs provided by the user, the model then predicts the hydrology at each HRU using a water balance equation which consists of daily precipitation, runoff,

evapotranspiration, percolation and return flow components. The generated flow of all the HRUs in a sub-basin are then summed together and are then routed through channels, ponds and reservoirs to the basin outlet.

The surface runoff in SWAT can be estimated using either the Soil Conservation Service (SCS) curve number method or the Green and Ampt infiltration method. The peak runoff estimations are based on the modified rational formula and the percolation through each soil layer is predicted using storage routing techniques. The evapotranspiration can be estimated in SWAT using the Priestley-Taylor method, the Penman-Monteith method or the Hargreaves method. The flow routing in the river channels is computed using either the variable storage coefficient method or the Muskingum routing. Detailed descriptions of the model can be found in Arnold et al (1998). The basic input data required for SWAT includes daily precipitation, maximum and minimum temperature, land use/land cover map, soil map, and DEM, a description of which are given in the following sections.

1.3.2 Input data and model setup

1.3.2.1 Topography, land use/land cover, soil data

The topography of the area to be modeled has to be provided to SWAT in the form of a DEM, for which a hydrologically conditioned version of the Shuttle Radar Topography Mission (SRTM) DEM of 90 m resolution was collected from the HydroSHEDS database of the United States Geological Survey (<http://hydrosheds.cr.usgs.gov>, 28 June 2016). A global land use/land cover map of 300 m resolution called GlobCover prepared by the European Space Agency for the year 2009 was collected (<http://due.esrin.esa.int>, 28 June 2016) and its legend was reclassified to match with the land classes in the SWAT database. For using as a soil map in SWAT, the Digital Soil Map of The World prepared by the Food and Agriculture Organization of the United Nations in 1995 was collected (<http://www.fao.org/geonetwork/srv/en/metadata.show?id=14116>, 28 June 2016).

1.3.2.2 Weather data

For using as weather inputs to SWAT, daily time series of observed precipitation and maximum/minimum temperature were collected. Version 7 of the 3B42 product of Tropical Rainfall Measuring Mission (TRMM) was collected as daily observed precipitation for grid points over the study area (http://mirador.gsfc.nasa.gov/collections/TRMM_3B42__007.shtml, 28 June 2016). The TRMM grid points have a resolution of 0.25°. As for the daily maximum and minimum temperature required in SWAT, atmospheric reanalysis products from ERA-Interim database was collected for grid points over the study area. ERA-Interim grid points also have a resolution of 0.25° (<http://www.ecmwf.int/en/research/climate-reanalysis/era-interim>, 28 June 2016).

1.3.2.3 Model setup

Using the provided DEM, the automatic watershed delineation command of SWAT initially defined a stream network given a minimum drainage area threshold of 2600 km² and later delineated the outline of the complete basin with an area of 519695 km² given the location of the basin outlet. The outlet of the whole Brahmaputra River basin was considered to be at the Bahadurabad gaging station of Bangladesh Water Development Board (BWDB) – the location of which is shown in **Fig. 1** – so that the observed discharge data from that location can be compared with the SWAT generated discharge in order to calibrate and validate the model. Later, the HRU Analysis command was performed which divided the whole basin into 113 sub-basins and created 3387 HRUs. The Hargreaves method was selected for estimating potential evapotranspiration, the SCS curve number method for estimating surface runoff volume and the variable storage coefficient method was selected for channel routing. The SWAT model was run at a daily time-step for all purposes, i.e. for calibration, validation and simulation of future discharges.

1.3.3 Calibration and validation of SWAT model

1.3.3.1 Observed discharge data

As mentioned before in section 3.2.3, the outlet of the whole Brahmaputra River basin was selected to be at the Bahadurabad gaging station of BWDB, the official station number of which is SW46.9L. Observed discharges from the station have been collected of the time duration 2000 to 2013 corresponding with the calibration and validation period of the SWAT model. Since BWDB does not measure discharge on a daily basis but does measure the daily water levels, a rating curve was generated with the partial discharge data series using which the daily discharges were later estimated from the daily water levels. The rating curve used in this study was of the form (Equation 1.1)-

$$Q = C (h + a)^N \dots\dots\dots(1.1)$$

where Q = discharge, C and N = constants, h = water level and a = water level at which discharge is zero.

1.3.3.2 Calibration and validation

The available weather data of 14 years was divided into two equal periods of 7 years each, one for using in calibration (2000-2006) of the model and the other for validation (2007-2013). For both calibration and validation periods, 1 year has been kept as warm-up or equilibration period which is required to get the hydrologic cycle of the SWAT model fully operational. Before initializing the calibration process, a global sensitivity analysis was performed on 26 hydrology-related parameters of SWAT using a separate independent tool called SWAT-CUP (Calibration and Uncertainty Program). Here the parameter sensitivities were determined by calculating a multiple regression system that regresses Latin hypercube generated parameters against some set objective function values and then a t-test is performed to identify the relative significance of each parameter (Abbaspour 2015). Afterwards the 14 most sensitive parameters were selected for performing the calibration process using Sequential Uncertainty Fitting II (SUFI-2) algorithm of SWAT-CUP (Abbaspour et al 2007). A list of the 14 selected parameters are given in **Table 1.1** along with their respective t-stats and P-values as calculated by the sensitivity analysis.

Table 1.1 Parameters used for calibration of SWAT model, ranked by sensitivity.

Sensitivity Rank	Parameter	t-stat	P-value
1	CN2 (Curve number)	3.22	0.002
2	SOL_BD (Moist bulk density of first soil layer)	2.98	0.003
3	SOL_K (Saturated hydraulic conductivity of first soil layer)	2.92	0.004
4	CH_N2 (Manning's n value for the main channel)	2.50	0.014
5	GWQMN (Threshold depth of water in the shallow aquifer for return flow to occur)	-2.30	0.023
6	ALPHA_BNK (Baseflow alpha factor for bank storage)	2.26	0.025
7	SLSUBBSN (Average slope length)	-1.63	0.105
8	EPCO (Plant uptake compensation factor)	-1.57	0.117
9	SOL_AWC (Available water capacity of the first soil layer)	1.52	0.130
10	SFTMP (Snowfall temperature)	1.32	0.190
11	REVAPMN (Threshold depth of water in the shallow aquifer for revap to occur)	-1.21	0.230
12	GW_DELAY (Groundwater delay)	-1.10	0.274
13	ALPHA_BF (Baseflow alpha factor)	-0.42	0.675
14	OV_N (Manning's n value for overland flow)	0.41	0.683

After the calibration process was completed, the SWAT model was run for the validation period with the optimized parameters kept unchanged. To determine the most optimum parameter values during calibration by comparing the performances of different models with different parameter values and also to evaluate the performance of the model during validation, the Nash-Sutcliffe efficiency (NSE) value was used, which has the form (Equation 1.2),

$$NSE = 1 - \left[\frac{\sum_{i=1}^n (Q_i^{obs} - Q_i^{sim})^2}{\sum_{i=1}^n (Q_i^{obs} - Q^{mean})^2} \right] \dots\dots\dots (1.2)$$

where Q^{obs} is the observed discharge, Q^{sim} is the simulated discharge, Q^{mean} is the mean of all the observed discharge data and n is the total number of observations. The values of NSE range from 1 to $-\infty$ where a value of 1 corresponds to a perfect fit between simulated and observed datasets.

Some other statistical indicators were also calculated but they were not used as a deciding factor for selecting the most optimum parameters during calibration, rather they only served the purpose of providing some additional insight to the level of match/mismatch between the observed and simulated datasets. The additional indicators were the coefficient of determination (R^2), RMSE-observations standard deviation ratio (RSR) and percent bias (PBIAS). R^2 values have a range of 0 to 1 where 1 is the optimum value, RSR values have a range of 0 to ∞ where 1 is the optimum value and PBIAS values have a range of $-\infty$ to ∞ where 0 is the optimum value.

1.3.4 Climate change impact analysis

1.3.4.1 Future climate projections

For simulating future discharges of the Brahmaputra River, bias corrected daily precipitation and daily maximum/minimum temperature data of 11 future climate projections were used as weather inputs in running the calibrated SWAT model. The details of the climate projections are given in **Table 1.2**. The raw RCM outputs were collected from the Coordinated Regional Climate Downscaling Experiment (CORDEX) - South Asia domain database, after which they were bias corrected by the multi-segment statistical bias correction (MSBC) method (Grillakis et al 2013). The CORDEX–South Asia domain database contains high resolution datasets with a grid resolution of 0.5° and of the time duration 1971 to 2100. The reference dataset used for the bias correction was the hybrid dataset of Watch Forcing Data (WFD) and the Watch Forcing Data methodology applied to ERA-Interim data (WFDEI) (Weedon et al 2014). For bias correction, the reference period was considered to be 1980 to 2009 and the regular 0.5° grid of WFD was used as reference grids.

Table 1.2 CORDEX-South Asia climate projections used in the study.

Institute	GCM	RCM	Resolution	RCP
CSIRO	ACCESS1.0	CCAM-1391M	0.5°	8.5
CSIRO	CCSM4.0	CCAM-1391M	0.5°	8.5
SMHI	CNRM-CERFACS-CNRM-CM5	RCA4	0.5°	8.5
CSIRO	CNRM-CM5	CCAM-1391M	0.5°	8.5
SMHI	ICHEC-EC-EARTH	RCA4	0.5°	8.5
CSIRO	MPI-ESM-LR	CCAM-1391M	0.5°	8.5
MPI-CSC	MPI-M-MPI-ESM-LR	REMO2009	0.5°	8.5
SMHI	MPI-M-MPI-ESM-LR	RCA4	0.5°	8.5
SMHI	NOAA-GFDL-GFDL-ESM2M	RCA4	0.5°	8.5
SMHI	IPSL-CM5A-MR	RCA4	0.5°	8.5
SMHI	MIROC-MIROC5	RCA4	0.5°	8.5

As mentioned before, only the extreme RCP8.5 emission scenario was considered among the three RCPs. The ensemble range of basin averaged temperature and precipitation values used in this study are shown in **Fig. 1.2** and **Fig. 1.3** respectively. In **Fig. 1.2** the changes in temperature are shown compared to pre-industrial period for which a constant value of 0.5 °C was added to the baseline scenario (Alfieri et al 2015). Based on a 10-year moving average it is seen that for the emission scenario of RCP8.5, the annual mean temperature over the Brahmaputra River basin will increase by 2 °C and 4 °C in the years 2046 and 2074 respectively, compared to pre-industrial period. From **Fig. 1.3** it is seen that the basin averaged total annual precipitation is projected to rise at a rate of 1.69 mm/year.

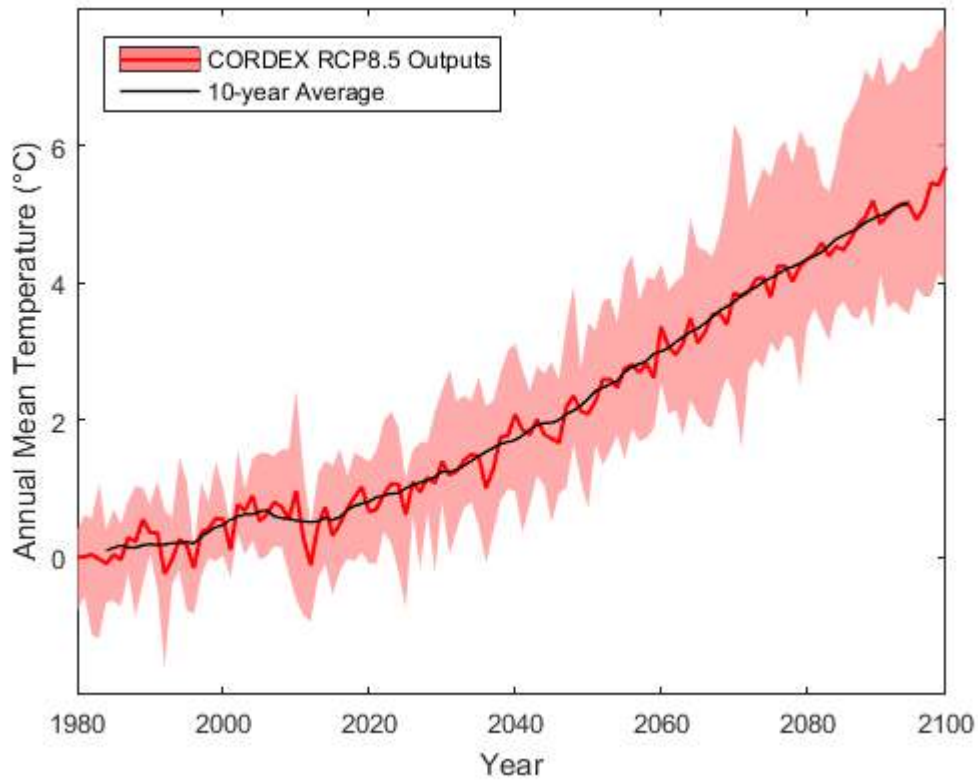


Fig. 1.2 Changes in ensemble range of basin averaged temperature compared to pre-industrial period.

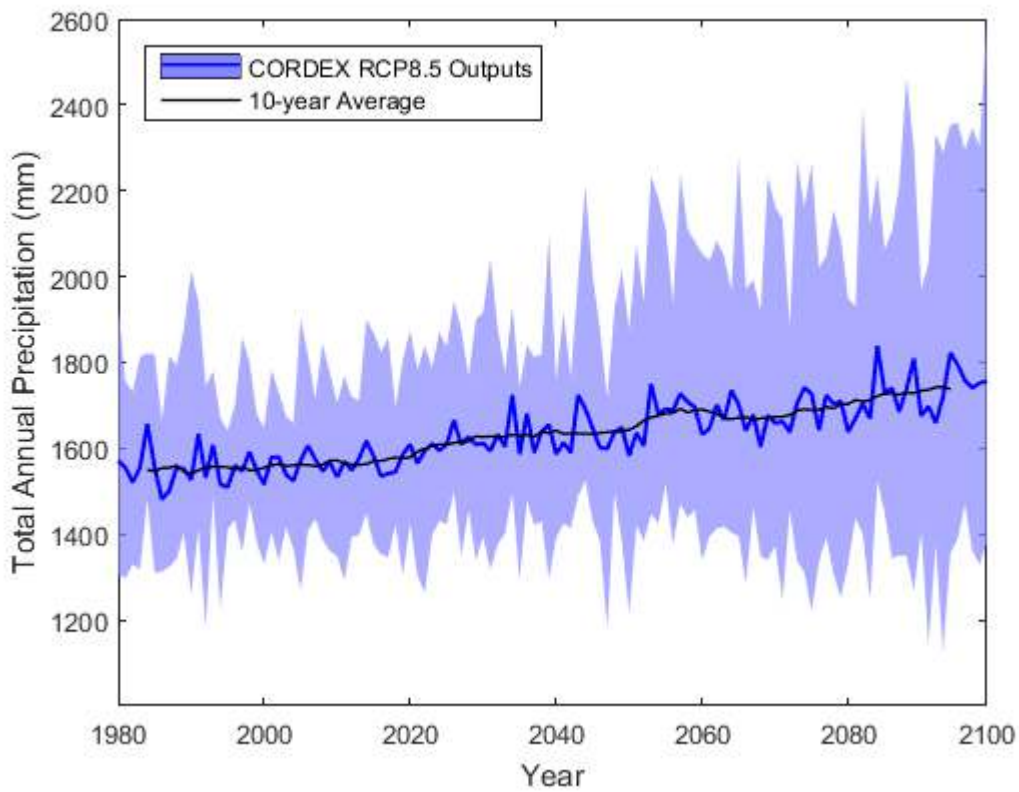


Fig. 1.3 Changes in ensemble range of basin averaged precipitation.

When analyzing the changes in future river discharges, 4 time periods were considered, which are the baseline period (1980-2009), the 2020s (2010-2039), the 2050s (2040-2079) and the 2080s (2080-2099). A key assumption is that while simulating the future discharges with SWAT using the downscaled future precipitation and temperature data was that the terrain, soil and land use/land cover will be static in the future. Another assumption is that anthropogenic changes to the stream network through dams, reservoirs or other structural measures will be minimal.

1.3.4.2 Analysis of extreme discharges

After all the future daily discharges of the Brahmaputra River at the selected basin outlet location of Bahadurabad for all 4 time periods were simulated with the calibrated SWAT model using the future weather data, annual maximum/minimum discharge time series were extracted from all the simulated daily datasets in order to analyze the changes in frequency, magnitude and timing of extreme discharges at different time periods compared to the baseline period. Before carrying out frequency analysis the data must be tested to check if they are independent, stationary and homogenous, as these are the assumptions of the frequency analysis. In this study, the Spearman rank order serial correlation coefficient test for independence, the Spearman rank order correlation coefficient test for trend and the Mann-Whitney test for homogeneity were performed on all the datasets that were used in further frequency analysis and were found to pass the tests at 1% significance level. All the above mentioned tests are non-parametric and a description of them can be found in Pilon and Harvey (1993).

Afterwards, parametric frequency analysis was performed on annual maximum series using the Consolidated Frequency Analysis (CFA) program and on annual minimum series using the Low Flow Frequency Analysis (LFA) program, both written by Environment Canada (Pilon and Harvey 1993; Pilon and Jackson 1988). The probability distributions used to fit the datasets during frequency analysis were the Generalized Extreme Value distribution and the Weibull distribution for annual maximum series and annual minimum series respectively. As for analyzing the changes in magnitude of extreme discharges at different time periods compared to the baseline period, a probability density function was

drawn for each time period. While drawing each probability density function for a time period, all 11 of the annual maximum discharge series (when analyzing maximum discharge) or all 11 of the annual minimum discharge series (when analyzing minimum discharge) of that particular time period - corresponding to the 11 climate projections used to derive them - were compiled together into one single series. Similar to the frequency analysis, the probability density functions were fitted to a Generalized Extreme Value distribution and Weibull distribution for annual maximum series and annual minimum series, respectively.

Changes in the timing of extreme discharges were also analyzed in this study because the severity of floods in Bangladesh largely depends on the coincidence of the timing of the peak discharges of the Ganges River and the Brahmaputra River. Hence it is important to see whether the timing of the peak discharge in future time periods shift in either direction i.e., earlier or later from the baseline period. Usually the peak discharge of the Brahmaputra River happens to occur earlier than that of the Ganges River. In case the timing of the peak discharge of the Brahmaputra River shifts in the future due to climate change and coincide with the timing of the peak discharge of the Ganges River, it would increase the severity of floods in Bangladesh. Similarly, a change in the timing of the low flow extremes of the Brahmaputra River due to climate change may cause the timing to coincide with the timing of the low flow extremes of other major rivers, thus creating extreme water shortages.

1.4 Results

1.4.1 Calibration and validation of SWAT model

A comparison of observed and simulated hydrographs for calibration and validation period is shown in **Fig. 1.4**. The values of the statistical indicators for evaluating model performances in both periods are given in **Table 1.3**. It can be seen that the NSE values are 0.84 and 0.83 for calibration and validation periods respectively, which indicates a very good agreement between the observed and simulated

discharges. Similarly, the R^2 values for calibration and validation periods are 0.86 and 0.87 respectively, which also indicates a very good model performance.

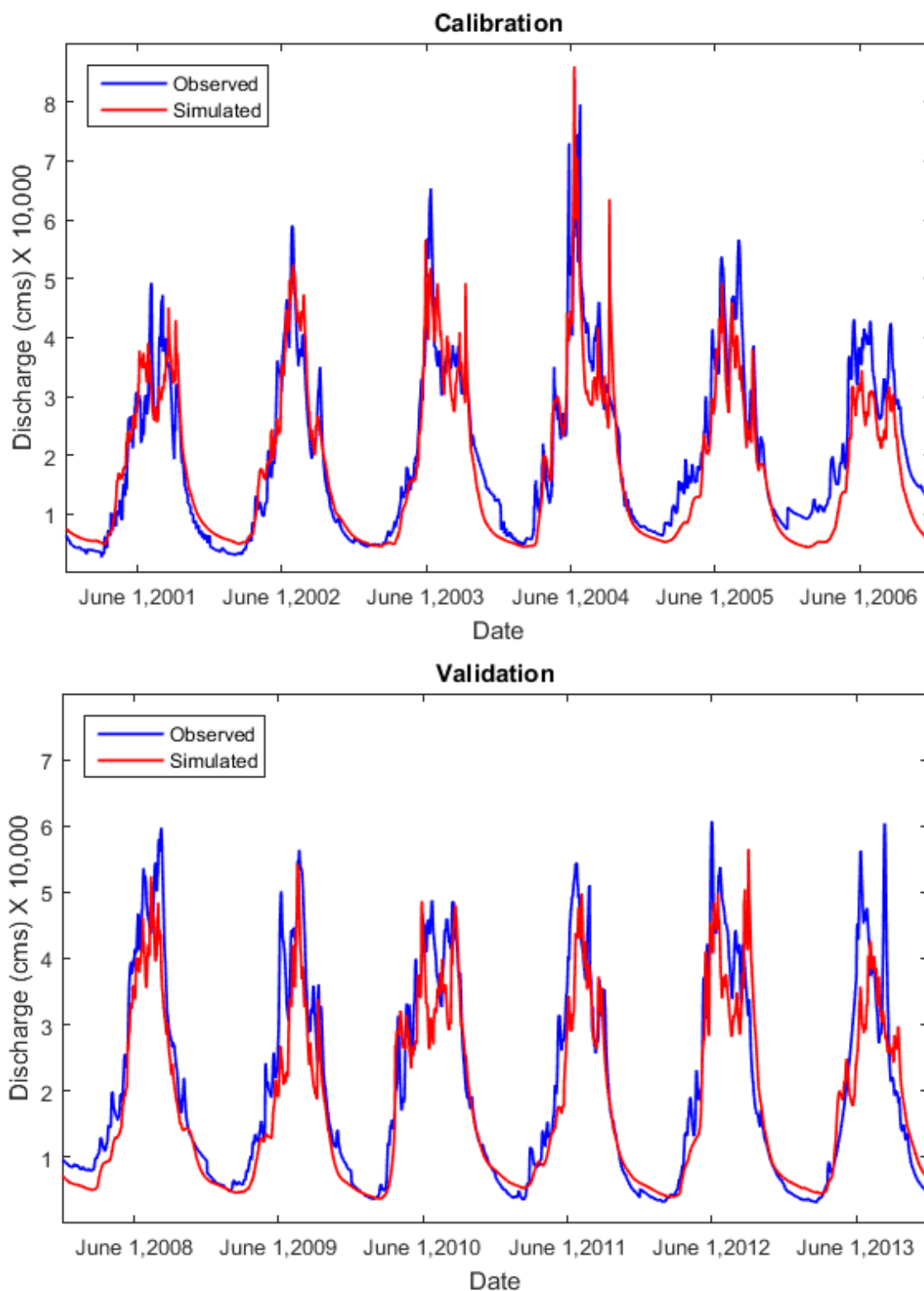


Fig. 1.4 Comparison of observed and simulated hydrographs.

Table 1.3 Performance of SWAT model during the calibration and validation periods.

Statistical Indicator	Calibration (2001 - 2006)	Validation (2007 - 2013)
NSE	0.844	0.833
R ²	0.862	0.865
RSR	0.087	0.660
PBIAS	-0.003	0.006

1.4.2 Climate change impact analysis

The time series of annual mean discharge, annual maximum discharge and annual minimum discharge as simulated by the calibrated SWAT model for all 11 scenarios are shown in **Fig. 1.5**, **Fig. 1.6** and **Fig. 1.7** respectively. Based on a 10-year moving average it is seen that for the emission scenario of RCP8.5, the annual mean discharge of Brahmaputra River at Bahadurabad station is projected to rise at a rate of 18.01 m³/s/year, the annual maximum discharge is projected to rise at a rate of 131.47 m³/s/year and the annual minimum discharge is projected to rise at a rate of 1.45 m³/s/year.

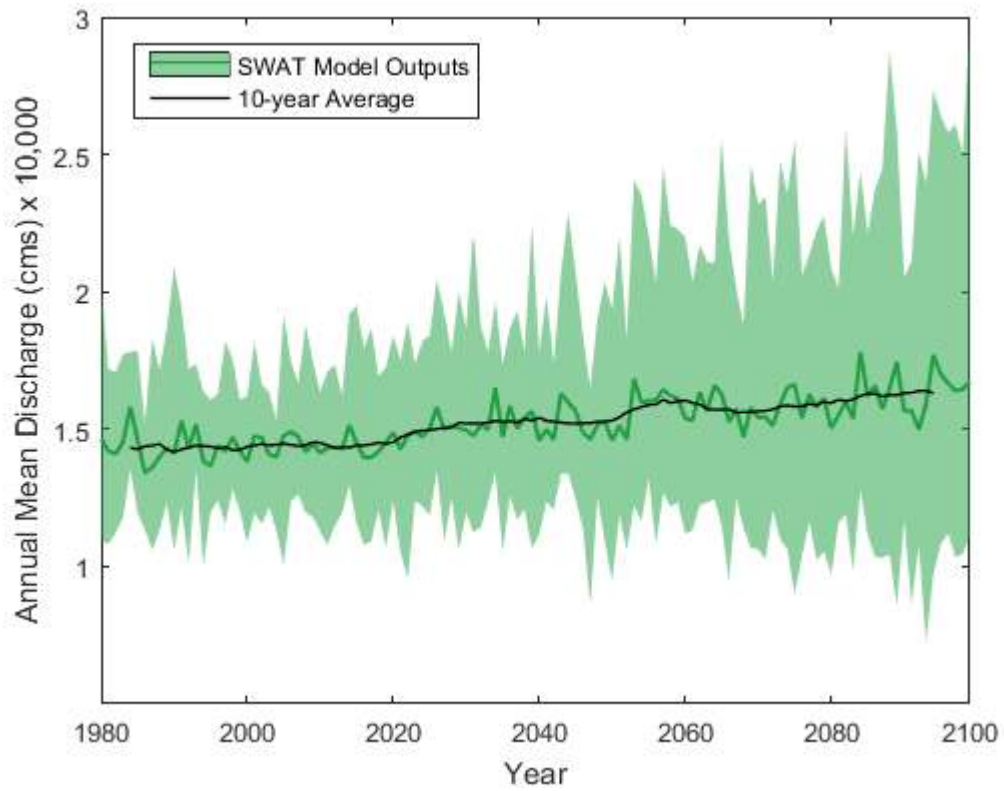


Fig. 1.5 Changes in ensemble range of annual mean discharge.

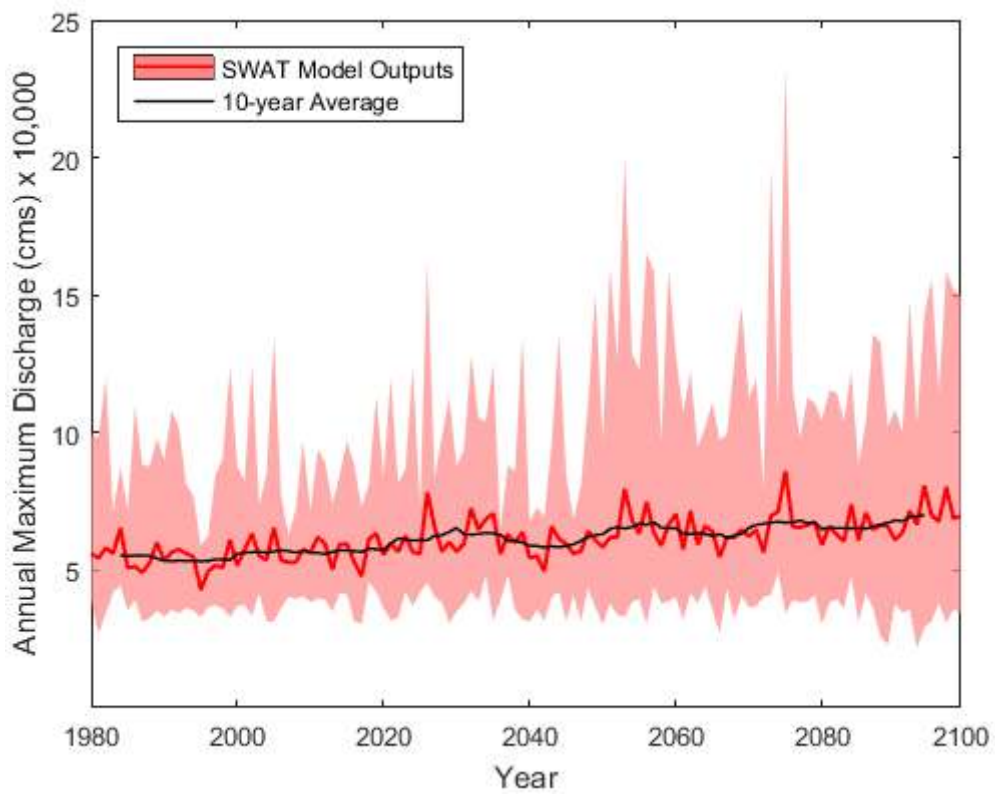


Fig. 1.6 Changes in ensemble range of annual maximum discharge.

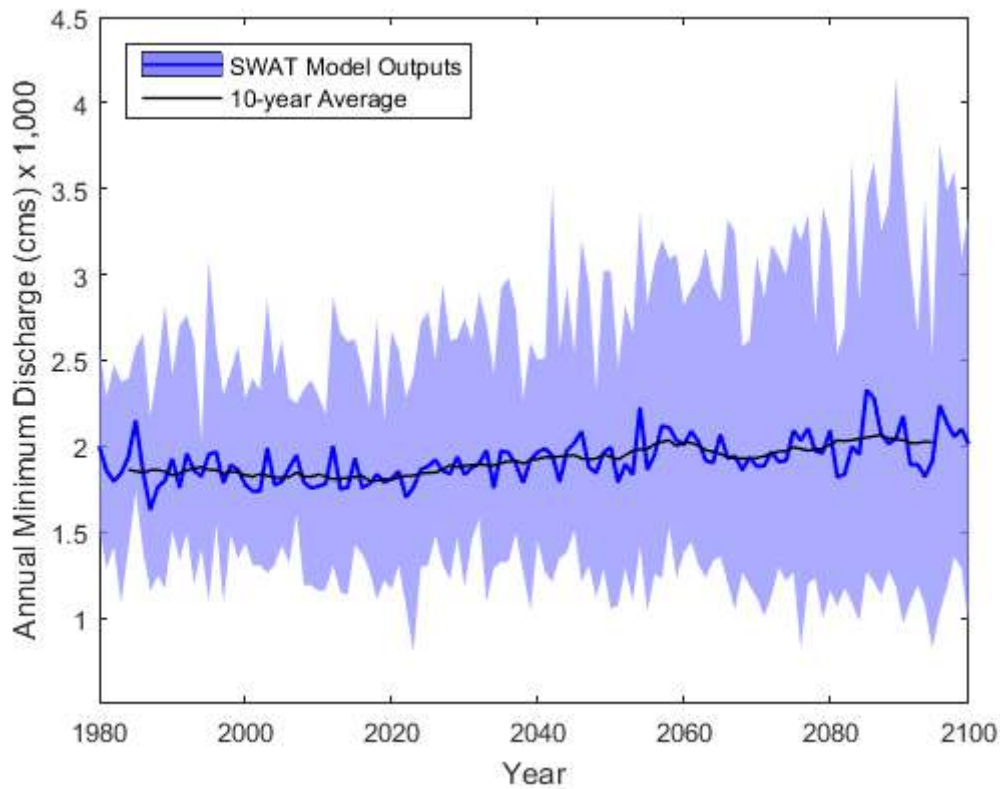


Fig. 1.7 Changes in ensemble range of annual minimum discharge.

1.4.2.1 Changes in frequency of annual maximum discharge

The return periods estimated by the parametric frequency analysis performed on the annual maximum discharge series are shown in **Fig. 1.8**. Here, 4 shaded regions correspond to the 4 time periods and each shaded region shows the range of 11 return period curves estimated by 11 climate projections. It can be seen that as the return period value increases, the range of uncertainty in their corresponding annual maximum discharge value also increases gradually. The largest range of uncertainty is displayed by the 2080s for all return periods. In order to quantify the changes in different time periods, a mean of the ranges were drawn which are shown by the solid line within each shaded region. For every return period, the percentage change of the corresponding annual maximum discharge value in 2020s, 2050s and 2080s compared to the baseline period are shown in **Table 1.4** where a positive value indicates an increase. It can be seen that for all return periods, the corresponding discharge values will increase in 2020s, 2050s and 2080s compared to the baseline period and the increase is largest in 2080s. For instance, the annual

maximum discharge with a 500 year return period will increase 50.14% in the 2080s compared to the baseline period. In other words, floods will become more frequent in the future.

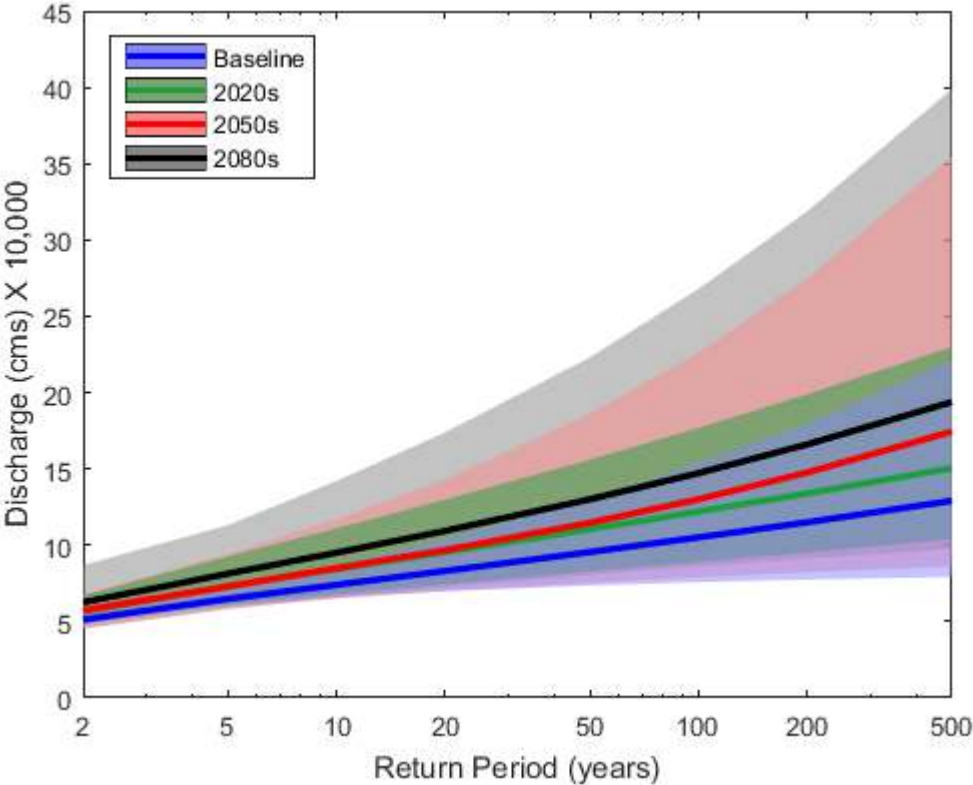


Fig. 1.8 Return period curves of annual maximum discharge for different time periods.

Table 1.4 Percentage change in annual maximum discharge for different return periods.

Return period (years)	Percentage change in annual maximum discharge compared to baseline		
	2020s	2050s	2080s
2	10.76	12.08	22.34
5	12.84	12.53	25.44
10	13.95	14.80	28.43
20	14.78	16.32	31.61
50	15.68	20.08	36.19
100	16.11	23.72	40.02
200	16.44	28.39	44.41
500	16.60	35.17	50.14

1.4.2.2 Changes in magnitude of annual maximum discharge

The probability density functions of the annual maximum discharge series for the 4 time periods are shown in **Fig. 1.9**. It can be seen that as time periods progress from baseline to 2080s, the maximum probability density function value gradually decreases, i.e. the uncertainty of possible ranges of annual maximum discharge value increases. Also, the modes of the probability density functions appear to shift to the right. In order to understand the quantitative changes in different time periods, the percentage change of the mean, median and mode of the probability density functions of annual maximum discharges in 2020s, 2050s and 2080s compared to the baseline period are shown in **Table 1.5** where a positive value indicates an increase. It can be seen that the mean, median and mode will all increase in 2020s, 2050s and 2080s compared to the baseline period and the increase is largest in 2080s. For instance, the mean value of all the annual maximum discharges in the 2080s will be 22.67% greater than the mean value of all the annual maximum discharges in the baseline period. In other words, the magnitude of floods will be increased in the future, i.e. they will become more severe.

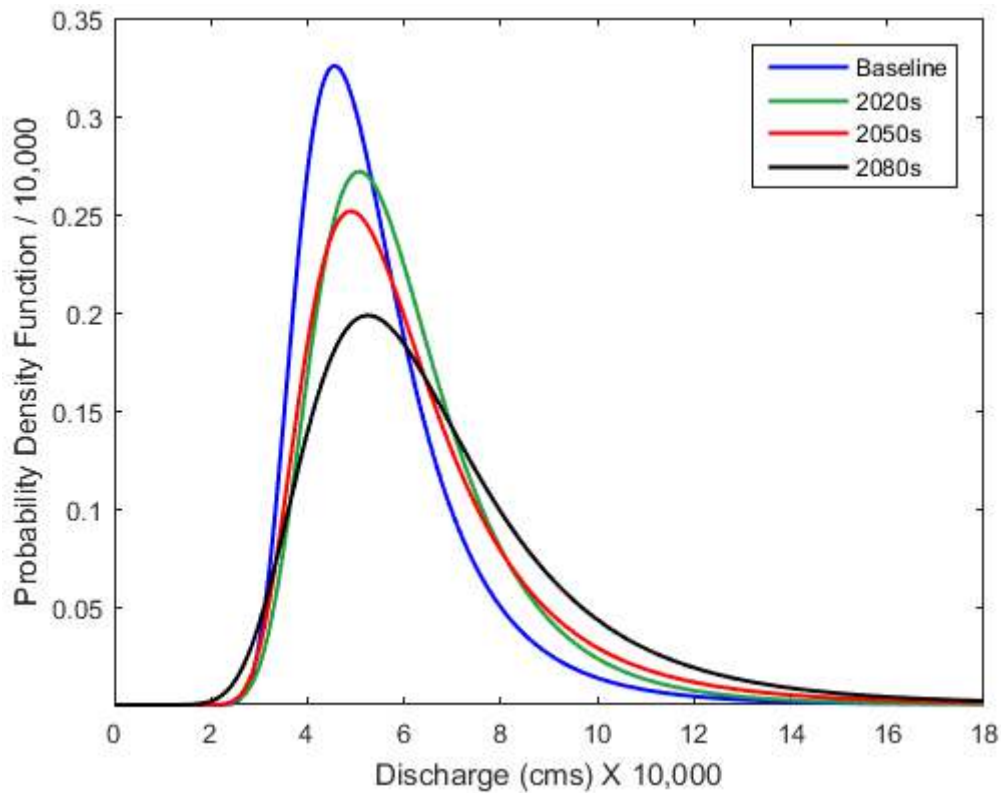


Fig. 1.9 Probability density functions of annual maximum discharge for different time periods.

Table 1.5 Percentage change in properties of probability density function of annual maximum discharge.

Property of probability density function	Percentage change compared to baseline period		
	2020s	2050s	2080s
Mean	9.88	13.28	22.67
Median	10.76	10.77	20.04
Mode	11.24	7.38	15.12

1.4.2.3 Changes in timing of annual maximum discharge

The date of occurrences of the annual maximum discharges for all 4 time periods are shown in **Fig. 1.10**.

For each time period, a scatter plot was made with data from all 11 of the annual maximum discharge

series of that particular period, corresponding to the 11 climate projections used to derive them. In order to compare the change in timing of annual maximum discharge of different time periods, a dashed line was drawn on each scatter plot representing the average date of all the dates of the particular time period of that scatter plot. It can be seen that the average date of occurrence of annual maximum discharge is virtually unchanged. The average dates are July 28, July 27, July 26 and July 27 for the baseline period, 2020s, 2050s and 2080s respectively. In other words, timing of the floods will not change in the future.

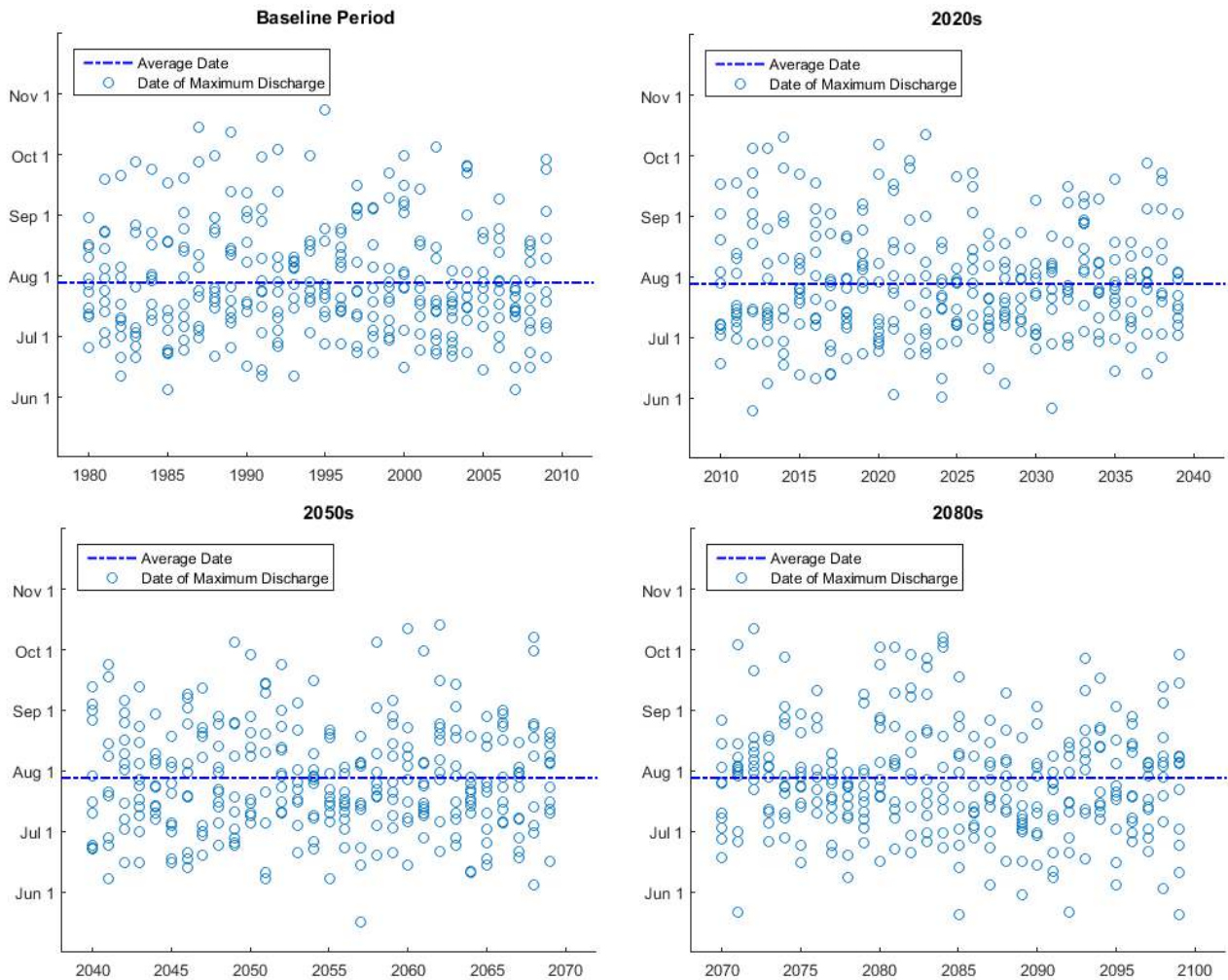


Fig. 1.10 Timing of annual maximum discharge for different time periods.

1.4.2.4 Changes in frequency of annual minimum discharge

The return periods estimated by the parametric frequency analysis performed on the annual minimum discharge series are shown in **Fig. 1.11**. Here, 4 shaded regions correspond to the 4 time periods and each shaded region shows the range of 11 return period curves estimated by 11 climate projections. It

can be seen that similar to the return periods of annual maximum discharge, the range of uncertainty is largest for 2080s, but unlike **Fig. 1.8** the range of uncertainty does not increase proportionally with the return period. Rather the uncertainty is approximately the same for all return periods. In order to quantify the changes in different time periods, a mean of the ranges were drawn which are shown by the solid line within each shaded region. For every return period, the percentage change of the corresponding annual minimum discharge value in 2020s, 2050s and 2080s compared to the baseline period are shown in **Table 1.6** where a positive value indicates an increase. It can be seen that for all return periods, the corresponding discharge values will increase in 2020s, 2050s and 2080s compared to the baseline period and the increase is largest in 2080s. For instance, the annual minimum discharge with a 2 year return period will increase 9.34% in the 2080s compared to the baseline period. In other words, low flow extremes will become less frequent in the future.

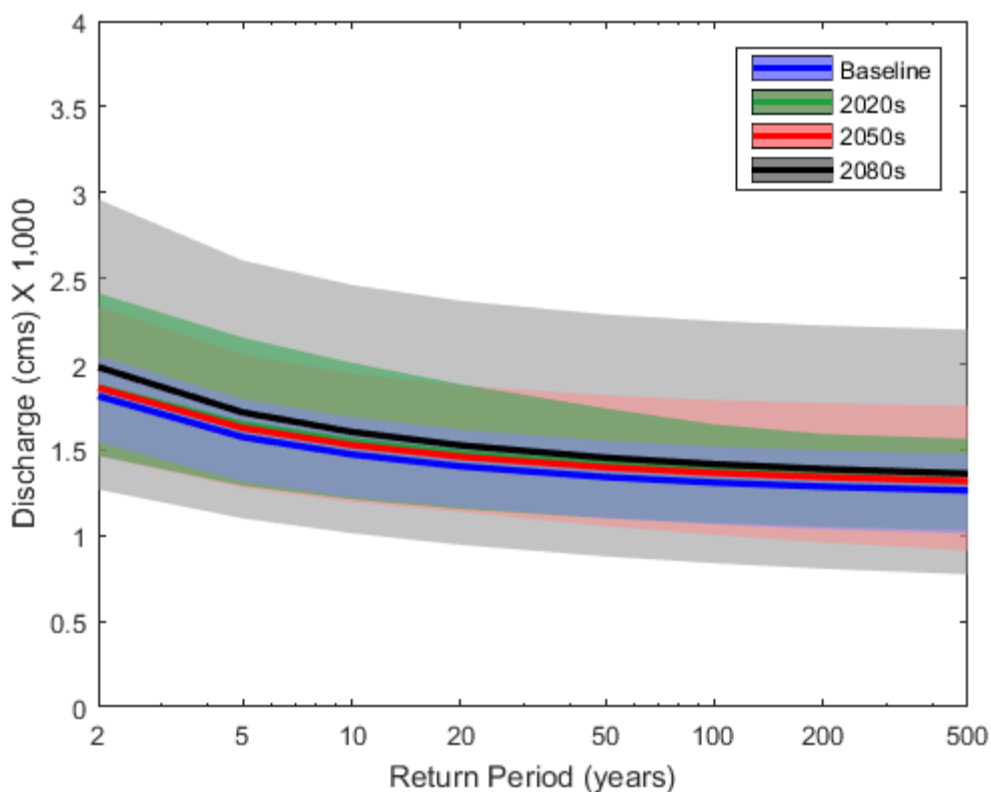


Fig. 1.11 Return period curves of annual minimum discharge for different time periods.

Table 1.6 Percentage change in annual minimum discharge for different return periods.

Return period (years)	Percentage change in annual minimum discharge compared to baseline
-----------------------	--

	2020s	2050s	2080s
2	2.90	2.68	9.34
5	4.75	3.37	9.13
10	5.32	3.73	8.91
20	5.55	4.03	8.72
50	5.46	4.25	8.42
100	5.19	4.32	8.19
200	4.86	4.35	8.01
500	4.37	4.35	7.81

1.4.2.5 Changes in magnitude of annual minimum discharge

The probability density functions of the annual minimum discharge series for the 4 time periods are shown in **Fig. 1.12**. It can be seen that as time periods progress from baseline to 2080s, the maximum probability density function value gradually decreases, i.e. the uncertainty of possible ranges of annual minimum discharge value increases. Also, the modes of the probability density functions appear to shift slightly to the right. In order to understand the quantitative changes in different time periods, the percentage change of the mean, median and mode of the probability density functions of annual minimum discharges in 2020s, 2050s and 2080s compared to the baseline period are shown in **Table 1.7** where a positive value indicates an increase. It can be seen that the mean, median and mode will all slightly decrease in 2020s but then increase in 2050s and 2080s compared to the baseline period. For instance, the mean value of all the annual minimum discharges in the 2080s will be 9.35% greater than the mean value of all the annual minimum discharges in the baseline period. In other words, the magnitude of low flow extremes will be increased in the future, i.e. they will become less severe, except in the near future (2020s).

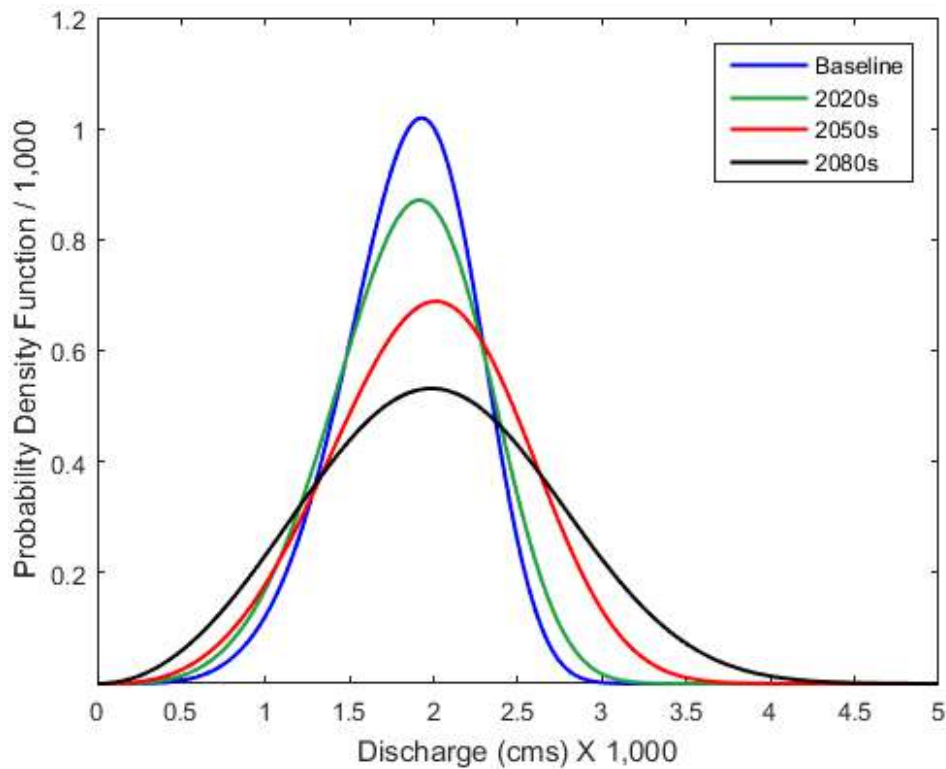


Fig. 1.12 Probability density functions of annual minimum discharge for different time periods.

Table 1.7 Percentage change in properties of probability density function of annual minimum discharge.

Property of probability density function	Percentage change compared to baseline period		
	2020s	2050s	2080s
Mean	-0.04	6.40	9.35
Median	-0.27	5.64	7.16
Mode	-0.57	4.41	3.11

1.4.2.6 Changes in timing of annual minimum discharge

The date of occurrences of the annual minimum discharges for all 4 time periods are shown in **Fig. 1.13**. For each time period, a scatter plot was made with data from all 11 of the annual minimum discharge series of that particular period, corresponding to the 11 climate projections used to derive them. In order

to compare the change in timing of annual minimum discharge of different time periods, a dashed line was drawn on each scatter plot representing the average date of all the dates of the particular time period of that scatter plot. It can be seen that the average date of occurrence of annual minimum discharge is virtually unchanged. The average dates are March 5, March 9, March 4 and March 7 for the baseline period, 2020s, 2050s and 2080s respectively. In other words, timing of the low flow extremes will not change in the future.

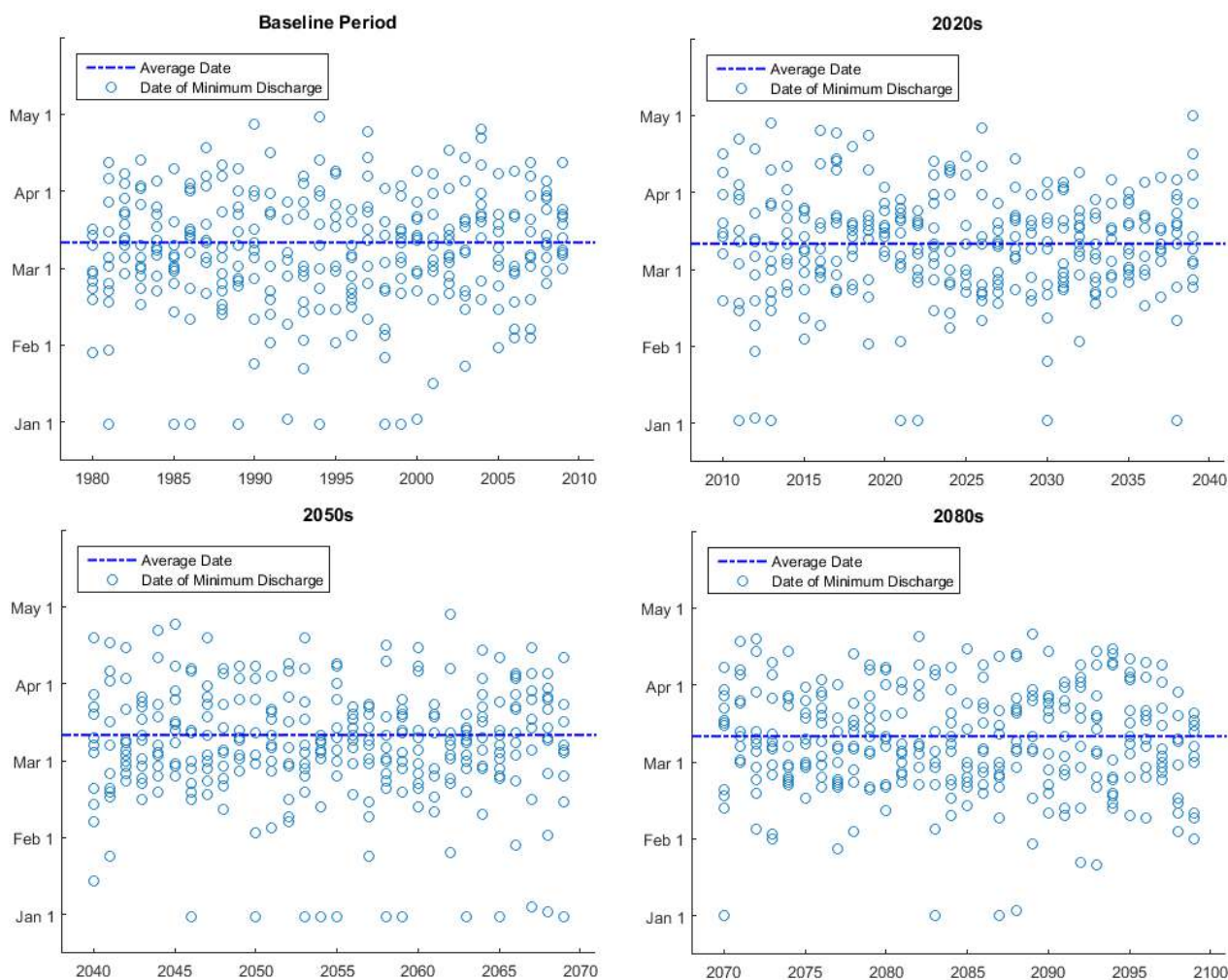


Fig. 1.13 Timing of annual minimum discharge for different time periods.

1.4.2.7 Changes in median of mean monthly discharge

In order to understand the change in mean monthly discharges in different time periods, the daily time series of SWAT simulated discharges were converted to mean monthly discharge time series. Then a boxplot was drawn using the mean monthly discharge time series as shown in **Fig. 1.14**. Here, each box

represents the mean monthly discharges of a particular month and a particular time period from all 11 SWAT simulated discharge time series, corresponding to the 11 climate projections used to derive them. The black dots inside white circles on each box represents the median value. It can be seen that the range of uncertainty is largest during the monsoon months of June, July, August and September for all 4 time periods. In order to understand the quantitative changes in different time periods, the percentage change of discharge values in 2020s, 2050s and 2080s compared to the baseline period for all 11 climate projections were calculated which are shown in **Fig. 1.15** as another boxplot. The median values of these boxes are shown in **Table 1.8**. It can be seen that in every time period, majority of the months will see an increase in mean monthly discharge and the remaining will see a slight decrease. In the 2020s, March and April will see a decrease while in the 2050s and 2080s, October and November will see a decrease in mean monthly discharge. The largest increase for all 3 time periods will be in May, with values of 7.85%, 18.34% and 24.08% for 2020s, 2050s and 2080s respectively.

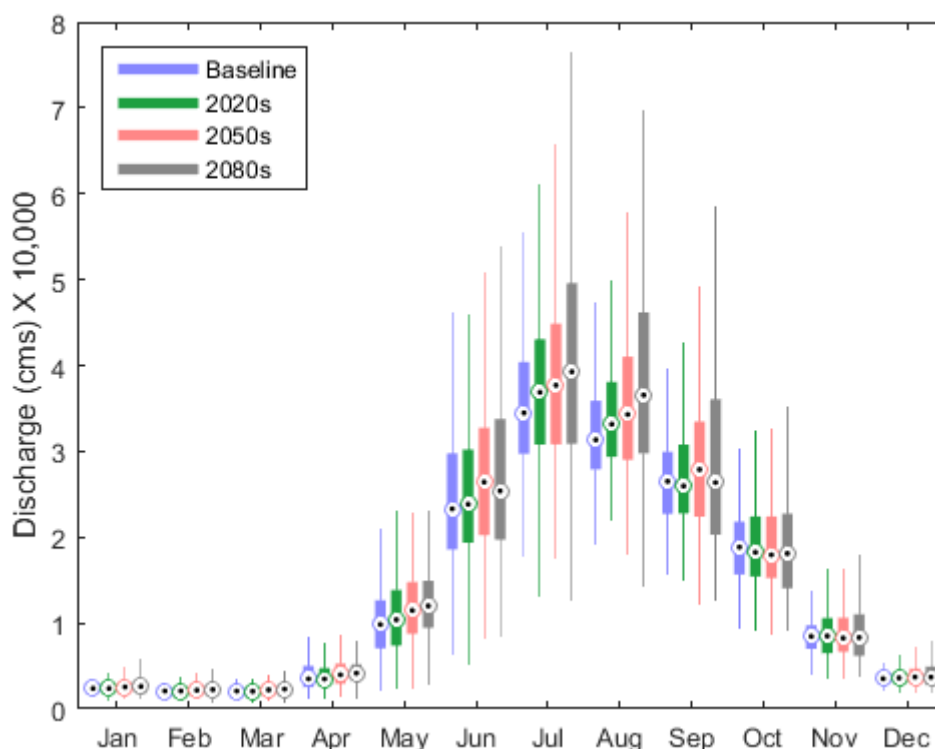


Fig. 1.14 Boxplot of mean monthly discharge for different time periods.

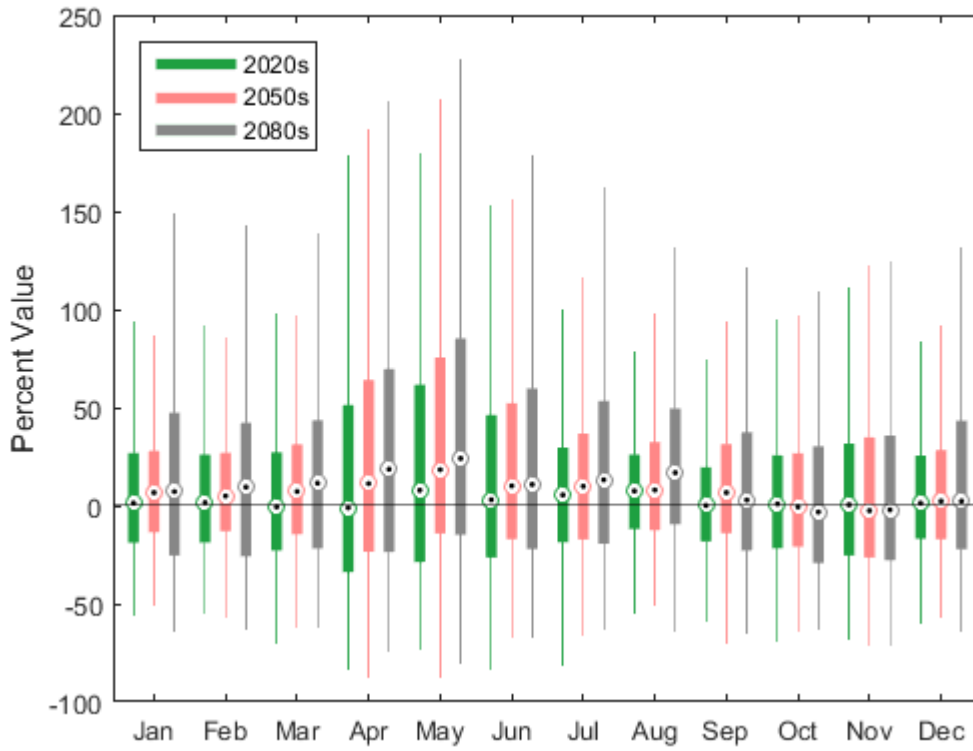


Fig. 1.15 Boxplot of percentage change in mean monthly discharge.

Table 1.8 Median of percentage changes of mean monthly discharge.

Month	Percentage change compared to baseline period		
	2020s	2050s	2080s
Jan	1.30	6.65	7.16
Feb	1.57	4.96	9.47
Mar	-0.61	7.23	11.45
Apr	-1.08	11.24	18.55
May	7.85	18.34	24.08
Jun	3.03	10.10	10.81
Jul	5.47	9.88	13.17
Aug	7.47	8.00	16.81
Sep	0.09	6.67	2.89
Oct	0.89	-0.63	-3.22
Nov	0.47	-2.53	-2.15
Dec	1.25	2.29	2.29

1.5 Summary

This study was undertaken to assess the impact of climate change on the frequency, magnitude and timing of extreme discharges and the mean monthly discharges of Brahmaputra River at the location of Bahadurabad gaging station of BWDB. For this purpose the SWAT hydrological model was used at a daily time-step. For calibrating the parameters of SWAT model the SUFI-2 algorithm SWAT-CUP program was used. The calibrated model used in further analysis had NSE values of 0.84 and 0.83 and R^2 values of 0.86 and 0.87 during calibration and validation periods, respectively. For simulating future discharges, precipitation and temperature data of an ensemble of 11 different future climate projections were used. Also, only the emission scenario of RCP8.5 was considered.

When analysing the changes in future river discharges, 4 time periods were considered. Annual maximum/minimum discharge series were extracted from the SWAT simulated daily discharges. Return periods were calculated for estimating the changes in frequency of extreme discharges and probability density functions were drawn for estimating the changes in magnitude of extreme discharges. For estimating the changes in timing of extreme discharges, scatter plots were drawn with the date of occurrences of extreme events. Finally, simulated daily discharges were converted to mean monthly discharges and a boxplot was drawn to compare changes in mean monthly discharges of the 4 time periods.

Results of the analysis of annual maximum discharge data show that floods will become more frequent in the future and their magnitudes will become greater, i.e. they will become more severe, but the mean timing of flood events will not change. Results of the analysis of annual minimum discharge data show that low flow extremes will become less frequent in the future and their magnitudes will become greater, i.e. they will become less severe, but the mean timing of low flow extremes will not change. Results of the analysis of mean monthly discharge data show that in every time period, majority of the months will see an increase in mean monthly discharge and the remaining will see a slight decrease. But for all time periods the month of May will see the highest increase in discharge compared to the other months.

CHAPTER TWO

ASSESSMENT OF THE UNCERTAINTY AND SENSITIVITY OF CLIMATE CHANGE ON THE PRODUCTION OF BORO RICE IN BANGLADESH USING DSSAT CROP MODEL

2.1 Introduction

Bangladesh is an agriculture based country. Here, 76% of the population lives in rural areas and 47.5% of the total manpower is involved in agriculture. Agriculture contributes 19.3% of the gross domestic product (GDP) of the land (Shelley et al., 2016). Rice is a crop that is grown almost throughout the country. The physiological, agricultural and climatic conditions of Bangladesh are suitable for growing rice throughout the year. But, average rice yield of Bangladesh is lower (2.94 t/ha) than that of other rice-growing countries (BBS, 2012). Rice is the staple food for about 156 million people of the country. With the present population growth rate of 2 million per year, the total population would be 238 million by 2050. Bangladesh will require more than 55.0 million tons of rice to feed its people by the year 2050 (Basak, 2010). The ever increasing demand on agriculture is added with problems like decreasing agricultural lands and water source depletion (Ahmed et al., 2000). The total cultivable land is decreasing at a rate of 1% per year due to the multifarious land use in construction of industries, factories, houses, roads, and highways. Moreover, with urbanization and changed food habits, the demand of the cultivation of new crops has raised which would decrease the share of land used for rice cultivation. Therefore, attempts should be made to increase the yield per unit area of rice. Moreover, due to climate change, agriculture is experiencing impediments like drought, flood, salinity, extreme temperature stress, and low soil fertility. Even though we live in the modern age with numerous technological advances featuring improved crop varieties, improved fertilizers and irrigation systems, the effect of climate is still dominating over these advancements.

The impacts of climate change on food production are global concerns, and they are very important for Bangladesh. Irrigated rice or Boro rice is a potential area for increasing rice yield, which currently

accounts for about 55% of total rice production in the country though it was around 50% before 2006. (BRRI, 2006 and Risingbd, 2014). As the demand of rice rises, so is that of Boro rice which has the most share. However, climate change is the major threat towards attaining this objective. So, it is very important to evaluate the effect of climate change on Boro production.

For the last 15 years, DSSAT (Decision Support System for Agrotechnology Transfer) has been a useful tool that has brought many applications under experiment like N fertilization, irrigation and planting or sowing date. (Iqbal et.al., 2011). Simulation studies have been carried out to assess the impacts of climate change and variability on rice productivity in Bangladesh using the CERES-Rice model previously. (e.g., Basak 2010; Mahmood et al., 2003; Mahmood, 1998; Karim et al., 1996). These studies mainly focused on the effects of higher air temperature on rice yield. For instance, Basak (2010) has carried out simulations of 12 representative regions from various zones of the country using the regional climate model PRECIS. However, this study covers simulation over all the 64 districts of the country using seven numbers of bias corrected ensembles of regional climate models.

As the regional variations in natural and anthropogenic factors governing the response of the crop, the impact of climate change on crop also depends on the region, scenarios and the type of crop (Tubiello et.al., 2002). The impact of temperature depends both on the change of temperature and the crop growth stage (Hatfield, 2008). However, the impact of climate change on agriculture is bolstered by the addition of the effects of CO₂ fertilization with plant physiological processes (Salinger et al., 2005). A study has been done on 2xCO₂ scenario which witnessed a positive change of yield than the normal emission scenarios (Pongratz et. al., 2012).

2.2 Materials and methods

2.2.1 Study area

The study was focused on Bangladesh (20°34" North Latitude to 26°38" North Latitude and from 88°01" East Longitude to 92°41" East Longitude) which has almost 0.15 million km² territory. This South Asian country is the largest delta of the world as 80% of the land is formed by the floodplains of the Ganges, Brahmaputra and Meghna (GBM) rivers making it a fertile land for rice production. The country experiences most of the rainfall due to monsoon. However, some flash floods prior to the monsoon season also occur. This tropical country has annual average rainfall of 1600 mm and a temperature ranging from 8° to 38°C during the growth season of Boro rice (Nov-April) over the last 30 years (1981-2010). This study covers the whole country which is divided into 64 districts (administrative boundary) as shown in Figure 2.1.

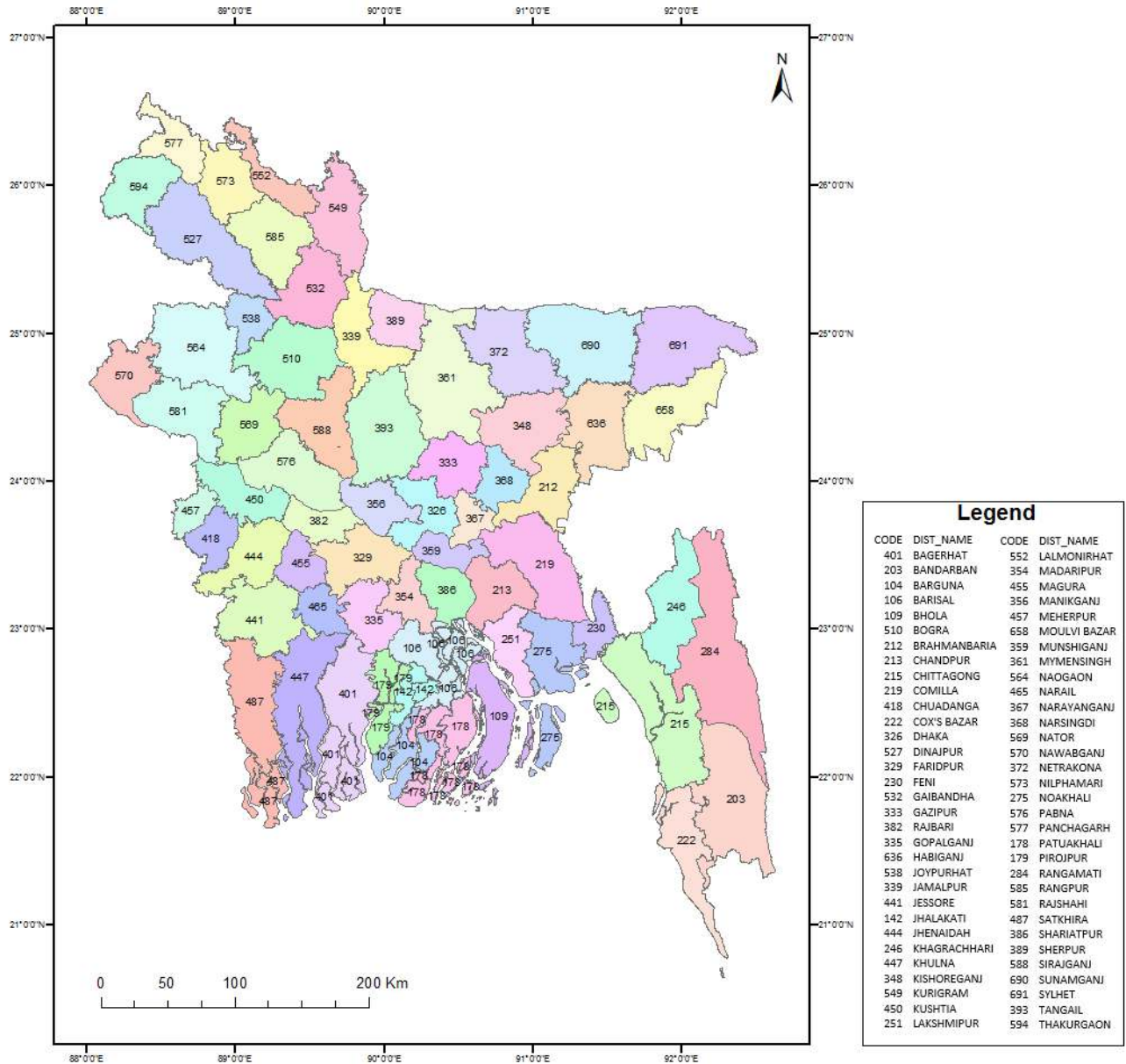


Fig. 2.1 District maps of Bangladesh.

2.2.2 Selection of crop simulation model

From several crop modeling software, DSSAT 4.6 was chosen for the simulation. The CERES-Rice model of the DSSAT modeling system is an advanced physiologically based rice crop growth simulation model and has been widely applied to understanding the relationship between rice and its environment. The model estimates yield of irrigated and non-irrigated rice, determine duration of growth stages, dry matter production and partitioning, root system dynamics, effect of soil water and soil nitrogen contents

on photosynthesis, carbon balance and water balance. Ritchie et al. (1987) and Hoogenboom et al. (2003) have provided a detailed description of the model.

2.2.3 Integrating field data in DSSAT

The model requires a quite detailed set of input data on soil and hydrologic characteristics (i.e., pedological and hydrological data), and crop management. Input data related to soil characteristics include soil texture, number of layers in soil profile, soil layer depth, pH of soil in water for each depth, clay, silt and sand contents, organic matter, cation exchange capacity, etc. However, we are concerned only about the impact of climatologic parameters due to shifted date of transplantation. Nevertheless, we have set some defaults of soil parameters like 15 cm depth of base layer and pH calculation in pH of water etc. The DSSAT software team has recently done experiments on 17 soil stations across Bangladesh. The soil station data has been stored in WISE 1.1 database. Once a region is selected from the global map, it enables the user to access the soil station data. This set of data is simply copied and pasted on the soil database file. Thus the soil stations can easily be integrated in DSSAT.

2.2.4 Selection of rice variety

The CERES-Rice model is variety-specific and is able to predict rice yield and rice plant response to various environmental conditions. In predicting crop growth and yield, the model takes into effect of weather, crop management, genetics, and soil water, C and N. The model uses a detailed set of crop specific genetic coefficients, which allows the model to respond to diverse weather and management conditions. Therefore, in order to get reliable results from model simulations, it is necessary to have the appropriate genetic coefficients for the selected cultivars. The Boro rice variety BR29 has been selected as most of the Boro rice produced here is BR29. The genetic coefficients of BR29 have been calibrated by the model as shown in **Table 2.1**.

Table 2.1 Key information of the BR29 variety of Boro rice.

Item	Value
Real Name	Brridhan29
Height	95 cm
Duration of growth	160 days
Grain quality	Medium
Yield (Kg/hectares)	7500
Developed on	1994
Developed by	Bangladesh Rice Research Institute (BRRI)

2.2.5 Weather data

In this study, the historic weather data was taken from 34 stations of Bangladesh Meteorological Department (BMD). The weather data contains daily rainfall (mm), maximum and minimum temperature (°C) and daily solar hours. Rainfall and temperatures are used directly in DSSAT. However, the weather manager of DSSAT itself converts solar hours into solar radiation. As simulations were carried out over 64 districts, the data of the nearest station of the corresponding district was taken. **Fig. 2.2** indicates the location of the meteorological stations of BMD. For calibrating the model, data of the years from 2007-2010 was taken and 2011-2014 was taken for validation. Although the weather data was available for last 35 years (1981-2015), those particular years was taken because, before 2007, individual data for Boro rice production was not available for every individual district.

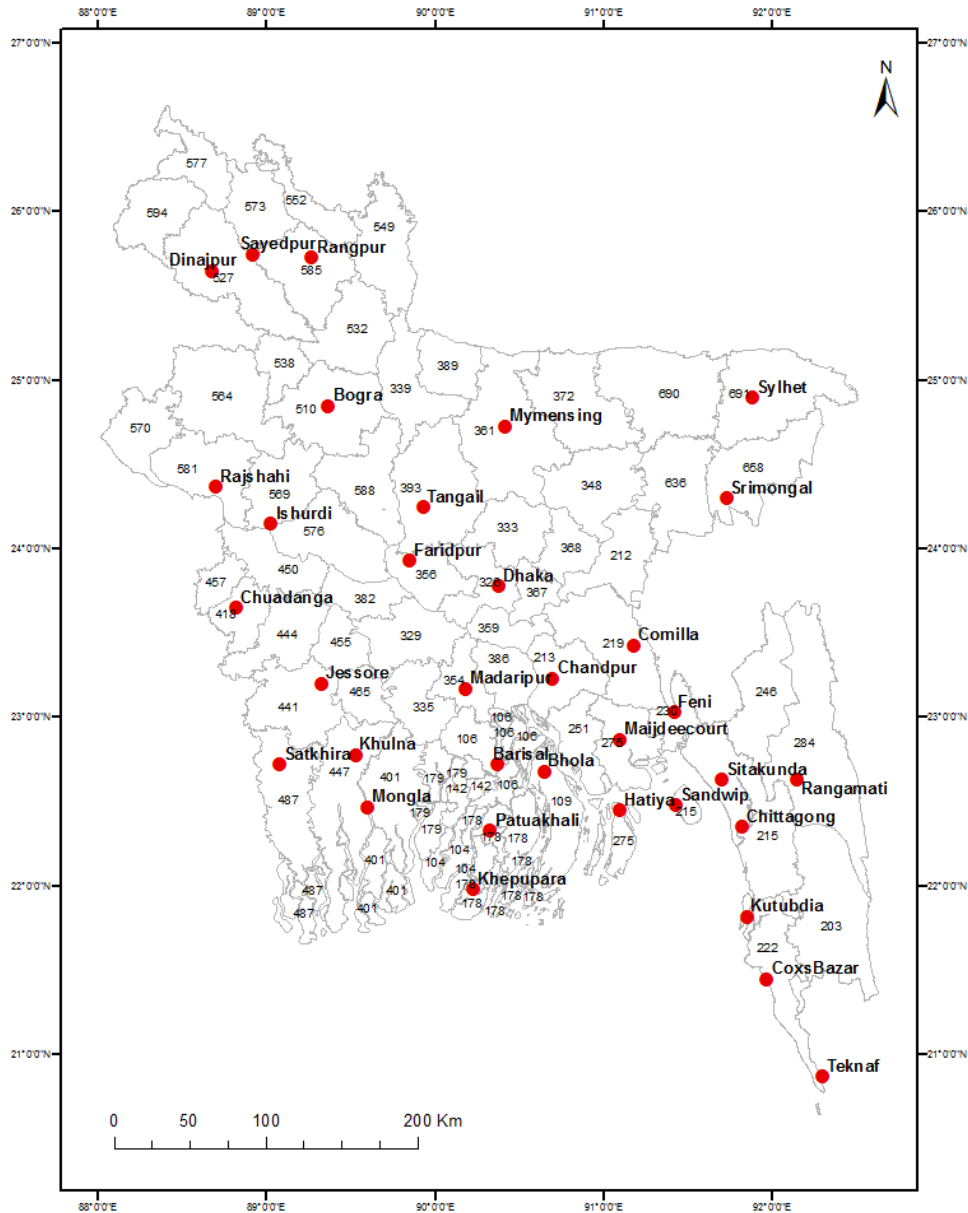


Fig. 2.2 Thirty four ground base measuring stations of Bangladesh Meteorological Department.

2.2.6 Climatic data

The future projected data was collected from 7 bias corrected ensembles with RCP 8.5 scenario of regional climate models RCM's under 4 GCM's. The baseline period was 30 years (1981-2010) and the projection was made for 2030's (2021-2050) and 2080's (2070-2099). **Table 2.2** describes the details of the ensembles.

Table 2.2 Details of the bias corrected ensembles of regional climate models.

Institute	GCM	RCM	Driving Ensemble Member	Res.	RCP
SMHI	CNRM-CERFACS- CNRM-CM5	RCA4	r1i1p1	0.5°	8.5
SMHI	ICHEC-EC-EARTH	RCA4	r1i1p1	0.5°	8.5
MPI- CSC	MPI-M-MPI-ESM-LR	REMO2009	r1i1p1	0.5°	8.5
SMHI	MPI-M-MPI-ESM-LR	RCA4	r1i1p1	0.5°	8.5
SMHI	NOAA-GFDL-GFDL- ESM2M	RCA4	r1i1p1	0.5°	8.5
SMHI	IPSL-CM5A-MR	RCA4	r1i1p1	0.5°	8.5
SMHI	MIROC-MIROC5	RCA4	r1i1p1	0.5°	8.5

2.2.7 Crop management

The crop management includes planting details, transplanted date, irrigation and fertilizer management, tillage, harvest and chemical applications. After calibration and validation, the transplant date was set as November 21. **Table 2.3** describes the details of crop management data for BR29 rice. **Fig. 2.3** shows the development stage of the BRRI 29 varieties of Boro rice in a field located at the Bangladesh Rice Research Institute, Gazipur, Bangladesh.



Fig. 2.3 BR29 variety of Boro rice in Bangladesh.

Table 2.3 Crop management data for simulations of BR29 in DSSAT.

Parameter	Input Data
Planting Method	Transplant
Transplantation Date	November 21
Planting distribution	Hill
Plant population at seedling	40 plants/ m ²
Plant population at emergence	35 plants/ m ²
Row spacing	20 cm
Planting Depth	5 cm
Transplant age	15-20 days
Fertilizer Application	90 kg/ha applied equally in 3 phases after 15, 35 and 55 days of transplant respectively
Irrigation	1000 mm applied in 15 applications with 7 days interval in 1 st month and 10 days interval later
Harvest	May 1

2.2.8 Calibration and validation

The model was calibrated to find the genetic coefficients for BR29 variety of Boro rice. Statistical parameters root mean square error (RMSE) was mainly used for the calibration. Trial and error methods were used by matching the grain yield previously in order to find the appropriate genetic coefficient (Sarkar and Kar 2006; Saseendran et. al.; 2013 and Ma et. al., 2006). The value of RMSE varied from 100- 300 depending on the soil profile and climatic scenario of the region. **Table 2.4** shows the default

values of the genetic coefficients and **Table 2.5** shows the calibrated value of these parameters in some important locations (divisions).

Table 2.4 Default values of the genetic coefficients of Boro rice.

Coefficient ID	Name of coefficient	Default Value
P1	Basic vegetative phase coefficient	650
P20	Critical photoperiod at maximum growth rate	90
P2R	Extent in delay of panicle initiation	400
P5	Time from emergence to maturity	13
G1	Potential spikelet number coefficient)	0.65
G2	Single grain weight in gm in ideal condition	0.25
G3	Tillering coefficient	1.0
G4	Temperature tolerance coefficient	1.0

Table 2.5 Values of the genetic coefficients in some important locations (divisions).

Region	P1	P2R	P5	P20	G1	G2	G3	G4	RMSE (Calibration)	RMSE (Validation)
Dhaka	647	93	415	12.9	67	0.26	1	1	260	125
Chittagong	645	87	395	12.9	62	0.25	1	1	312	213
Rajshahi	647	93	415	12.9	67	0.26	1	1	317	106
Barisal	648	90	400	13	67	0.25	1	1	192	141
Khulna	648	90	400	13	67	0.25	1	1	211	139
Sylhet	650	90	400	13	67	0.25	1	1	169	140
Rangpur	650	90	400	13	65	0.25	1	1	315	154

2.3 Results and discussion

2.3.1 Climatic scenarios

Fig. 2.4 shows that in the 2030's (2021-2050), the maximum temperature would cross 1⁰C and the minimum temperature will cross 1.5⁰C during the emergence to end period of Boro rice. Again, in the 2080's (2070-2099), the maximum temperature would cross 4⁰C and minimum temperature will cross 5⁰C during the emergence to end period of Boro rice. However, the rainfall also increases in future. In 2080's the increase is more than the 2030's. **Fig 2.5** shows the spatial pattern of the rainfall. The results show a spatial distribution of the change of rice yield.

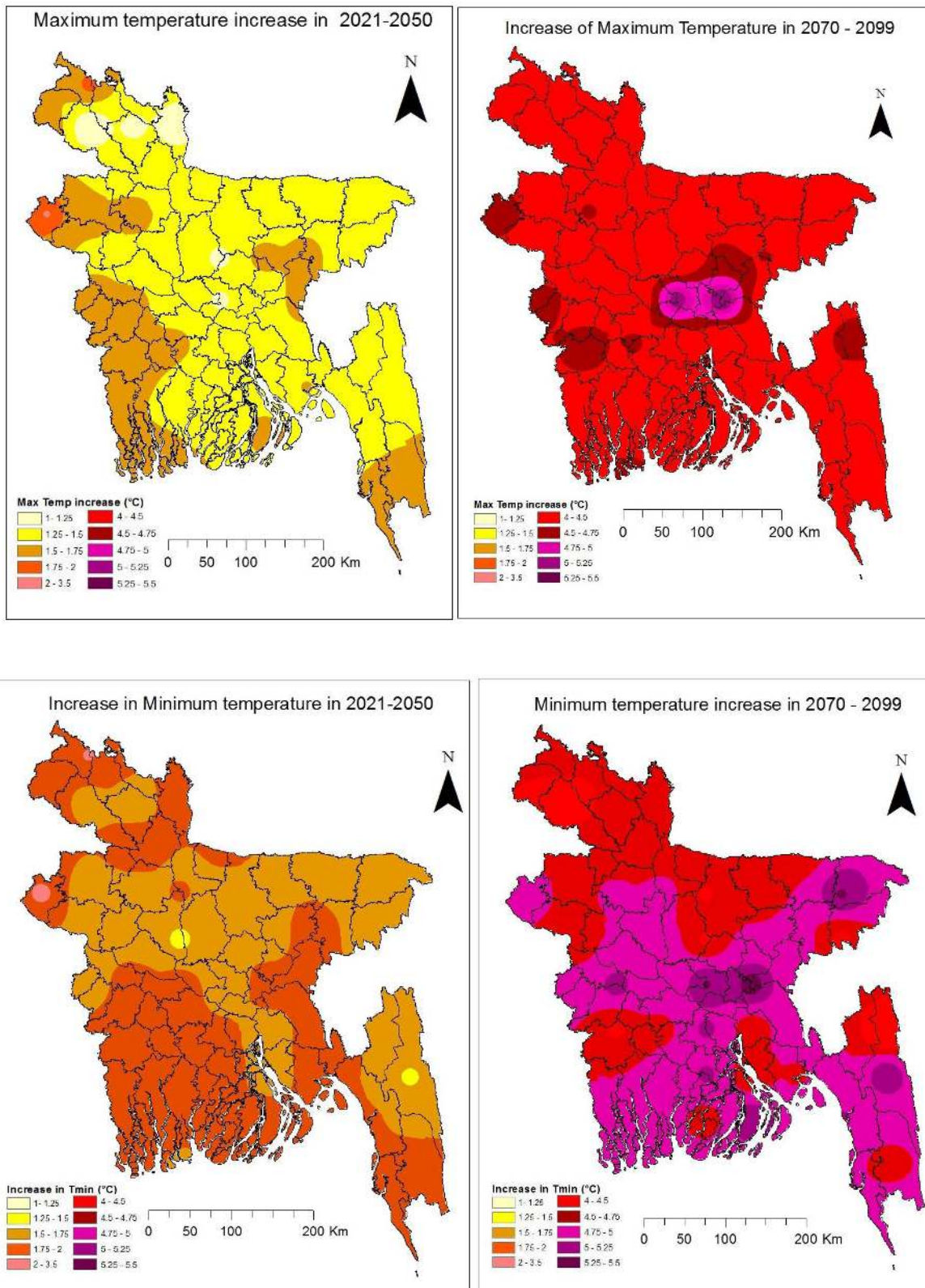


Fig. 2.4 Changes of the maximum temperature (top) and minimum temperature (bottom) in 2021-2050 (left) and 2070-2099 (right).

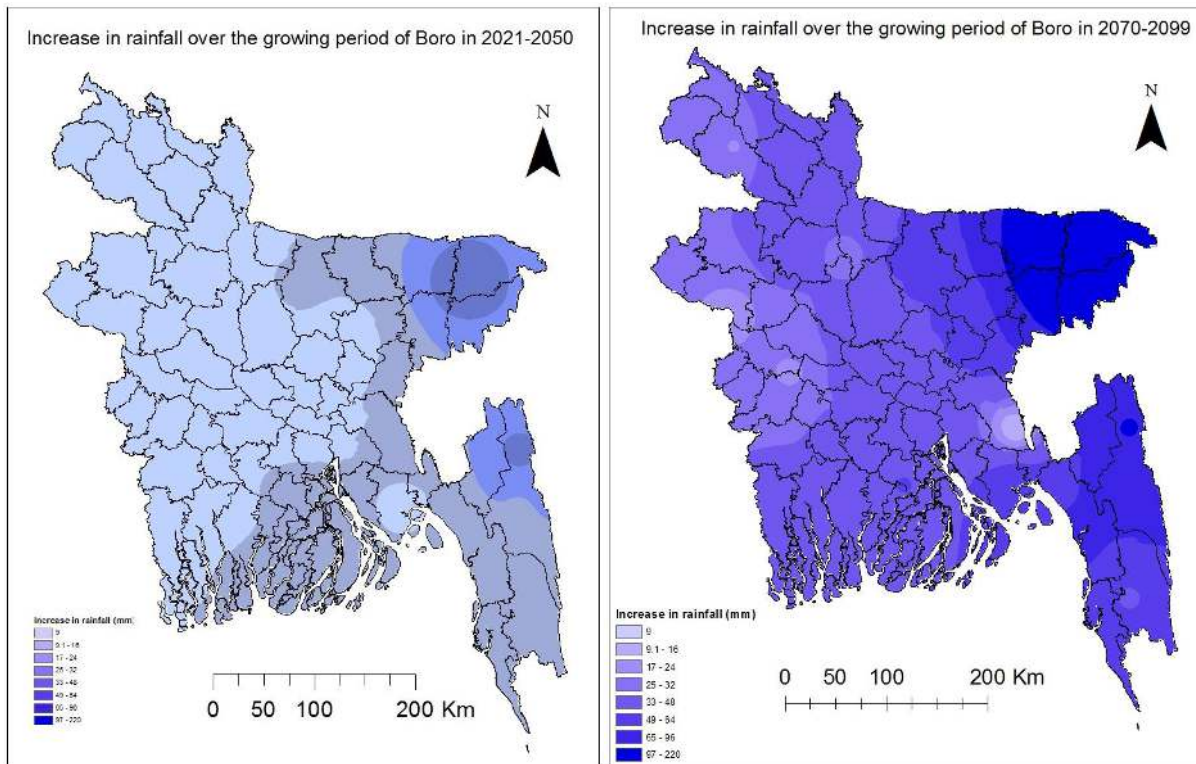


Fig. 2.5 Change of rainfall in 2021-2050 (left) and 2070-2099 (right).

2.3.2 Change of the yield

Fig. 2.6 (a) and Fig. 2.6(b) show a spatial distribution of the change of rice yield. As we can see in the figures, for both near (2021-2050) and far (2070-2099) future, the northeast zone encounters the minimum reduction in yield (2-6%). On the contrary, the southern zone is the most danger prone region experiencing a 14% to above 20% decrease in yields. Over the near and far future, the western zone of Bangladesh remains moderately affected by reduction of rice yield from 8% to 12%. However, the condition of the central zone is also affected in the far future which indicates how severe the impact of climate change is going to endanger the whole country in future. **Fig. 2.7** and **Fig. 2.8** show the range of the variations of the yield simulated by the various ensembles in 2021-2050 and 2070-2099, respectively.

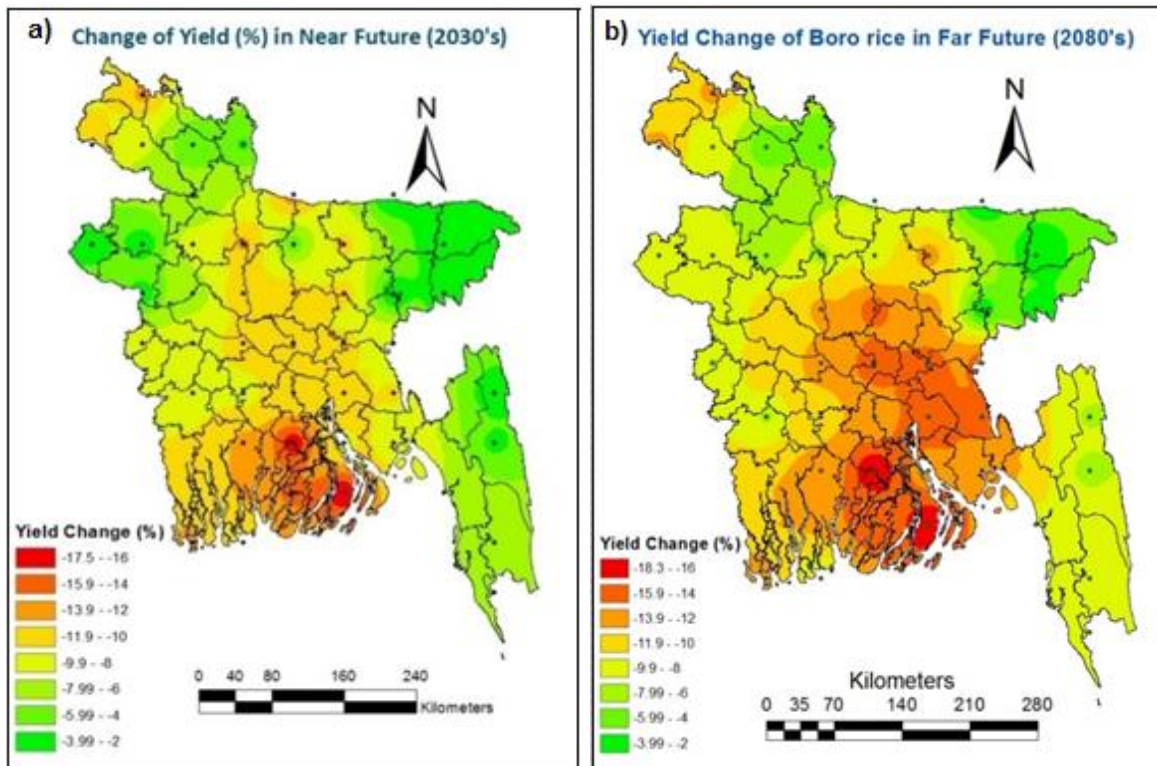


Fig. 2.6 (a) Change of Boro yield in 2021-2050 and (b) Change of Boro yield in 2070-2099.

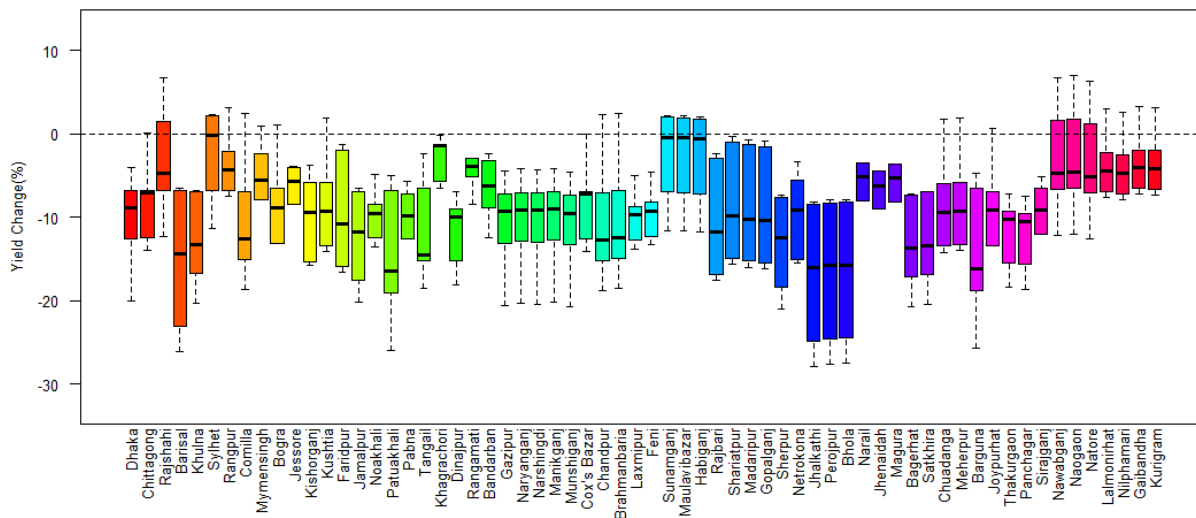


Fig. 2.7 Change of yield of Boro rice in 2021-2050.

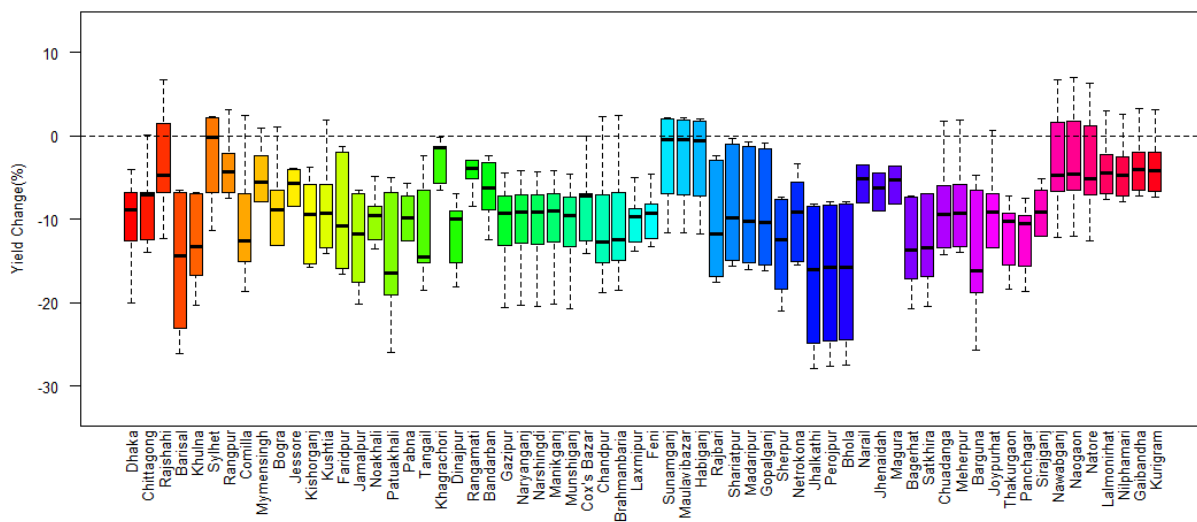


Fig. 2.8 Change of yield of Boro rice in 2070-2099.

2.3.3 Sensitivity of the increasing CO₂ on yield

Previously, many simulations were carried out (Pongratz et. al., 2012) at elevated CO₂ emission and the results were found to be positive on the yield of crops. The fixed emission of 380 ppm was considered to find out the changes in yield. However, according to RCP 8.5 scenario, the emission is not fixed. It is about 500 ppm over the 2030's and 950 ppm over the 2080's (IPCC, 2007). For this test we have selected

the major 8 districts or the divisional districts of Bangladesh: Dhaka, Chittagong, Rajshahi, Barisal, Khulna, Sylhet, Rangpur and Mymensingh. From **Fig. 2.9** and **Fig. 2.10**, it is seen that, the yield in almost all the regions has increased in the elevated CO₂ level than the fixed CO₂ emission in 2030's and 2080's. So, it is obvious that, elevated CO₂ would compensate some of the negative impacts of temperature. However, the range of unpredictability in rice yield has increased with the elevated CO₂ emissions. This might indicate the complex correlation between temperature and elevated CO₂ emission in the yield of crop.

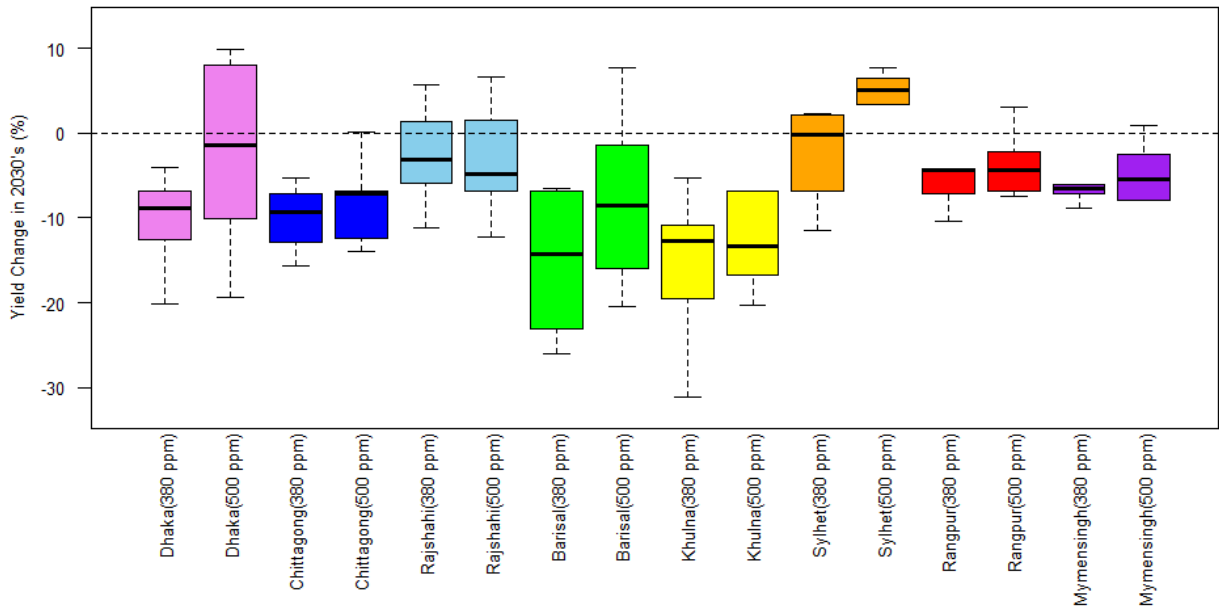


Fig. 2.9 Comparison of the yield change in fixed (380 ppm) and elevated (500 ppm) CO₂ in 2021-2050.

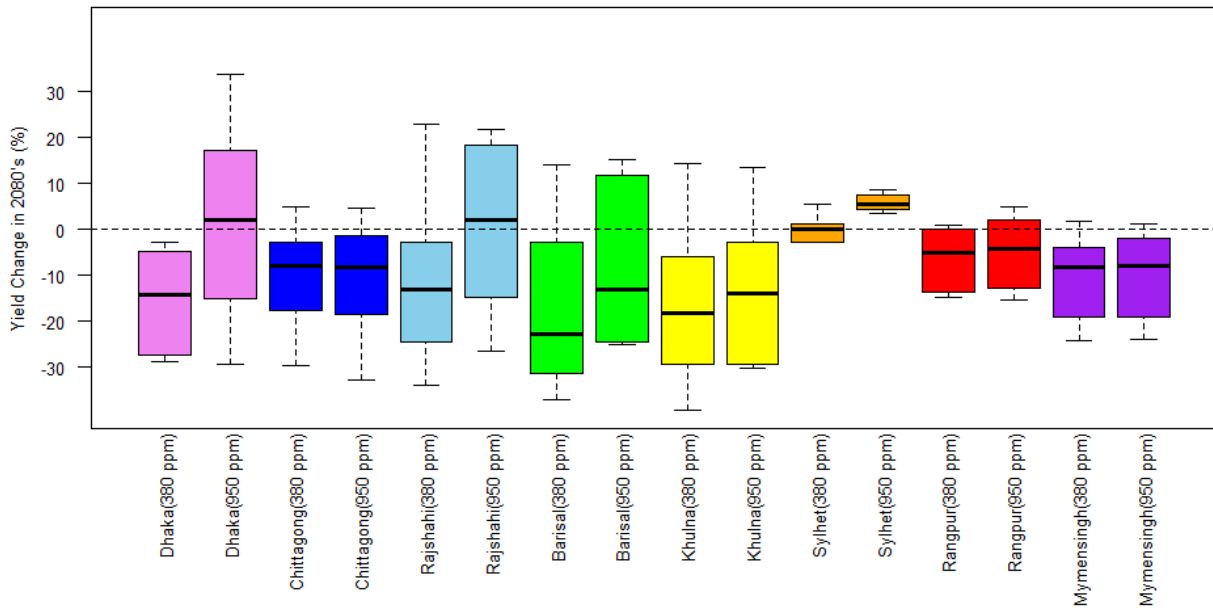


Fig. 2.10 Comparison of the yield change in fixed (380 ppm) and elevated (950 ppm) CO₂ in 2070-2099.

2.4 Summary

Most of the regions encountered extreme change in the maximum and minimum temperature over the emergence to end period of Boro crop. The yield trend is gradually decreasing at an alarming rate; crossing 10% decrease in 2030's to 20% decrease in 2080's. The growth and yield of crops are directly related to the rate of photosynthesis and their response to temperature, solar radiation and rainfall. Optimum temperatures for maximum photosynthesis range from 25°C to 30°C for rice under the climatic conditions of Bangladesh. Increased temperatures during the growing season cause grain sterility. Maximum temperatures cause the reduction in rice yield mainly. However CO₂ is also increasing which pose a positive impact on crop production. But, it is not dominant over the impact of temperature (Basak et al., 2010). We have also observed the positive impacts of elevated CO₂ emissions in our study.

It was evident that, the yield in 2030's is more than that of 2080's. The reasons behind this are, both maximum and minimum temperature would increase in 2080's than the 2030's. However, the rainfall is also increasing during the growing period of Boro rice in the 2080's than that of 2030's. But, it's positive impact was not sufficient to offset the negative impacts of temperatures. It is clear that, the south east zone is least affected by the climate change. This reason experiences the highest rainfall in future. Moreover, the rise of temperature is not the highest for these districts. Again, the southern zone is mostly affected by the climate change. It is observed that, these districts do not experience worst impact of any parameters, but the cumulative impacts of all the parameters have worsen their yield. Over the growing period of Boro rice experiences no Monsoon at all. For this reason, the probable cause behind the reduction in yield of any zone is supposed to be drought. This finding calls for a more detailed works on SPI (standardized precipitation index) in future. DSSAT crop modeling could prove very effective for this potential study. Moreover, the high end emission as the IPCC could be simulated to assess how intense is the impact of increased emission on Boro rice.

REFERENCES

- Abbaspour, K.C. (2015). *SWAT-CUP: SWAT Calibration and Uncertainty Programs – A User Manual*. Swiss Federal Institute of Aquatic Science and Technology, Switzerland.
- Abbaspour, K.C., Faramarzi, M., Ghasemi, S.S. and Yang, H. (2009). Assessing the impact of climate change on water resources in Iran. *Water Resour. Res.*, 45, W10434.
- Abbaspour, K.C., Vejdani, M. and Haghghat, S. (2007). SWAT-CUP calibration and uncertainty programs for SWAT. Proceedings of the International Congress on Modelling and Simulation (MODSIM07), Modelling and Simulation Society of Australia and New Zealand, Melbourne, 1603-1609.
- Ahmed, A. and Ryosuke, S. (2000). Climate change and agricultural food production of Bangladesh: an impact assessment using GIS-based biophysical crop simulation model. Center for Spatial Information Science, University of Tokyo, 4-6-1 Komaba, Japan.
- Alfieri, L., Burek, P., Feyen, L. and Forzieri, G. (2015) Global warming increases the frequency of river floods in Europe. *Hydrol. Earth Syst. Sc.*, 19, 2247–2260.
- Andersen, T.K. and Shepherd, J.M. (2013). Floods in a changing climate. *Geogr. Compass*, 7, 95–115.
- Arnell, N. (1999) Climate change and global water resources. *Global Environ. Change*, 9, 31-49.
- Arnold, J.G., Srinivasan, R., Muttiyah, R.S. and Williams, J.R. (1998). Large area hydrologic modeling and assessment Part I: Model development. *J. Am. Water Resour. Assoc.*, 34(1), 73-89.
- Basak, J.K. (2010). Effects of Increasing Temperature and Population Growth on Rice Production in Bangladesh: Implications for Food Security.
- Basak, J.K., Ali, M.A., Islam, M.N. and Rashid, M.A. (2010). Assessment of the effect of climate change on boro rice production in Bangladesh using DSSAT model. *Journal of Civil Engineering*, 38 (2), 95-108.
- BBS (Bangladesh Bureau of Statistics) (2012). Statistical Year Book of Bangladesh. Ministry of Planning, Government of the People’s Republic of Bangladesh: 33–36.
- Bharati, L., Gurung, P., Maharjan, L. and Bhattarai, U. (2016). Past and future variability in the hydrological regime of the Koshi Basin, Nepal. *Hydrol. Sci. J.*, 61(1), 79-93.

- BRRI (2006). Improvement of standard Boro rice. BRRI (Bangladesh Rice Research Institute) Annual Report for July 2005-June 2006. Plant Breeding Division, BRRI, Gazipur, Bangladesh.
- Gain, A.K., Immerzeel, W.W., Weiland, F.C.S. and Bierkens, M.F.P. (2011). Impact of climate change on the stream flow of the lower Brahmaputra: trends in high and low flows based on discharge-weighted ensemble modelling. *Hydrol. Earth Syst. Sc.*, 15, 1537–1545.
- Gosain, A.K., Rao, S. and Arora, A. (2011). Climate change impact assessment of water resources of India. *Curr. Sci.*, 101(3), 356-371.
- Grillakis, M.G., Koutroulis, A.G. and Tsanis, I.K. (2013). Multisegment statistical bias correction of daily GCM precipitation output. *J. Geophys. Res.: Atmos.*, 118(8), 3150–3162.
- Hasson, S., Lucarini, V. and Pascale, S. (2013). Hydrological cycle over South and Southeast Asian river basins as simulated by PCMDI/CMIP3 experiments. *Earth Syst. Dyn.*, 4, 199–217.
- Hatfield, J. (2008). Agriculture. In: P. Backlund, A. Janetos and D. Schimel (eds.) The effects of climate change on agriculture, land resources, water resources, and biodiversity in the United States. Synthesis and Assessment Product 4.3. Climate Change Science Program, Washington, DC, USA, pp 21-74.
- Hoogenboom, G., Jones, J.W., Porter, C.H., Wilkens, P.W., Boote, K.J., Batchelor, W.D., Hunt, L.A. and Tsuji, G.Y. (Editors). (2003) Decision Support System for Agrotechnology Transfer Version 4.0., Volume 1: Overview. University of Hawaii, Honolulu, HI.
- Huang, S., Krysanova, V. and Hattermann, F. (2015). Projections of climate change impacts on floods and droughts in Germany using an ensemble of climate change scenarios. *Reg. Environ. Change*, 15, 461-473.
- Immerzeel, W.W. (2008). Historical trends and future predictions of climate variability in the Brahmaputra basin. *Int. J. Climatol.*, 28, 243-254.
- Immerzeel, W.W., van Beek, L.P.H. and Bierkens, M.F.P. (2010). Climate change will affect the Asian Water Towers. *Science*, 328, 1382-1385.
- IPCC (2013). *Climate Change 2013: The Physical Science Basis. Contribution of Working Group I to the Fifth Assessment Report of the Intergovernmental Panel on Climate Change*. Cambridge University Press, Cambridge, United Kingdom and New York, NY, USA.

- Iqbal, M.A., Eitzinger, J., Formayer, H., Hassan, A., Heng, L.K. (2011). A simulation study for assessing yield optimization and potential for water reduction for summer-sown maize under different climate change scenarios. *J. Agr. Sci.* 149:129-143.
- Islam, A.S. (2008). Analyzing Changes of temperature over Bangladesh due to global warming using historic data. Institute of water and flood management, Bangladesh University of Engineering and Technology, Dhaka-1000
- Jha, M.K., Arnold, J.G., Gassman, P.W., Giorgi, F. and Gu, R.R. (2006). Climate change sensitivity assessment on upper Mississippi River basin streamflows using SWAT. *J. Am. Water Resour. Assoc.*, 42(4), 997-1016.
- Jian, J., Webster, P.J. and Hoyos, C.D. (2009). Large-scale controls on Ganges and Brahmaputra river discharge on intraseasonal and seasonal time-scales. *Q. J. R. Meteorolog. Soc.*, 135, 353–370.
- Karim, Z., Hussain, S.G. and Ahmed, M. (1996) Assessing Impact of Climate Variations on Foodgrain Production in Bangladesh, *Water Air and Soil Pollution*, 92, 53-62.
- Ma, L., Hoogenboom, G., Ahuja, L.R., Ascough II, J.C., Saseendran, S.A., (2006). Evaluation of the RZWQM-CERES-Maize hybrid model for maize production. *Agric. Syst.* 87 (3), 274–295.
- Mahmood, R. (1998) Air temperature variations and rice productivity in Bangladesh: A comparative study of the performance of the YIELD and CERES-Rice models. *Ecological Modeling*, 106, 201-212.
- Mahmood, R., Meo, M., Legates, D. R., & Morrissey, M. L. (2003). The CERES-Rice model-based estimates of potential monsoon season rainfed rice productivity in Bangladesh. *The Professional Geographer*, 55(2), 259-273.
- Narsimlu, B., Gosain, A.K., Chahar, B.R., Singh, S.K. and Srivastava, P.K. (2015). SWAT model calibration and uncertainty analysis for streamflow prediction in the Kunwari River basin, India, using Sequential Uncertainty Fitting. *Environ. Proc.*, 2, 79–95.
- Nepal, S. and Shrestha, A.B. (2015). Impact of climate change on the hydrological regime of the Indus, Ganges and Brahmaputra river basins: a review of the literature. *Int. J. Water Resour. Dev.*, 31(2), 201-218.
- Oki, T. and Kanae, S. (2006). Global hydrological cycles and world water resources. *Science*, 313, 1068-1072.

- Ouyang, F., Zhu, Y., Fu, G., Lu, H., Zhang, A., Yu, Z. and Chen, X. (2015). Impacts of climate change under CMIP5 RCP scenarios on streamflow in the Huangnizhuang catchment. *Stoch. Environ. Res. Risk Assess.*, 29, 1781–1795.
- Pervez, M.S. and Henebry, G.M. (2015). Assessing the impacts of climate and land use and land cover change on the freshwater availability in the Brahmaputra River basin. *J. Hydrol.: Reg. Stud.*, 3, 285–311.
- Pilon, P.J. and Harvey, K.D. (1993). Consolidated Frequency Analysis – Reference Manual. Environment Canada, Ottawa, Canada.
- Pilon, P.J., Jackson, R.J. (1988). *Low Flow Frequency Analysis Package – LFA*. Environment Canada, Ottawa, Canada.
- Pongratz, J., Lobell, D. B., Cao, L. and Caldeira, K. (2012). Crop yields in a geoengineered climate, *Nature Climate Change*, 22 January 2012, DOI:10.1038/NCLIMATE1373
- Risingbd (2014) [www.risingbd.com/english/Rice_ production_reaches_34449_million_ton_in_FY_2013-14/16217](http://www.risingbd.com/english/Rice_production_reaches_34449_million_ton_in_FY_2013-14/16217).
- Ritchie, J. T., Alocilja, E. C., Singh, U., Uehara, G. (1987). IBSNAT and the CERES-Rice model.
- Sarkar, R., Kar, S., 2006. Evaluation of management strategies for sustainable rice–wheat cropping system, using DSSAT seasonal analysis. *J. Agric. Sci.* 144 (05), 421–434.
- Saseendran, S.A., Nielsen, D.C., Ahuja, L.R., Ma, L., Lyon, D.J., (2013). Simulated yield and profitability of five potential crops for intensifying the dry land wheat fallow production system. *Agric. Water Manage.* 116, 175–192.
- Shelley, I. J., Takahashi-Nosaka, M., Kano-Nakata, M., Haque, M. S., & Inukai, Y. (2016). Rice Cultivation in Bangladesh: Present Scenario, Problems, and Prospects, *J Intl Cooper Agric Dev* 2016; 14: 20–29.
- Tubiello FN, Rosenzweig C, Goldberg RA, Jones JW, (2002). Effects of climate change on US crop production: simulation results using two different GCM scenarios. Part one: wheat, potato, maize and citrus. *Clim. Res.* 20:25-270.
- Uniyal, B., Jha, M.K. and Verma, A.K. (2015). Assessing climate change impact on water balance components of a river basin using SWAT model. *Water Resour. Manage.*, 29, 4767–4785.

Weedon, G.P., Balsamo, G., Bellouin, N., Gomes, S., Best, M.J. and Viterbo, P. (2014). The WFDEI meteorological forcing data set: WATCH Forcing Data methodology applied to ERA-Interim reanalysis data. *Water Resour. Res.*, 50(9), 7505–7514.

Xu, H. and Luo, Y. (2015). Climate change and its impacts on river discharge in two climate regions in China. *Hydrol. Earth Syst. Sc.*, 19, 4609–4618.